MAREES TERRESTRES

BULLETIN D'INFORMATIONS

INTERNATIONAL CENTER FOR EARTH TIDES
CENTRE INTERNATIONAL DES MAREES TERRESTRES

International Association of Geodesy - International Gravity Field Service
(IAG – IGFS)

Publié par l'Université de la Polynésie française

BIM n°146

ISSN n° 0542-6766

15 DECEMBRE 2010

BIM 146

December 15, 2010

New Challenges in Earth Dynamics (ETS2008) - end

Additional scientific papers

Importance of the ocean tide modeling of regional scale in the Earth tide study

Tadahiro Sato

Research Center for Prediction of Earthquakes and Volcanic Eruptions,

Tohoku University

6-6 Aza-Aoba, Aramaki, Aoba-ku, Sendai, 980-8578, Japan

E-mail: tsato@aob.geophys.tohoku.ac.jp

Abstract

This is a summary of an invited talk presented by Sato at the ETS 2008 International Conference 'New Challenges in Earth's Dynamics' that was held in Jena, Germany in September 2008. Main part of the presentation is referred to Sato et al. (2008). Recent improving of the accuracy of the tidal observations and model predictions including the ocean tidal loading (OTL) effects is remarkable. The observed Earth tide data may use to improve the model of the Earth's inside structure, which exhibits a viscoelastic property as well as the laterally inhomogeneous elastic structure. For these, it is essential to improve the accuracy of both the global and regional ocean tide models. An attempt in the region of Southeast Alaska is introduced.

1. Accuracy of the global ocean tide models

Based on the Schwiderski's ocean tide model (Schwiderski, 1980), Schenewerk et al. (2001) computed the ocean tide effects on the vertical components at the IGS-GPS sites in the world, and compared the observed loading effects. A remarkable point of their comparison results is large discrepancy exceeding 3 cm between the observed loading effect of the M_2 constituent and the computed one along the Pacific coast of Alaska.

Thanks to the satellite sea surface altimeters such as TOPEX/Poseidon and Jason-1, the accuracy of the recent global ocean tide models has been much improved compared with those in the 1980s. For example, according to Matsumoto et al. (2000), the vector differences for the M_2 constituent between NAO.99b (Matsumoto et al., 2000) and GOT99.2b (Ray, 1999) are the order of 1 cm or smaller than it almost everywhere in the open seas in the world. Matsumoto et al. (2006) also compared the recent global ocean tide models with the actual ocean bottom pressure gauge (OBPG) measurements in the western Pacific, off Sanriku in northern Japan, and they conclude that the difference between the observation and the five global ocean tide models was less than 1.3 cm in terms of root sum square of the vector differences for eight major tidal constituents (i.e. Q_1, O_1, P_1, K_1, N_2, M_2, S_2, and K_2). The ocean models they compared are NAO.99 (an old version of NAO.99b), NAO.99b, GOT99.2b, CSR4.0 (Eanes and Bettadpur,

1994), and TPXO.6 (Egbert et al., 1994). Consequently the accuracy of estimation of loading effect has been remarkably improved (e.g. Bos et al., 2002, Sato et al., 2004, Neumeyer et al., 2005 for the gravity, and Thomas et al., 2007 for the Global Positioning System (GPS) observation).

However, in contrast to the open seas, accuracy of the global ocean tide models is still questionable in the coastal regions. For example, Southeastern Alaska (SE-AK) is one of the places which show large discrepancy between the observations and the models. The total tidal range at Juneau exceeds 8 m (NOAA website, http://tidesandcurrents.noaa.gov/index.shtml), for instance. The analysis results for the 3-years tide gauge data at Juneau indicate that the observed amplitude and phase of M_2 tide are 198.612+/-0.064 cm and 282.736+/-0.018 degrees, respectively. On the other hand, those of the five global ocean tide models mentioned above are 133 cm to 353 cm in the amplitude and 206.9 deg to 277.0 deg in the phase at the grid close to Juneau. The differences in the proposed global models are considered to be mainly due to the complex bathymetry and coastline in SE-AK, which are not well represented with the grid size of these global models.

2. Southeast Alaska (SE-AK)

From the point of view of the geodesy and geophysics, SE-AK is an interest place, because very rapid uplift rates exceeding 30 mm/yr at maximum are observed there, which are mainly caused by glacial isostatic adjustment (GIA), including the effects of past and present-day ice melting. During 'Little Ice Age' (LIA), this area was completely covered with glaciers of up to 1.5 km in thickness. Since the middle of the 19th century (i.e. about 250 years ago), when LIA began to wane, this thick ice coverage has rapidly retreated (e.g. Molina, 2008). Therefore, it is considered that, for the effect of the past ice, the melting of the ice of LIA mainly contributes to the observed uplift rates (Larsen et al., 2005 and Larsen et al., 2007).

A joint Japanese-American observation project called ISEA (International geodetic project SouthEastern Alaska) was initiated in 2005 to follow up the work of the University of Alaska Fairbanks (UAF) by adding new geodetic data sets (Miura et al., 2007). In this project, three kinds of geodetic measurements are carried out to study GIA, loading deformation and tidal variations in and around Glacier Bay in SE-AK: (1) the absolute gravity (AG) and relative gravity surveys, (2) surveys with GPS and the establishment of new continuous GPS sites and (3) gravity tide observations. For the GPS, EarthScope (http://earthscope.org) continuous GPS data are also used in this project.

In the SE-AK region, the tides including the OTL effects are the major signal in the observed gravity and displacement signals over periods less than seasonal. The OTL effect is 15-30 times larger than the nominal precision of the absolute gravity measurements (i.e. 1-2 μGal).

Therefore, precise estimation of the ocean tide effects (i.e. the effects of attraction and loading) is indispensable to increase the accuracy of gravity and GPS observations made to study GIA, when they are carried out over a short period, because it is highly possible that inaccurate OTL correction may easily originate a spurious long-period signal, as pointed out by Penna et al. (2007).

3. Problem in the determination of viscoelasticity of the Earth

Viscoelasticity is important property of the Earth for many geodetic and geophysical phenomena such as the mantle convection, the plate tectonics, the figure of the Earth (J2 and other orders), and the post glacial rebound, etc. Observation of the GIA process gives us the 1st-order information on the viscoelastic property of the Earth. However, we meet a difficulty in the comparison between the observations and the model predictions of the effects of post glacial rebound (PGR) , because there exist a problem due to the tradeoff between the viscoelastic parameters, i.e. tradeoff between the magnitude of the upper mantle viscosity and the thickness of the lithosphere in the estimation of the effects of PGR, and also ambiguity of the past ice models, i.e. their extent and thickness of the glaciers (for example, see a paper by Sato et al., 2007, which discusses the GIA problem in Ny-Alesund, Svalbard). In addition to this, present-day ice melting (PDIM) is accelerating in SE-AK as well as other glacier areas in the world, which is considered partly to be the effect of recent 'Global Warming'. GPS and gravity observations in SE-AK clearly detect not only the effect of mass changes in the past ices but also that of PDIM. Error in the estimation of PDIM effects may introduce an additional ambiguity in the estimation of the PGR effects from the observed data.

The magnitude of Earth's viscoelasticity depends on the frequency that is used in the observations (i.e. frequency dependency). Therefore, it is important to constrain the parameters related to the viscoelasticity with the observations over wide frequency bands. If we take a difference from the static (elastic) gravity tidal factor, then the effect of viscoelasticity is estimated at the orders of 0.3% to 0.4% over the frequencies between the semidiurnal and the fortnightly tides (e.g. Lambeck, 1988). For the loading Green's function, its effect is estimated at the order of 0.1% to 0.2% at the frequency band between the semidiurnal and diurnal tides (Okubo and Tsuji, 2001). As well known, the loading Green's function has a nature that it is sensitive to the elastic and/or viscous structure at the depth almost corresponding to the loading distance (i.e. distance between the observation point and the loading point). Therefore, we may have a chance to discuss the viscoelastic structure especially for that of the upper part of the mantle from the OTL effect, because the spatial scale of the variation in the OTL effect is much smaller than that of the body tide.

4. An attempt to improve the regional ocean tide model in SE-AK

The area of our regional model is 5.6 deg. by 7.1 deg. in latitude and longitude, respectively, i.e. 54.5N to 60.1N and 221.9E to 230.0E (see Fig.1, which is taken from Sato et al., 2008). The computation was carried out with a simple method that integrates the simultaneous equations of the Navier-Stokes equation in a coordinate system rotating with the earth and the equation of continuity (Fujii, 1967). The topography and bathymetry are modeled based on the ETOPO2 bathymetry data with the spatial resolution of 2 minutes by 2 minutes (http://www.ngdc.noaa.gov/mgg/fliers/01mgg04.html). The model was driven by giving the time variations in the tidal height on the boundary lines at the west and south edges of the model. We used here the NAO.99b model (Matsumoto et al., 2000) for the boundary values. We also took into account the tide gauge data at 12 stations available in the study area, five NOAA continuous tide stations and seven of temporary sites installed by UAF. Their locations are shown in Fig. 1.

The computation is sensitive to the assumed magnitude of the bottom friction (BF). We have searched for the best value in our model computation by changing the BF value within the range of 0.0001 to 0.1 in CGS unit. We may expect that the best BF value should give the amplitude close to the observed one. We have tested at two tide gauge sites, one is faced the open sea and located at the entrance of a long strait. Other one is the back of the strait. The best BF values for the M_2 constituent are slightly different at two sites mainly due to the difference in the geographical condition. However, the difference in the best BF is not so large comparing the range of amplitudes obtained by changing the BF coefficients by the three orders tested here. Therefore, we used here the average value obtained from the test computations for these two sites over the whole sea area of the model considered here, i.e. 0.0029 in CGS unit. We also tested the BF values for the K_1 constituent which has the major amplitude in the diurnal tide. Different from the case of the M_2 constituent, the peak of the curve for the K_1 constituent was broad. Since the wave length of K_1 is longer than that of M_2, the K_1 wave is not so sensitive to the assumed BF values than that of M_2.

To examine the effects of the tide gauge data on our modeling in SE-AK, we compared two cases. One does not use the tide gauge data as a boundary condition (Model A) and other uses them (Model B). In general, the amplitudes of Model A are larger than Model B in our computation. The areas show the difference exceeding 100 cm at around Juneau and over the region of Glacier Bay, however, the large amplitude in Model A is suppressed in Model B by introducing the actual tide gauge data into the model computation as expected.

5. Comparison between the observation and prediction

The gravity data were obtained from a Scintrex CG-3M AUTOGRAV gravimeter set at the

Egan library of the University of Alaska, Southeast (UAS) in Juneau. The GPS data obtained at three PBO continuous GPS sites, AB48, AB50 and AB51. PBO is part of a US research facility called EarthScope. To estimate the tidal displacement, we used a PPP method, which was initially introduced by Zumberge et al. (1997). The software used here is 'GpsTools ver. 0.6.3' (Takasu et al., 2005 and Takasu, 2006), which is a GPS/GNSS (Global Navigation Satellite System) analysis software package. The analysis was performed using the BAYTAP-G tidal analysis program (Tamura et al., 1991).

We compared here the predicted tides consisting of the body tide and the OTL effects to the observations. For the body tide, we tested three tidal factors. One is given by Wahr (1981) for the 1066A earth model (Gilbert and Dziewonski, 1975) and other two are given by Dehant, Defraigne and Wahr (1999, here after DDW) for the PREM model (Dziwonski and Anderson, 1981), that is, one for the elastic and hydrostatic (EL-HY) earth and one for the inelastic and non-hydrostatic (IE-NH) earth. Following Farrell's method (1972), we estimated the amplitude and phase of OTL effects by convolving respectively the cosine and sine amplitudes with the loading Green's function over the whole oceans in the world. For the Green's function, we used the PREM earth model (Dziewonski. and Anderson, 1981). In order to represent the topography, a small grid system of 5 by 10 in arc-seconds in latitudinal and longitudinal directions (i.e. about 154 m by 162 m in the respective directions) for the land-sea masking around the observation sites. Fig.2 (This figure taken from Sato et al., 2008) shows the phasor plots of the observations and the predictions.

In Fig. 2, Three kinds of tidal factors are compared. One is by Wahr (1981) for the 1066A earth model (here WAHR), other two for the PREM earth model by Dhant, Defraigne and Wahr (1999), i.e. two of the elastic hydrostatic earth (DDW_EL_HY) and the inelastic and non-hydrostatic earth model (DDW_IE_NH). In each plot, the solid black circles are the observed values with the open sector that shows the observation error estimated by the BAYTAP-G tidal analysis. The Body Tides Amplitude (BTA) shows the amplitude computed using the tidal factors for the DDW_EL-HY model. The phase lag of the body tides was assumed to be zero.

For gravity, Model B is remarkably consistent with the observed M_2 tide and the K_1 constituent is also improved relative to Model A. The actual tide gauge data at Juneau was used in Model B for one of the boundary conditions in the area around EGAN. This may contribute to the improvement. However, for the S_2 and O_1 components, the improvement from including the tide gauge data is relatively small, even though the phase of S_2 is improved. For the displacement, Fig. 2 plots the vector sums of three components NS, EW, and UD. This figure indicates that, except for the K_1 constituent, agreement between the observations and the predictions is generally good in both the amplitude and phase at all the sites compared here.

From Fig. 2, we also see that, the differences between Model A and Model B in the displacements are small compared with the difference in the gravity predictions. For gravity, the attraction part may contribute to the difference in sensitivity. In this connection, for the M_2 tides at the EGAN gravity site, which is located at about 7 km away from the AB50 GPS site, the amplitudes and phases of the attraction part are 3.35 μGal and 185.01 deg. and 2.72 μGal and 185.44 deg. for Model A and Model B, respectively. As shown in Fig.2, for the M2 constituent, the difference between Model A and B is relatively large at AB51 compared with other sites. Large ocean tide amplitude exceeding 3 m may contribute to this.

It is known that, in GPS time series, the vertical coordinates are much noisier than the horizontal ones, mainly caused by the satellite constellation and by error in the wet zenith delay estimation. The similar situation is shown in Table 1 (This table is taken from Sato et al., 2008), and the UD component shows larger observation errors and generally larger amplitude differences than the horizontal components. On the other hand, Table 1 indicates that, for the semi-diurnal tides, the amplitude difference of the vector sum is smaller than the UD component, and sometimes smaller than the NS and EW components. This means that the magnitude of the tidal displacement vector is determined more accurately than its orientation; the most likely cause for such an error is a small rotation of the tidal displacement vector due to correlations between the coordinate components. However, this clear tendency is not observed in the diurnal tides, suggesting that the observed diurnal tides of the horizontal components might be also affected by the tropospheric error much more than the semi-diurnal tides.

From our comparison results, we may say; (1) Compared with the case only using the global ocean tide models, by taking into account the regional ocean tide effect, the amplitude differences between the observation and the predicted tide in SE-AK is remarkably reduced for both the gravity and displacement (e.g. for the M_2 constituent, 8.5 μGal to 0.3 μGal, and 2.4 cm to 0.1 cm at the AB50 GPS site in Juneau in terms of the vector sum of three components of the north-south, east-west and up-down) , even though the ocean tide loading is large in SE-AK. (2) We have confirmed the PPP (Precise Point Positioning) method, which was used to extract the tidal signals from the original GPS time series, works well to recover the tidal signals. Although the GPS analysis results still contain noise due to the atmosphere and multipath, we may conclude that the GPS observation surely detects the tidal signals with the sub cm accuracy or better than it for some of the tidal constituents. (3) In order to increase the accuracy of the tidal prediction in SE-AK, it is indispensable to improve the regional ocean tide model such as those developed in this study, especially for the phase.

6.   Effect of the viscoelasticity

The gravity effect of the loading tide at the EGAN site has a magnitude as large as 6 μGal

for the M_2 tide due to the large ocean tide amplitude, and it is about twice as large as the effect of attraction. We estimated effect of inelasticity on our gravity observation based on a complex Green's function for the inelastic earth given by Okubo and Tsujii (2001), and we obtained a value of 0.05 μGal as the inelastic loading effect on the M_2 constituent at EGAN. On the other hand, the effect of inelasticity on the body tide is estimated at the order of 0.03 μGal from the difference between DDW_EL-HY and DDW_IE-NH (i.e. 23.976 μGal and 24.008 μGal for the former and the latter). The total inelastic effect is to be estimated at the order of 0.08 μGal. Unfortunately, its effect is similar in magnitude to the tidal analysis error of our gravity data or slightly larger than it. Therefore, it is difficult to constrain the inelastic effect precisely by the present analysis results, but it should be possible to measure its effect by using an updated well calibrated stable gravimeter better than that used here, because of large amplitude of OTL effects in SE-AK.

Related to a possible source affecting the observed gravity tide, based on the tidal gravity profile obtained in Alaska (north of our study area), Zürn et al. (1976) discussed an effect of geological structure associated with the downgoing lithospheric slab beneath Alaska, and they concluded that this effect on tidal gravity perturbations will be detected when the observation and the estimation of the ocean tide effect achieve an accuracy of 0.1 % and of 1 %, respectively. For the ocean tide effect on M_2 constituent, Fig.2 indicates that, for the estimation by Model B, the difference between the observation and the prediction is about 0.3 μGal and it is at the order of about 1.3 % of the amplitude of predicted body tide (i.e. the ratio of 0.3 μGal to 23.98 μGal). Most of the difference is considered to be due to the error in the estimation of the ocean tide effect. Therefore, improvement of the accuracy of the regional ocean tide model in SE-AK is essential for the further discussion of the tidal gravity response observed in SE-AK.

To improve the accuracy of the regional ocean tide model, we have started the following two items; (1) The ocean bottom pressure (OBP) gauge observation has been initiated off Juneau in June 2007. We expect this observation may reveal a possible systematic modification in the existing tide gauge data obtained at the back of the narrow channel. (2) New modeling using more accurate bathymetry data than that by Sato et al. (2008) and considering the spatial variation in the bottom friction, because of very large spatial variation in the speed of tidal currents in the sea area in SE-AK.

7. Additional note

Last, the poster presented by Ito at this symposium is interest related to the title of this symposium 'New Challenges in Earth's Dynamics'. By using a kinematic precise point positioning (KPPP) method, he analyzed the GPS data obtained from 1200 sites of a Japanese

GPS network called GEONET (GPS Earth Observation Network system) operated by GSI (Geographical Survey Institute), and he examined the residuals after subtracting the model tides computed by a GOTIC2 program developed by Matsumoto et al. (2001). In this program, 1066A Earth model and NAO.99b ocean tide model are used to compute the body and ocean loading tides. The obtained M_2 residuals for the vertical tidal displacement indicate that their averaged phase difference is 0.11 degrees across the Japanese islands and most of the sites show a phase delay with respect to the predicted tide. More over, the averaged amplitude ratio of the observation to the prediction is 1.007. From these, he concludes that it may show an Earth's compliant against the response of the Earth obtained from the model computation. Related to this, it may be noted that the 1066A earth model used in GOTIC2 has a soft upper layer compared with other earth models such as PREM model.

Although we should carefully test other models for both the body tide and the OTL effects and check the accuracy of the global ocean tide models, there is a possibility that, from this kind of study, we may reveal the departure of the tidal response of the Earth from that expected from the layered Earth, which is shown for instance by the theoretical estimation by Wang (1991).

Related to this topic, seismic tomography models have revealed the precise 3D image of the Earth's interior. Based on the constructed tomography models, a new image of the mantle dynamics such as mantle plume rising up from the core-mantle boundary is proposed. Basically tomography models are constructed from the body and surface wave data such as travel times and waveforms. However, these data have a defect in the sensitivity to density variations, because the density is a common parameter for both of the P- and S-wave velocities. More over, it is known that the density variations estimated by scaling seismic wave speed models may not be accurate.

To figure out more reliable 3D structure of the Earth's mantle including that of the density, two different kinds of approaches are noticed. One is the utilization of lowest frequency data of the free oscillations of the Earth so called 'gravest seismic normal modes', which depend on lateral variations in density as well as elasticity, because the gravitational restoring force plays an important role to the amplitude and the frequency splitting of these normal modes (e.g. Ritzwoller Lavely, 1995, Widmer-Schnidrig, 2003, Rosat et al., 2005, 2007). Other is the utilization of the forced oscillations of the Earth such as in the solid Earth tides, because the inside the Earth is deformed by the tidal force as well as its surface, therefore, study of the tidal response of the Earth may be an useful way to reveal in detail about the structure of Earth's inner including the 3D distribution of the density. Such study has been tried by a group of seismologists of America and Canada (Ishii et al., 2008).

An important issue in the tidal tomography is how we can accurately evaluate a possible systematic error in the estimation of the OTL effects and that due to the effect of spatial distribution of the observation sites which are biased toward the continental land areas on the globe. Anyway, improving the ocean tide models of both the global and regional scales is essential to obtain the reliable image of the 3D structure of inside of the Earth from the tidal observations. But, at least, it can be said that the tidal study is coming to a new stage and its importance increases in the study for the Earth's 3D model constructions and related geosciences based on these models.

References

Bos, M. S., Baker, T. F., Røthing, K., Plag, H.-P., 2002., Testing ocean tide models in the Nordic seas with tidal gravity observations, Geophys. J. Int., 150 (3), 687–694 doi: 10.1046/j.1365-246X.2002.01729.x.

Dehant, V., Defraigne, P. and Wahr; J. M., 1999. Tides for a convective Earth, J. Geophys. Res., 104, No. B1, 1035-1058.

Dziwonski, A. D. and D. L. Anderson, 1981. Preliminary Reference Earth Model, Phys. Earth Planet. Inter., 25, 297-356. Eanes, R. J., and S. V. Bettadpur, 1994. Ocean tides from two year of TOPEX/POSEIDON altimetry, EOS Trans. AGU, 75(44), Fall Meet. Suppl., 61.

Eanes, R. J. and S. V. Bettadpur; 1994. Ocean tides from two year of TOPEX/POSEIDON altimetry (abstract), EOS Trans., AGU, 75 (44), Fall Meet., Suppl., 61.

Egbert, G. D., A. F. Bennette, and M. G. G. Foreman, 1994. TOPEX/POSEIDON tides estimated using a global inverse model, J. Geophys. Res., 99, 24,821 .24,852.

Farrell, W. E., 1972. Deformation of the Earth by surface loads, Rev. Geophys. Space Phys., 10, 761-797.

Fujii, Y., 1967. Nmerical Investigations of Tidal Currents in the Kurushima Straits, Bulle. Kobe Marine Obs. 179, 1-116.

Gilbert, F. and Dziewonski, A. M., 1975. An application of normal mode theory to the retrievals of structural parameters and source mechanisms from seismic spectra, Phil. Trans. R. Soc., 278A, 319-328.

Ishii, M., K., Latychev, J.X., Mitrovica, and J.L., Davis, 2008. Body Tides on a Three-Dimensional Elastic Earth: Toward a Joint Tidal and Seismological Tomography, Eos Trans. AGU, 89(53), Fall Meet. Suppl., abstract No. DI11A-08.

Ito, T., 2008. The high resolution mapping of earth tide responses from GPS network in Japan, Abstract Volume of the ETS 2008 Symposium 'New Challenges in Earth's Dynamics', Jena, Germany, ed. G. Jentzsch, p96.

Lambeck, K., 1988. Geophysical geodesy: the slow deformations of the earth, New York : Oxford University Press.

Larsen, C. F., 2003. Rapid uplift of southern Alaska caused by recent ice loss, PhD Thesis presented to the Faculty of the University of Alaska Fairbanks.

Larsen, C. F., R. J. Motyka, J. T. Freymuller, K. A. Echelmeyer, E. R. Ivins, 2005. Rapidviscoelastic uplift southern Alaska caused by post-Little Ice Age glacial retreat, Earth Planet. Sci. Lett., 237, 548-560.

Larsen, C. F., R. J. Motyka, A. A. Arendt, K. A. Echelmeyer, and P. E. Geissler, 2007. Glacier changes in southeast Alaska and northwest British Columbia and contribution to sea level

rise, 2007, J. Geophys. Res., VOL. 112, F01007, doi:10.1029/2006JF000586.

Matsumoto, K., T. Sato, T. Takanezawa, and M. Ooe, 2001. A Program for Computation of Oceanic Loading Effects, J. Geodetic Soc. Japan, Vol.47, No.1, 243-254.

Matsumoto, K., Takanezawa, T. and Ooe, M., 2000. Ocean tide models developed by assimilating TOPEX/Poseidon altimeter data into hydro-dynamical model: A global model and a regional model around Japan, J. Oceanogr., 56, 567-581.

Matsumoto, K., Sato, T., Fujimoto, H., Tamura, Y., Nishino, M., Hino, R., Higashi, T. and Kanazawa, T., 2006. Ocean bottom pressure observation off Sanriku and comparison with ocean tide models, altimetry, and barotropic signals from ocean models, Geophys. Res. Lett., 33, L16602, doi: 10.1029/2006GL026706.

Miura, S., Sato, T., Freymuller, J. T., Kaufman, M., Cross, R., Sun, W., and Fujimoto, H., 2007. Geodetic measurements for monitoring rapid crustal uplift in southeast Alaska caused by post-glacial rebound –Outline of the project–. Proc. 7th International Conference on Global Change: Connection to Arctic (GCCA-7), ed. by H. L. Tanaka, International Arctic Research Center, Univ. Alaska Fairbanks, 95–97.

Molnia, B.F., 2008. Glaciers of North America -- Glaciers of Alaska, *in* Williams, R.S., Jr., and Ferrigno, J.G., eds., Satellite image atlas of glaciers of the world: U.S. Geological Survey Professional Paper 1386-K, 525 p.

Neumeyer, J., del Pino, J., Dierks O., Sun, H.P., and Hartmut, P., 2005. Improvement of ocean loading correction on gravity data with additional tide gauge measurements, J. Geody., Vol. 40, No.1, 104-111.

Okubo, S. and Tsuji, D., 2001. Complex Green's Function for Diurnal/Semidiurnal Loading Problem, J. Geod. Soc. of Japan, Vol.47, No.1, 225-230.

Penna, N. T., M. A. King, and M. P. Stewart, 2007. GPS height time series: Short-period origins of spurious long-period signals, J. Geophys. Res., 112, B02402 (doi:10.1029/2005JB004047).

Ray, R. D., 1999. A global ocean tide model from TOPEX/POSEIDON altimetry: GOT99.2b, Tech. Memo. 209478, NASA Goddard Space Flight Cent., Greenbelt, Md.

Ritzwoller, M., and E. M. Lavely, 1995. Three-dimensional seismic models of the Earth's mantle, Rev. Geophys., 33, 1 – 66.

Rosat, S., T. Sato, Y. Imanishi, J. Hinderer, Y. Tamura, H. McQueen, and M. Ohashi, 2005. High resolution analysis of the gravest seismic normal modes after the 2004 Mw=9 Sumatra Earthquake using superconducting gravimeter data, *Geophys. Res. Lett.*, **32**, L13304, doi:10.1029/2005GL023128, 2005.

Rosat, S., S. Watada, and T. Sato, 2007. Geographical variations of the $_0S_0$ normal mode amplitude: predictions and observations after the Sumatra-Andaman Earthquake, Earth

Planets Space, **59**, 307–311.

Sato, T., Tamura, Y., Matsumoto, K., Imanishi, Y. and McQueen, H., 2004. Parameters of the fluid core resonance inferred from superconducting gravimeter data, J. Geodyn., 38, 375-389.

Sato, Tadahiro, Jun'ichi Okuno, Jacques Hinderer, Daniel S. MacMillan, Hans-Peter Plag, Olivier Francis, Reinhard Falk, and Yoichi Fukuda, 2006. A geophysical

interpretation of the secular displacement and gravity rates observed at Ny-Ålesund, Svalbard in the Arctic - Effects of post-glacial rebound and present-day ice melting -, G. J. Int., 165., 729-743, doi: 10.IIII/j.1365-246x.2006.02992.x.

T. Sato, S. Miura, Y. Ohta, H. Fujimoto, W. Sun, C.F. Larsen, M. Heavner, A.M. Kaufman, J.T. Freymueller, 2008. Earth tides observed by gravity and GPS in southeastern Alaska, J. Geodyn., 46, 78–89.

Schenewerk, M. S., J. Marshall and W. Dillingar (2001), Vertical Ocean-loading Deformations Derived from a Global GPS Network, J. Geod. Soc. Japan, Vol.47, No.1, 237-242.

Schwiderski, E. W. (1980), On charting global ocean tides, Rev. Geophys. Space Phys., 18, 243-268.

Takasu, T., and Kasai, S., 2005. Development of precise orbit/clock determination software for GPS/GNSS, Proce. the 49th Space Sciences and Technology Conference, Hiroshima, Japan (in Japanese), 1223-1227.

Takasu, T., 2006. High-rate Precise Point Positioning: Detection of crustal deformation by using 1-Hz GPS data, GPS/GNSS symposium 2006, Tokyo, 52-59.

Tamura Y., Sato, T., Ooe, M. and Ishiguro, M., 1991. A procedure for tidal analysis with a Bayesian information criterion, Geophys. J. Int., 104, 507-516.

Thomas, I. D., King, M. A., Clarke, P. J., 2007. A comparison of GPS, VLBI and model estimates of ocean tide loading displacements, J. Geodesy, 81(5), 359-268.

Wahr, J. M., 1981. Body tides of an elliptical, rotating, elastic and oceanless Earth, Geophys. R. Astron. Soc., 64, 677-703.

Wang, R., 1991. Tidal deformations of a rotating, spherically symmetric, visco-elastic and laterally heterogeneous Earth, Ph.D. Thesis, Univ. of Kiel, Kiel, Germany.

Widmer-Schnidrig, R., 2003. What can superconducting gravimeters contribute to normal mode seismology?, *Bull. Seism. Soc. Am.*, **93**(3), 1370–1380.

Zumberge, J. F., Heflin, M. B., Jefferson, D. C., Watkins, M. M., and Webb, F. H., 1997. Precise point positioning for the efficient and robust analysis of GPS data from large networks, J. Geophys. Res., 102 (B3), 5005-5017.

Zürn, W., Beaumont, C. and Slichter, L. B., 1976. Gravity tides and ocean loading in southern Alaska, J. Geophys. Res., Vol. 81, No. 26, 4923-4932.

Table 1. Amplitude differences between the observed tidal displacements from GPS and the predictions for the four constituents of O_1, K_1, M_2, and S_2. In this table, the predicted tides were computed with a combination of the Green's function for the elastic PREM given by Dehant, Defraigne and Wahr (1999), NAO.99b global tide model and the Model B regional tide model (see subsection 4). Results for three GPS sites of AB48, AB50 and AB51 are shown. Unit of the amplitude difference: cm. VSM: Vector sum of the NS, EW and UD components.

| Site	Wave	Amplitude difference				Observation error			
		NS	EW	UD	VSM	NS	EW	UD	VSM
AB48									
	O_1	0.38	0.12	0.49	0.50	0.03	0.03	0.04	0.06
	K_1	0.50	0.89	1.43	1.57	0.03	0.03	0.05	0.06
	M_2	0.02	0.08	0.59	0.08	0.03	0.03	0.06	0.07
	S_2	0.38	0.24	0.82	0.43	0.03	0.03	0.05	0.07
AB50									
	O_1	0.10	0.14	0.24	0.27	0.02	0.10	0.03	0.11
	K_1	0.25	1.01	0.78	0.89	0.02	0.10	0.03	0.10
	M_2	0.11	0.10	0.23	0.08	0.02	0.03	0.04	0.05
	S_2	0.77	0.40	0.58	0.38	0.02	0.03	0.04	0.05
AB51									
	O_1	0.02	0.10	0.31	0.32	0.01	0.01	0.03	0.03
	K_1	0.23	0.34	0.25	0.29	0.02	0.02	0.03	0.04
	M_2	0.08	0.10	0.37	0.31	0.02	0.02	0.03	0.04
	S_2	0.27	0.25	0.54	0.33	0.02	0.02	0.03	0.04
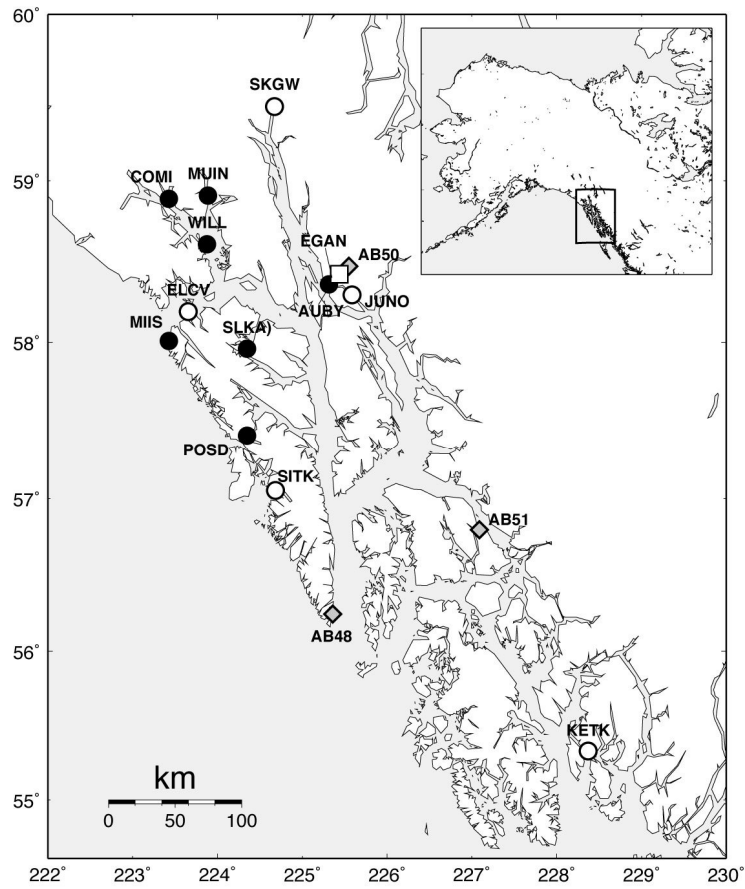
Fig. 1. Locations of the observation sites used in this study. An open square, a diamond, open circles, and closed circles indicate the tidal gravity, continuous GPS, continuous tide gauges, and temporal tide gauges installed by UAF (Larsen, 2003), respectively.
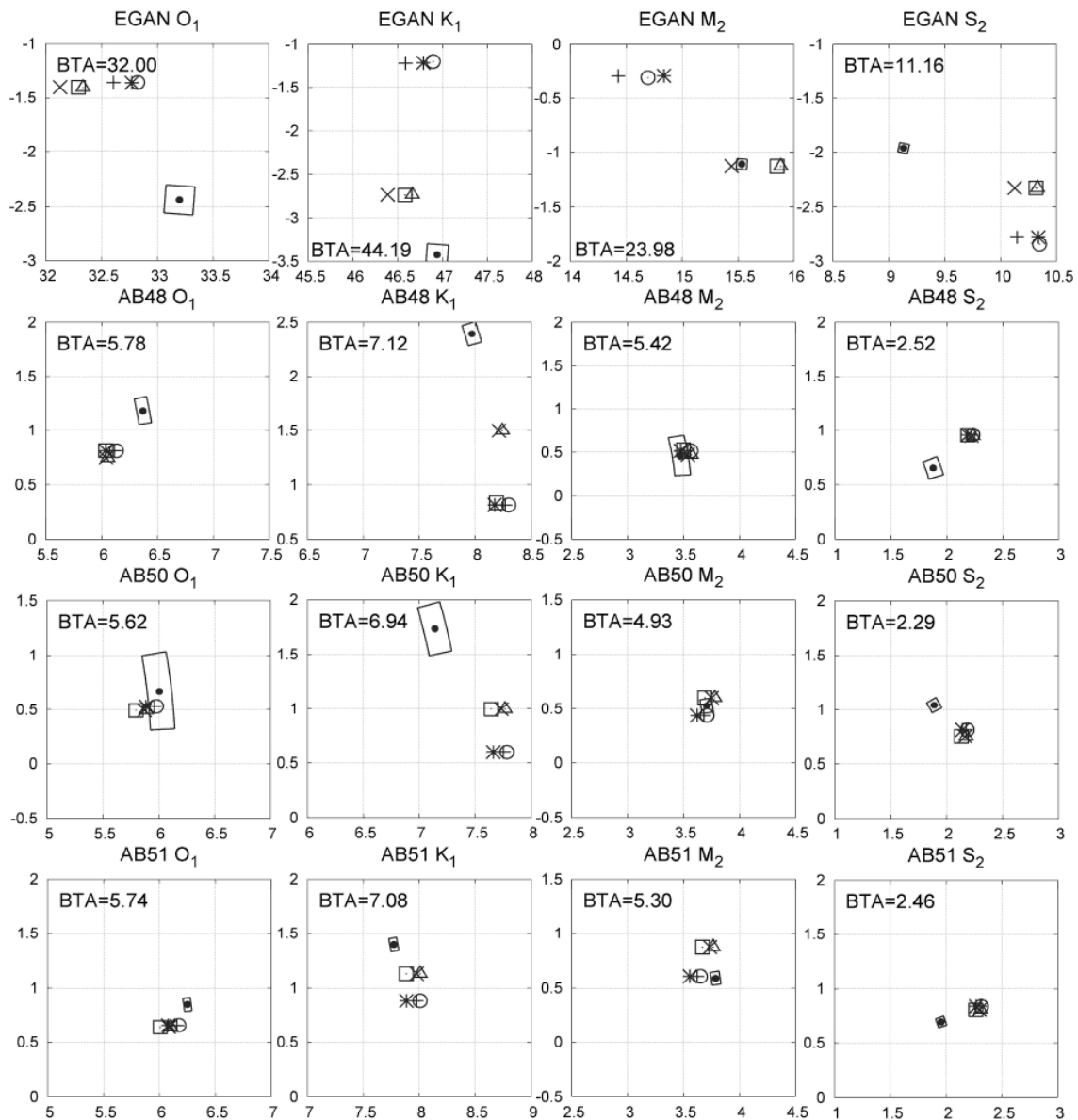
Fig. 2. Phasor plots for the observed and predicted tides at four sites of EGAN (gravity) and AB48, AB50, and AB51 (displacement). Units of both the horizontal and vertical axes are in μGal and cm for the gravity and displacement, respectively. For the displacement, the vector sums of three components of NS, EW and UD are plotted. The six combinations of the predicted body tide and the regional ocean tide model (Model A or B) are plotted with the following symbols; (1) Cross denoted with '+': Predictions from WAHR and Model A, (2) Stars: DDW_EL_HY and Model A; (3) Open circle: DDW_IE_NH and Model A, (4) Cross denoted with ' x': WAHR and Model B, (5) Open square: DDW_EL_HY and Model B, and (6) Open triangle: DDW_IE_NH and Model B. See Section 5 of the text for the abbreviations of the body tides.

Centenary Researches on Earth Tides in Kyoto University (1909 - 2008)

Shuzo Takemoto

Kyoto University, Yosida-honmachi, Sakyo-ku, Kyoto 606-8501, Japan

(takemoto@kugi.kyoto-u.ac.jp)

Abstract: This paper is a short historical review of centenary researches on Earth tides carried out in Kyoto University during the period of 1909 - 2008. Geophysical researches in Kyoto University started in 1909 when Toshi Shida arrived at Kyoto. He installed the tiltmeters of the E von Rebeur-Paschwitz type and the Pendulum seismographs of the Wiechert type at the Kamigamo Geophysical Observatory. Based on the data obtained from these instruments, he accomplished many pioneering achievements in geophysics. Among them, he first carried out tidal tilt observation in Japan and proposed the third parameter in spherical elasticity known as "Shida Number". First observation of tidal strains was carried out by Kenzo Sassa by employing extensometers of the Sassa type. Recent researches in the field of Earth tides with originalities in Kyoto University are tidal gravity measurements with superconducting gravimeters in Japan and Indonesia and development of laser interferometric devices for precise measurements of tidal strains. Combined use of laser strainmeters and superconducting gravimeter in Kamioka will be an effective tool to investigate physical properties of Earth's interior.

KEYWORDS: Tiltmeter, Extensometer, Laser strainmeter, Superconducting gravimeter, Shida Number

1. Introduction

Geophysical researches in Kyoto University started in 1909 when Toshi Shida (1876-1936) got his post as an associate professor in the Kyoto Imperial University (predecessor of Kyoto University). He graduated from the Institute of Physics of the Imperial University of Tokyo in 1901 and arrived at Kyoto Imperial University in September, 1909. After arriving at Kyoto, Shida immediately installed the tiltmeters of the E von Rebeur-Paschwitz type and the Pendulum seismographs of the Wiechert type at the Kamigamo Geophysical Observatory located about 4 km away from Kyoto University in direction of the north-northwest. Based on the data obtained from these instruments, Shida accomplished many pioneering achievements in geophysics;

(i) Precise observation of tidal tilts and proposal of the third parameter in spherical elasticity (Shida Number),
(ii) Discovery of quadrantal push-pull distribution of the first motion of seismic P waves,
(iii) Verification of deep earthquakes,
(iv) Proposal of a plan to detect free oscillation of the Earth.

Among these, topics (i) and (iv) are shown in the following chapters. In this chapter, we mention (ii) and (iii) briefly. With regard to (ii), Shida first pointed out the quadrantal push-pull distribution of the first motion of seismic P waves. Based on seismograms obtained at the Kamigamo observatory and other seismic observation network belonging to the Central Meteorological Observatory of Japan, Shida found out the quadrantal pattern of P-wave first impulses. This result was first reported at the meeting of the Tokyo Mathematico-Physical Society in April, 1917. Just after the meeting, a destructive shallow earthquake of M=6.3 occurred in Shizuoka Prefecture on May 18, 1917. Shida collected seismograms of this earthquake and confirmed that the distribution of P-wave first motions shows simple pattern of push-pull distribution divided by two orthogonal nodal lines (Shida 1929). Nowadays, it is well known that the first impulses of the seismic P-waves show a quadrantal pattern with compressional or dilatational distribution. This is a simple way to know the earthquake source mechanism.

In the research of deep earthquakes (iii), Kiyoo Wadati of Meteorological Agency of Japan is famous by his successive papers (Wadati, 1928 1929, .1931, 1935). He showed the convincing evidence of earthquakes occurring deeper than 300 km in and around Japan by employing the seismic data obtained from

the dense seismic observation network of the Central Meteorological Observatory of Japan. He distinguished the existence of a deep earthquake zone crossing the central Honshu, which was later called the Wadati-Benioff zone (a seismic zone with an inclined surface from the trench toward the continental margin).

Prior to Wadati's work, Shida pointed out the existence of deep earthquakes in the lecture given at the opening ceremony of the Beppu Geophysical Laboratory, Kyoto Imperial University on 28 October, 1926. In this lecture, he indicated the deep earthquake zone traversing central Honshu. Before the lecture, Shida examined in detail the arrival times of the seismic P waves observed at various stations in Japan and found some abnormal earthquakes at which the time-difference of arrival-times among various stations in Japan were very small compared with those of ordinary earthquakes. Moreover, the arrival-times of these earthquakes observed at far-field stations in foreign countries were ten seconds or more earlier compared with those of ordinary earthquakes. Meanwhile, a strong earthquake shook the central Honshu on 27 July, 1926. Based on data of the P wave initial motions obtained from different stations in Japan, Shida fixed the hypocenter of this earthquake near Lake Biwa, northeast in Kyoto. The depth of the epicenter was determined to be about 260 km. Shida came to the conclusion that deep earthquakes must have taken place in the Earth. The reprint of this lecture concerning the deep earthquakes was published ten years later (Shida, 1937). Shida hesitated to publish the result as the scientific papers, and only his lecture note is remaining. The following comments have been left in his lecture note about this. "The Earth must be statically stable in a zone deeper than 120km according to the isostatic theory, and it may be difficult to consider that the brittle fractures such as those occurring near the surface would occur in the deep zone near the depth of 300km. Therefore, it is necessary to renew the knowledge of the source mechanism of deep earthquakes and the detailed structure inside the Earth. Time has passed while I was keeping collecting various materials and preparing a high-pressure experiment device to know physical properties in the upper mantle."   Deep earthquakes with origins deeper than 60 km are approximately one-quarter of all earthquakes. Existence of deep earthquakes became one of the important grounds to find out the subduction zone in plate tectonics.

In 1929, Toshi Shida was awarded the 19th Imperial Prize from the Japan Academy on the title of "Investigations on the Rigidity of the Earth and on Earthquake Motions". In addition to his excellent achievements in research and education, Shida established the Beppu Geophysical Observatory in 1926, the Aso Volcanological Observatory in 1928, and the Abuyama Seismological Observatory in 1930. Since then, useful geodetic and seismological data have been obtained in these observatories until now.

In this paper, early research achievements on Earth tides performed by Toshi Shida and his successors (Kenzo Sassa and Eiichi Nishimura) are introduced first. Then some recent research activities in Kyoto University in the field of Earth tides, especially, tidal gravity measurements using superconducting gravimeters and development of laser interferometric devices for precise measurements of tidal strains are explained in the following chapters.

Figure 1.   Pioneering leaders in the research field of Earth tides in Kyoto University. From left to right: Toshi Shida (1876-1936), Kenzo Sassa (1900-1981) and Eiichi Nishimura (1907-1964).

2. First observation of Earth tides in Japan and proposal of "Shida Number"

Figures 2 and 3 show the general view of the observation room of the Kamigamo Geophysical Observatory and the arrangement of instruments in the observation room, respectively (Shida, 1912). The observation room stands on a small hill of Paleozoic rock in the northern part of Kyoto city. The natural rock of Paleozoic foundation was excavated to the depth of 3.5m over an area of 6m x 10m, and the floor was covered with concrete about 30cm thick except for the granite stone pillars on which instruments were installed.

As shown in the right side of Figure 3, the observation room was divided into two parts by two stone walls across stairs. In the eastern room (right upper part of Figure 3), the vertical seismograph of the Wiechert's inverted pendulum type with 1300kg-weight was installed at the NE corner, and his horizontal seismograph with 1000kg-weight was installed at the SE corner. The western room (right lower part of Figure 3) was used for the tiltmeter observation.

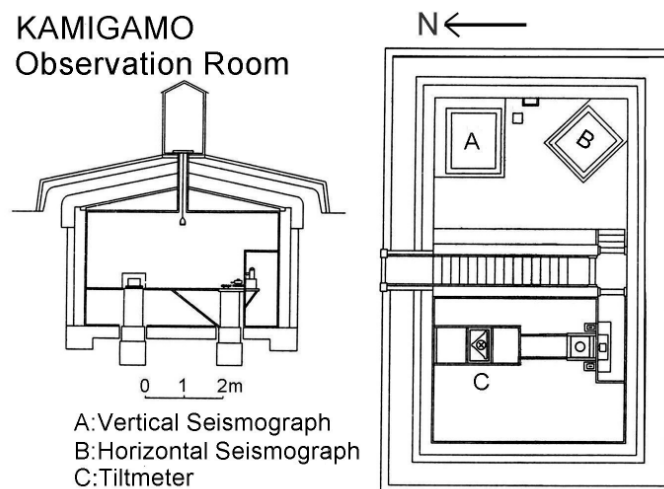**Figure 2.** General view of the Kamigamo Observatory in 1910 (After Shida,1912).

Figure 3. Construction of the observation room and arrangement of instruments (After Shida,1912)
(Left: side view (from west side), Right: plan view)

Using the tiltmeters of E von Rebeur-Paschwitz type in Kamigamo, Shida carried out first observation of tidal tilts in Japan. Based on tiltmetric data obtained from January 1910 to April 1911, he estimated the diminishing factor (D). At the first time, he was disappointed because D value obtained at the Kamigamo Geophysical Observatory was greatly different from those obtained at stations in Europe. This is due to the

difference of loading effects of ocean tides. Japan is surrounded by ocean and seas, and the loading effect in Japan is extremely large compared with those in European continent. He considered this weak point positive and succeeded to estimate the rigidity of Earth's crust from tidal loading effect at Kamigamo. After eliminating the tidal loading effect, he obtained the value of D =0.79, which is similar to those obtained in Europe, though it was still larger than the expected value.

The name of Shida is famous as the Shida Number in tidal studies. As well known, the tidal response on the Earth's surface can be represented by three dimensionless parameters in spherical elasticity. They are Love numbers h and k, and Shida Number l. Love (1909) showed that the disturbing potential can be represented with sufficient approximation by a spherical harmonic function of the second order, and all the deformations produced in the Earth by this potential may be represented by the same harmonic function multiplied by a numerical coefficient suitable for each aspect of the phenomenon. As the numerical coefficients, Love introduced two parameters (h and k). Shida (1912) pointed out that a third number parameter (l) should be necessary to obtain a complete representation of the phenomenon.

The tiltmetric observation started by Shida was succeeded by Eiichi Nishimura. He installed the fused silica tiltmeters of horizontal pendulum type at several stations in Japan and investigated local effects on tidal tilt observations over many years. In 1941, Nishimura carried out tiltmetric observation at Barim (N48° 18', E122°10', h=790m) in the China continent in order to obtain an accurate D value (Nishimura, 1950). The station is distant more than 1000km from the nearest sea. The observation room was in an old copper mine surrounded by hornfels. Using data obtained from tiltmeters installed at the 70m from entrance of the tunnel (44m in depth from the surface), Nishimura estimated the following D value;

$$D =0.661 +/- 0.024$$

This value was almost corresponding to a theoretically expected value. It took about 30 years to obtaining this reasonable value after Shida had started the tidal tilt observation at Kamigamo in 1910.
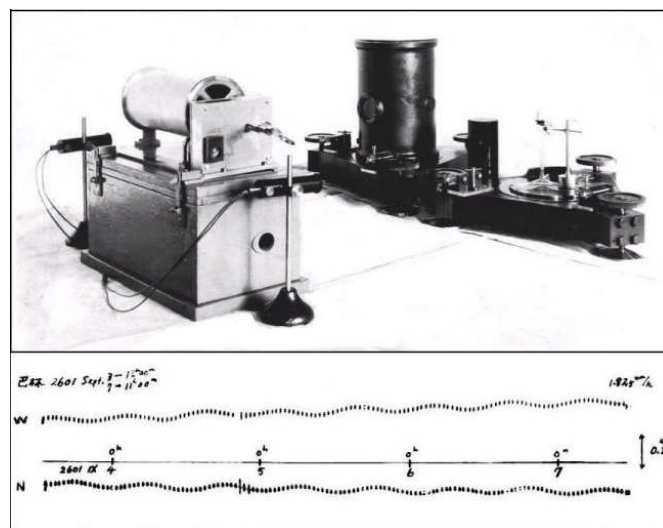

Figure 4. Fused silica tiltmeters of horizontal pendulum type used at the Barim station (upper) and example of tiltmetric records (lower).

3. Early proposal of observing free oscillations of the Earth

Existence of free oscillations of the "elastic" Earth had been theoretically predicted since the latter half of 19th century. However, observational verification of this had to wait until 1960 when the great Chilean earthquake of Mw=9.5 occurred off the east coast of Chili.

In order to observe the free oscillations of the Earth, it is inevitable to develop the instruments having high sensitivity in the range of periods from several minutes to 1 hour. Ordinary seismographs are not sensitive to such long periods. Before the Chilean earthquake of May 22, 1960, following effective

instruments had been developed: (i) Benioff extensometers (Benioff, 1935, 1959), (ii) Press-Ewing long-period seismometers (Press, *et al.*, 1958) and (iii) LaCoste and Romberg gravimeters (Clarkson and LaCoste, 1957). Using these instruments, convincing evidence of Earth's free oscillations was established in 1960s.

Prior to this, Toshi Shida considered to observe free oscillations of the Earth and designed a new observation system in 1920s (Shida, 1925). The system was a modified Galitzin's seismometer consisting of an extremely over-damped 5-minutes horizontal pendulum and a double coil galvanometer of low resistance, the needle of which was a Boys quartz fiber torsion balance with a 20-minutes period. Unfortunately, Shida and his group could not complete this observation system due to mainly financial difficulties.

After the World War II, Maurice Ewing and Frank Press of Columbia University in U.S.A. developed the long-period seismograph in the latter half of the 1940's and succeeded to observed free oscillations of the Earth (Benioff *et al.*, 1961). Their device so called the Press-Ewing seismograph was based on the almost same principle as that proposed by Shida in the first half of 1920s. The Press-Ewing seismograph consisted of a 30-second pendulum and a 90-second galvanometer.

During the Chilean earthquake on May 22, 1960, Ichiro Nakagawa observed free oscillations of the Earth at Kyoto by employing two Askania Gs-11 gravimeters of #105 and #111 (Nakagawa, 1962b). He improved the Pertzev's tidal filter (Nakagawa, 1961, 1962a).

4. First observation of tidal strains of the Earth

Shida also considered a linear extensometer to observe tidal strains and free oscillations of the Earth as shown in Figure 5 (Takemoto, 2007). This idea was latter improved by Kenzo Sassa and Izuo Ozawa, and was efficiently employed to observe the tidal strains of the Earth.
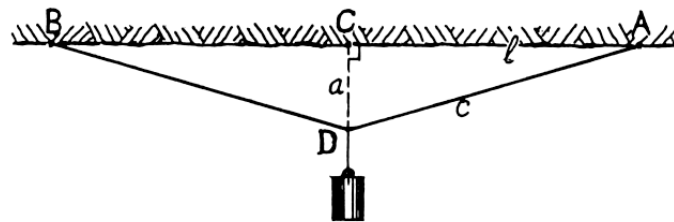

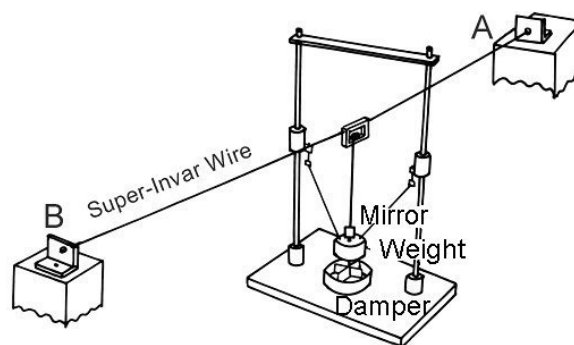**Figure 5.** Schematic representation of a wire extensometer designed by T. Shida.

Figure 6. Schematic representation of a wire extensometer of the Sassa type.

Kenzo Sassa developed an extensometer using a flexible wire as a length standard to measure the relative displacement between two piers fixed into the bedrock (Figure 6). In this device, a super-invar wire 1.6mm in diameter is fixed at both ends to concrete piers standing opposite each other at a distance of 20m. A weight of 350g is suspended from its center with an elinvar wire. Changes in the distance between the two piers cause an up-and-down movement of the weight. This motion is transformed into rotation of the weight through a bifilar suspension consisting of two super-invar wires 0.03mm in diameter. Photographic recording

is done with an optical lever using a small mirror mounted on the weight. Using this mechanical-optical extensometer, Sassa first succeeded to observe the tidal strain changes of the Earth in Ikuno and Makimine stations in 1943. Accordingly, the experimental investigation of the strain-tensor components of Earth tides started. Sassa and Ozawa installed the same type extensometer in Osakayama Observatory in 1947 and continued long-term tidal strain measurements. They first reported these result of tidal strain measurements at the IAG General Assembly held in Brussels in1951 (Sassa *et al.*(1952) and Ozawa (1952)).

Izuo Ozawa devised many kinds of mechanical extensometers with photographic recording systems. Figure 7 shows a high-sensitive super-invar bar extensometer with magnifier of Zollner suspension type (Ozawa, 1961). He continued precise tidal strain measurements in Osakayama, Kishu and Suhara in Japan over many years. In 1971, a super-invar bar extensometer of Ozawa type was installed in the Walferdange laboratory in Luxembourg (Ozawa *et al.*, 1973). This instrument was used to estimate the *l/h* ratio (Melchior and Ducarme, 1976).
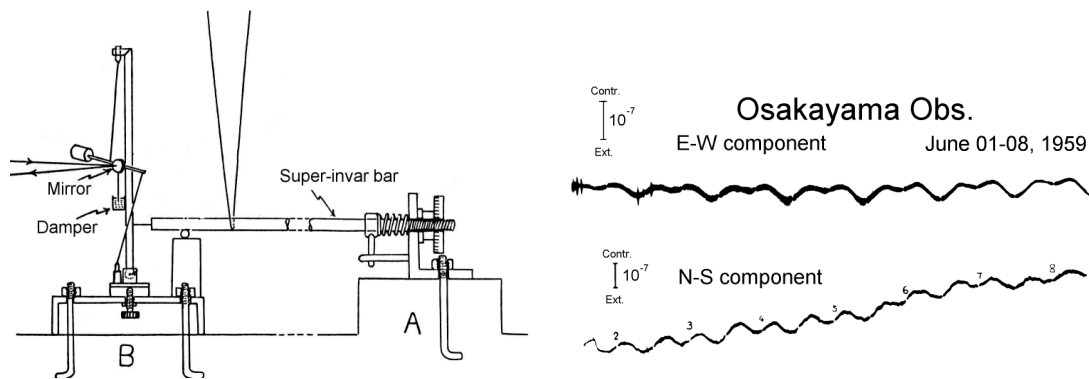

Figure 7. Schematic representation of a super-invar bar extensometer with magnifier of Zollner suspension type designed by I. Ozawa (left) and example of tidal strain records (right).

A continuous monitoring of crustal movements by tiltmeters and strainmeters has been considered to be an effective measure of earthquake precursors particularly on short time scales of hours to days. An early contribution in such an approach was due to Sassa and Nishimura (1951). They first reported anomalous changes of ground-strains and tilts observed before occurrences of some destructive earthquakes at observatories located near the source regions. Among them, a typical example was a precursory tilting motion associated with the 1943 Tottori earthquake of M=7.2. During 6 hours prior to the occurrence of the earthquake, an anomalous tilting motion with the order of 0.1" (0.5 μ rad.) was observed with a tiltmeter of the horizontal pendulum type installed at 800m under the ground surface in Ikuno mine located about 60km away from the epicenter. Although there remained some uncertainties to conclude it as a precursor, it played an important role in Japan for promoting the national project for earthquake prediction which started in 1965. Since then, many observatories and supplementary stations for monitoring crustal movements have been established in Japan. More than 100 stations are operating under the national project for earthquake prediction. Despite such a dense arrangement of stations equipped with improved instruments, we have not been able to detect "reliable precursors" immediately before the occurrence of earthquakes.

In the early morning of January 17, 1995 (in Japanese Standard Time), a destructive earthquake of M_w=6.9 occurred near the Kobe City. The death toll from the earthquake reached more than 6,300 due to collapse of buildings and bridges, fires and diseases induced by the earthquake. We have carried on continuous observation of crustal strains with a laser strainmeter at the Rokko-Takao station in Kobe since 1989 (Takemoto *et al.*, 1998b, 2003). The distance from the station to the epicenter is about 20 km and the station is located almost above the fault plane. Based on the laser strainmeter data, we searched for anomalous strain changes before and after the earthquake mainly focusing to the period of one week before the

earthquake, but could not find out distinct evidences. It will be difficult to find out reliable precursors immediately before the occurrence of earthquakes from continuous monitoring of crustal movements by tiltmeters and strainmeters.

5. Tidal observation with superconducting gravimeters

Two superconducting gravimeters (Model TT-70: #008 and #009) were introduced into Kyoto University in 1988. Since then, continuous observation of gravity changes by employing two superconducting gravimeters had been carried on in Kyoto until December 1997 (Takemoto *et al*., 1998c). During the period, we investigated instrumental noise (Higashi, 1996), atmospheric effect (Mukai *et al*., 1995a, 1995b) and the effect of ambient temperature change on gravity measurements (Mukai *et al*., 1995c). In December, 1997, one (#008) of the two superconducting gravimeters in Kyoto was shifted to Bandung in Indonesia under the cooperation between the Graduate School of Science, Kyoto University and the Volcanological Survey of Indonesia (now, Directorate of Volcanology and Geological Hazard Mitigation), Ministry of Mines and Energy of the Republic of Indonesia (Takemoto *et al*., 1998d). We installed the SG #008 in the underground observation room where Baron Melchior and his colleagues carried out gravity observation in 1987 by employing the LaCoste & Romberg gravimeter:L336 (Melchior *et al*., 1995). The Bandung station (BA) was located at 06°53'47"S, 107°37'54"E, and 713m above the sea level. The SG #008 was installed on the concrete base of 1.2m x 1.2m which was constructed 1 m below the floor on the under layer of very thick volcanic deposit of sand and other volcanic products. The distance from the nearest sea is about 50km. The Bandung station was the only one station existing near the equator in the GGP network and provided important gravity data from December, 1997. After eliminating tidal changes and long-term drift from the SG data in Bandung, we found that the gravity residual is correlated with ambient groundwater changes. The rise of 1m of the groundwater level increase the gravity residual of 4.2-4.4µGal with a time lag of about 13-20 days (Takemoto *et al*., 2002).
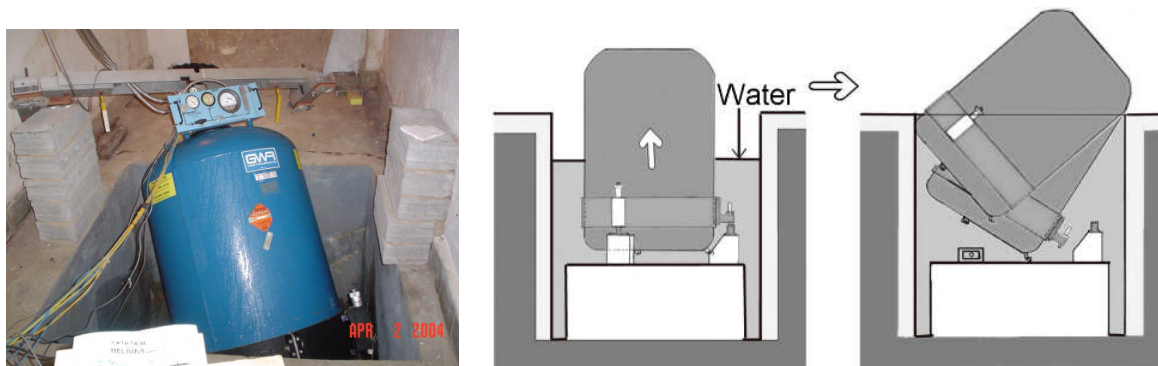

Figure 8. Accident of SG#008 due to heavy rainfall of March 27, 2004.

On March 27, 2004, the SG in Bandung suddenly broke down due to the natural disaster of flood after heavy rainfall of 140mm/hour. The SG floated due to the buoyancy of the flowing water (Figure 8). We thus continued the effort to repair the instrument but it was unfortunately impossible. We were obliged to close the SG station in Bandung in 2004.

Then we searched for possibility to restart SG observation in Indonesia because it was the only SG station that existed near the equator. In consideration of various conditions, we decided to shift another superconducting gravimeter of CT type, which was used in Aso volcano from 1996, to the National Coordination Agency for Surveys and Mapping in Indonesia (BAKOSURTANAL) in Cibinong, Indonesia. In 2008, Yoichi Fukuda and Toshihiro Higashi of Kyoto University installed the SG in the newly constructed gravity measurement room in the building belonging to BAKOSURTANAL (6°29'28"S, 106.50'56"E, h=138m) and we can restart the SG observation in Indonesia.

6. Application of laser interferometric devices to precise observation of Earth tidal deformations

In order to observe crustal deformations, various types of extensometers (strainmeters) have been developed during the last half of 20th century (e.g. Sassa type and Ozawa type extensometers). These meters are essentially using solid materials of low thermal conductivity as a "length standard" for measuring a relative displacement between two piers fixed into the bedrock (see Figure 6). Super-Invar wires (rods) or fused quartz tubes are commonly used as the length standard.

On the other hand, the appearance of the laser at the beginnings of 1960s opened up new possibilities in crustal strain measurements. Using the coherent and stable laser source, interferometric strainmeters have been developed (e.g. Berger and Lovberg (1969). The laser interferometric strainmeter enables the small strain to be measured quantitatively in terms of the wavelength of the laser light without using a length standard of any solid materials.

In Kyoto University, the laser interferometric device was used for calibrating conventional rod type extensometers at first. Then, laser strainmeters of the Michelson type were installed at the Amagase Crustal Movement Observatory, Kyoto in 1977 (Takemoto, 1979). The same type laser strainmeter was installed at the Rokko-Takao station in 1988 (Takemoto *et al.*, 1998b). As mentioned before, precursory strain changes could not be detected before the earthquake of January 17, 1995, but we could estimate the fluid core resonance using the data of the laser strainmeter installed at the Rokko-Takao tunnel in Kobe (Mukai *et al.*, 2004).

On the other hand, a new technique based on holographic interferometry was developed for measuring crustal deformations (Takemoto, 1986, 1990). The holographic recording system, consisting of an He-Ne gas laser and associated optical elements, was first installed in a tunnel at the Amagase Crustal Movement Observatory in 1984. Tunnel deformations caused by tidal and tectonic forces were precisely determined using 'real-time' technique of holographic interferometry. In this procedure, a hologram of the tunnel wall within a section 1-2 m in diameter was directly recorded on a photographic plate and then the plate was carefully reset in the same position at which the hologram had been taken. When the reconstructed image of the hologram was superimposed on the current image of the tunnel wall, many interferometric fringes could be seen through the hologram. The fringe displacement, formed by the deformation of the tunnel, was continuously recorded on a video cassette tape using a video camera and a time-lapse video recorder. The change in the fringe patterns was analyzed using the image-processing system. Tidal deformations obtained from the holographic method were consistent with the strain changes observed with laser strainmeters in the same tunnel. These observational results substantiated the tunnel deformation estimated by the finite-element calculations.

The holographic system, however, has a margin for improvement in use of the long-term strain measurements because the fringe pattern observed through the photographic plate gradually blurs over the course of the time. Thus, a clear record of holographic interferometry cannot be obtained even over a week. Therefore, we attempted to use the Electronic Speckle Pattern Interferometry (ESPI) technique, in which the interference fringe pattern can be produced without using photographic processing but instead using electronic processing (Takemoto *et al.*, 1998a). This attempt, however, did not succeed due to technical difficulty in detecting slowly moving crustal deformation.

In 2002, we installed a 100m laser strainmeter system in a deep tunnel about 1,000m below the ground surface at the Kamioka mine, Gifu, Japan (Figure 9). As shown in Figure 10, the system consists of three types of independent interferometers: (1) an EW linear strainmeter of the Michelson type with unequal arms, (2) an NS-EW differential strainmeter of the Michelson type with equal arms and (3) a NS absolute strainmeter of the Fabry-Perot type. These are configured in L-shaped vacuum pipes, each of which has a length of 100 m. (1) and (2) are highly sensitive (order of 10^{-13} strain) and have wide dynamical range (10^{-13} -10^{-6}). (3) is a new device for absolute-length measurements of a long-baseline (100 m) Fabry-Perot cavity with a precision of the order of 10^{-9} by the use of phase-modulated light (Takemoto *et al.*, 2004, 2006). The

11774

laser source of strainmeters (1) and (2) is a frequency-doubled YAG laser with a wavelength of 532 nm. The laser frequency is locked onto an iodine absorption line and a stability of 2×10^{-13} is attained. (3) uses another laser source of the same type as used for (1) and (2).The light paths of the laser strainmeter system are enclosed in SUS304 stainless steel pipes. The inside pressure is kept to be 10^{-4} Pa. Consequently, quantitative measurement of crustal strains of the order of 10^{-13} can be attained by employing the laser strainmeter system of (1) and (2) at Kamioka. This resolving power corresponds to that of a superconducting gravimeter. The noise level recorded at Kamioka is lowest in the range of 10^{-3} to 10^{-1} Hz among laser strainmeters now operating in the world.

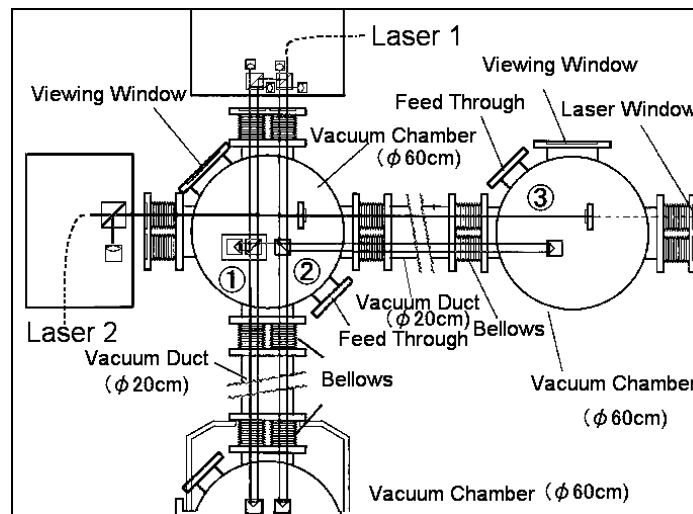**Figure 9.** View of the 100m laser strainmeter system in the Kamioka mine, Gifu, Japan.

Figure 10. Schematic view of the laser strainmeter system at Kamioka consists of three types of laser interferometers. (1) A simple Michelson type interferometer of unequal arms installed in the EW direction. (2) An equal arm laser interferometer detecting difference of linear strains in the NS and EW directions. The third type (3) is a new device for absolute-length measurements of a long-baseline (100 m) Fabry–Perot cavity with a precision of the order of 10^{-9} by the use of phase-modulated light.

Figure 11 shows the strain seismograms obtained from the Kamioka laser strainmeters ((1) and (2)) at the time of the great Sumatra-Andaman earthquake of December 26, 2004. In this figure, the left side is a high-passed and the right side a low-passed (1000sec) record, respectively. We can recognize that the maximum amplitude of seismic wave is in the order of 1μ strain (left side) and coseismic strain step is in the order of 1 nano strain at the epicentral distance of 5600km.
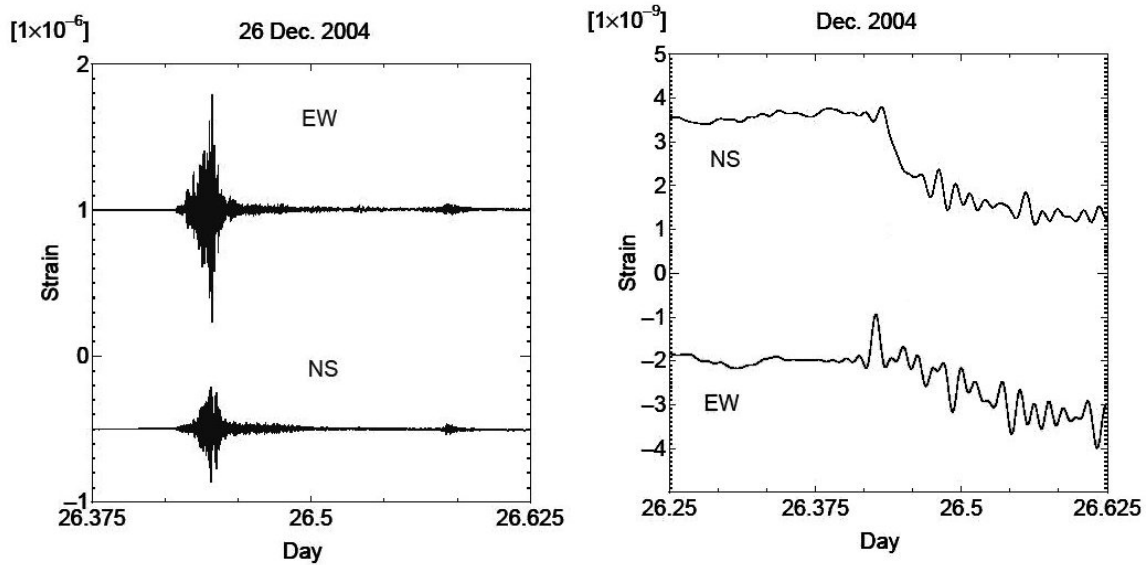
Figure 11. Strain seismograms of the great Sumatra-Andaman earthquake of December 26, 2004 observed at Kamioka.

In 2004, the Superconducting Gravimeter (T016) which had been used in the Showa station in Antarctica was installed in the same tunnel in Kamioka mine. Figure 12 shows the comparison of the tidal strain changes in NS and EW directions obtained from laser strainmeters and the gravity changes obtained from the superconducting gravimeter. Figure 13 shows the comparison of spectra obtained from laser strainmeters and the superconducting gravimeter after the earthquake (M=7.4) of Jan. 06, 2006 occurred at South Sandwich Islands. We can expect that combined use of laser strainmeters and superconducting gravimeter nearby installed will be an effective tool to investigate keen geophysical problems such as to separate "spheroidal modes" and "torsional modes of Earth's free oscillations and to search for Slichter triplet.
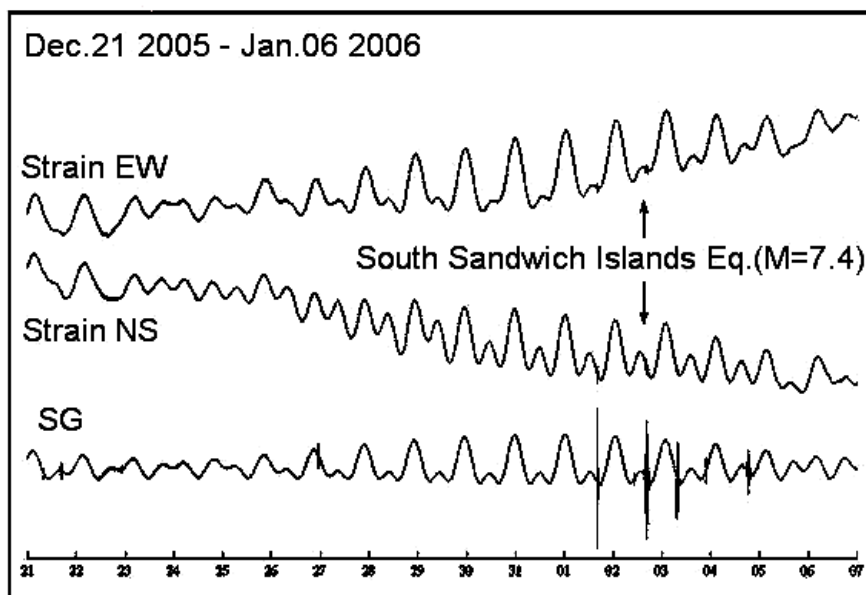

Figure 12. Comparison of tidal changes observed with laser strainmeters (NS and EW) and superconducting gravimeter installed in the same tunnel in Kamioka.
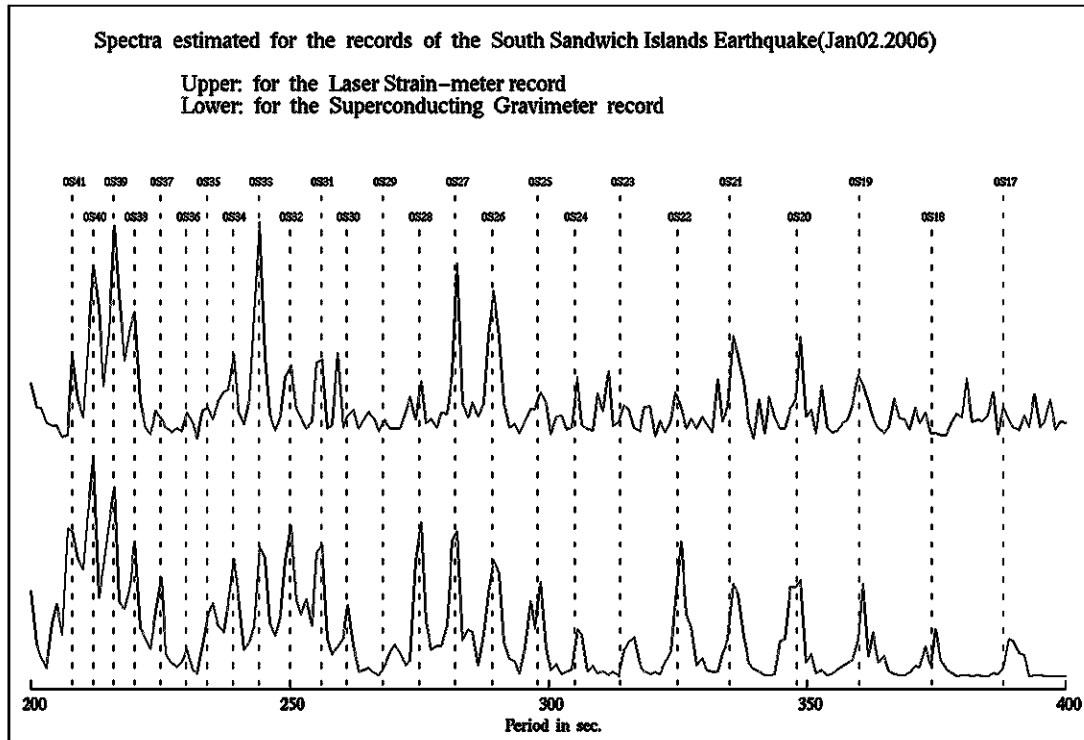
11776

Figure 13. Comparison of spectra obtained from laser strainmeters and the superconducting gravimeter at the earthquake (M=7.4) of Jan. 06, 2006 occurred at South Sandwich Islands.

Concluding remarks

In this paper, some of centenary researches on Earth tides carried out in Kyoto University during the period of 1909 - 2008 are presented. Early remarkable achievements are the proposal of "Shida Number" and the first observation of tidal strains by employing the Sassa type extensometers. Since then, we have continued studies on Earth tides based on observational data. Now, laser strainmeters and superconducting gravimeters are efficient tools to investigate Earth tides. Combined use of laser strainmeters and superconducting gravimeter will produce many new findings in geophysics. In the near future, the data obtained from these high-sensitive terrestrial instruments should be compared with the geodetic satellite data to improve geodetic and geophysical investigations.

Acknowledgements

References

Benioff, H., 1935, A linear strain seismograph, *Bull. Seism. Soc. Am.*, **25**, 283-309.

Benioff, H., 1959, Fused-quartz extensometer for secular, tidal, and seismic strains, *Bull. Geol. Soc. Am.*, **70**, 1092-1132.

Benioff, H., F. Press and S. Smith, 1961, Excitation of the free oscillation of the Earth by earthquakes, *J. Geophys. Res.*, **66**, 605-619.

Berger, J. and Lovberg, R. H., 1969, A laser strain meter, *Rev. Scientific Instrum.*, **40**, 1569-1576.

Clarkson, H. N., and LaCoste, L. J. B., 1957, Improvements in tidal gravity meters and their simultaneous comparison, *Trans. Am. Geophys. Union*, **38**, 8-16.

Higashi, T., 1996, A study on characteristics of tidal gravity observation by employing superconducting gravity mters at Kyoto, Japan, *Memoirs of Fac. Sci., Kyoto Univ., Series A*, **39**, No.3, 313-348.

Love, A. E. H., 1909, The yielding of the earth to disturbing forces, *Proc. of the Royal Society of London*, **82**, 73-88.

Melchior, P. and B. Ducarme, 1976, The ratio ℓ/h: A simple method for the prospection of tidal deformations of cavities in the Earth's crust, *Jour. Geod.*, **50**, 137-138.

Melchior, P., O. Francis and B. Ducarme, 1995, Tidal gravity measurements in southeast Asia, *Report for the IUGG General Assembly IAG Symposium "Geodesy in Southeast Asia"* pp.28.

Mukai, A., T. Higashi, S. Takemoto, I. Nakagawa and I. Naito, 1995a, Accurate estimation of atmospheric effects on gravity observations made with a superconducting gravity meter at Kyoto, *Phys. Earth Planet. Inter.* **91**, 149-159

Mukai, A., S. Takemoto, Y. Fukuyama, I. Nakagawa, 1995b, Effect of room temperature changes on gravity observation with superconducting gravity meters, *J. Geod. Soc. Japan*, **41**, 197-206 (in Japanese with English Abstract).

Mukai, A., T. Higashi, S. Takemoto, I. Naito and I. Nakagawa (1995c): Atmospheric effects on gravity observations within the diurnal band, *J. Geod. Soc. Japan*, **41**, 365-378.

Mukai, A., Takemoto S., and Yamamoto, T., 2004, Fluid core resonance revealed from a laser extensometer at the Rokko-Takao station, Kobe, Japan, *Geophys. J. Int.*, **156**, 22-28.

Nakagawa, I., 1961, General consideration concerning the elimination of the drift curve in the Earth tidal observations, *Comm. Obs. Roy. Belg., No. 188, Ser. Geophys.,* 201-210.

Nakagawa, I., 1962a, Some problems on time change of gravity, Part 2, On analytical treatments for data of the tidal variation of gravity, *Bull. Disas. Prev. Res. Inst., Kyoto Univ.*, No. 53, 67-105.

Nakagawa, I., 1962b, Some problems on time change of gravity, Part 5, On free oscillations of the Earth observed at the time of Chilean earthquake on May 22, 1960, Bull. Disas. Prev. Res. Inst., Kyoto Univ., No. 57, 85-107.

Nishimura, E. 1950, On Earth tides, *Trans. Am. Geophys. Union*, **31**, 357-376.

Ozawa, I., 1952, Observation of tidal strain of the earth by the extensometer (Part 2), *Bull. Disast. Prev. Res. Inst., Kyoto Univ.*, No. 3, 4-17.

Ozawa, I., 1961, On the observations of the earth tides by means of extensometers in horizontal components, *Bull. Disas. Prev. Res. Inst., Kyoto Univ.*, No. 46, 1-15.

Ozawa, I., P. Melchior, B. Decarme and J. Flick, 1973, Observations of the tidal extension at Walferdange, *Contributions of the Geophys. Inst., Kyoto Univ.*, **13**, 85-92.

Press, F., Ewing, M., and Lenner F., 1958, A long period seismograph system, *Trans. Am. Geophys. Union*, **39**, 106-108.

Sassa, K., and Nishimura, E., 1951, On phenomena forerunning earthquakes, *Trans. Am. Geophys. Union*, **32**, 1-6.

Sassa, K., Ozawa, I., and Yoshikawa, S., 1952, Observation of tidal strain of the earth by the extensometer, *Bull. Disast. Prev. Res. Inst., Kyoto Univ.*, No.3, 1-3.

Shida, T., 1912, On the elasticity of the earth and the earth's crust, *Memoirs of the College of Science and Engineering, Kyoto Imperial University*, **4**, 1-286.

Shida, T., 1925, On the possibility of observing free vibrations of the earth, in *Anniversary volume dedicated to professor Hantaro Nagaoka by his friends and pupils on the completion of twenty-five years of his professorship*, 109-120.

Shida, T., 1929, Review of the study of rigidity of the earth and the initial motion of seismic waves: *Toyo Gakugei Zasshi* (*East Asian Journal of Art and Science*), **45**, 275–289 (in Japanese).

Shida, T., 1937, An address at the opening ceremony of the Beppu Geophysical Institute : "A proposal for existence of deep earthquake": *Geophysics* (*the Japanese-language Journal of Geophysics of the Imperial University of Kyoto*), **1**, 1–5 (in Japanese).

Takemoto, S., 1979, Laser interferometer systems for precise measurements of ground-strains, *Bull. Disas. Prev. Res. Inst., Kyoto Univ.*, **29**, (No.262), 65-81.

Takemoto, S., 1986, Application of laser holographic techniques to investigate crustal deformations, *Nature*, **322**, 49-51.

Takemoto, S. 1990, Laser holographic measurements of tidal deformation of a tunnel, *Geophys. J. Int.*, Vol. **100**, 99-106.

Takemoto, S., Mukai, A., Magari, U., and Kondo, J. 1998a, A new measurement system of tidal strains by employing electronic speckle pattern interferometry (ESPI), *Proc. the 14th Inter. Sympo on Earth Tides, Brussels*, 69-73.

Takemoto, S., Yamamoto, T., Otsuka, S., Fujimori, K., and Mukai, A., 1998b, Tidal strain observation at Rokko-Takao station, Kobe, Japan, *Proc. the 14th Inter. Sympo. on Earth Tides, Brussel*s, 193-199.

Takemoto, S., T. Higashi, A. Mukai, Y. Fukuda and T. Tanaka, 1998c, Precise observation of gravity changes with superconducting gravimeters in Kyoto (1988-1997), *Annuals Disas. Prev. Res. Inst., Kyoto Univ.*, No. 41B-1, 77-85 (in Japanese with English Abstract).

Takemoto, S., S. Dwipa, Y. Fukuda, T. Higashi, A. Andan, D. S. Kusuma, R.Sukhyar, Wimpy S.Tjetjep, T. Tanaka and Leni S. Heliani, 1998d, Precise gravity observation in Bandung using a superconducting gravimeter, *Proc. of Symposium on Japan-Indonesia IDNDR Project, September 21-23, 1998, Bandung, Indonesia*, 223-230.

Takemoto, S., Y. Fukuda, T. Higashi, S. Ogasawara, M. Abe, S. Dwipa, D. S. Kusuma and A. Andan, 2002, Effect of groundwater changes on SG observations in Kyoto and Bandung, *Bulletin d'Information des Marees Terrestres (BIM)*, **136**, 10,839-10848.

Takemoto, S., Yamamoto, T., Mukai, A., Otsuka , S., and Fujimor, K., 2003, Crustal strain observation for nine years with a laser strainmeter in Kobe, Japan, *Jounal of Geodynamics*, **35**, 483 - 498.

Takemoto, S., Araya, A., Akamatsu, J., Morii, W., Momose, H., Ohashi, M., Kawasaki, I, Higashi, T., Fukuda, Y., Miyoki, S., Uchiyama, T., Tatsumi, D., Hanada, H., Naito, I., Telada, S., Ichikawa, N., Onoue, K. and Wada, Y., 2004, A 100m laser strainmeter system installed in a 1 km deep tunnel at Kamioka, Gifu, Japan, *Journal of Geodynamics*, **38**, 477-488.

Takemoto, S., Momose, H., Araya, A., Morii, W., Akamatsu, J., Ohashi, M., Takamori, A., Miyoki, S., Uchiyama, T., Tatsumi, D., Higashi, T., Telada, S., and. Fukuda, Y., 2006, A 100m laser strainmeter system in the Kamioka mine, Japan, for precise observations of tidal strains, *Journal of Geodynamics*, **41**, 23-29.

Takemoto, S., 2007, Short review of studies of crustal deformations in Kyoto University, *Jour. Geod. Soc. Japan*, **53**, 123-133 (in Japanese with English abstract).

Wadati, K., 1928, Shallow and deep earthquakes, *Geophysical Magazine*, **1**, 162-202.

Wadati, K., 1929, Shallow and deep earthquakes (2nd paper), *Geophysical Magazine*, **2**, 1–36.

Wadati, K., 1931, Shallow and deep earthquakes (3rd paper), *Geophysical Magazine*, **4**, 231–283.

Wadati, K., 1935, On the activity of deep-focus earthquakes in the Japan islands and neighborhoods, *Geophysical Magazine*, **8**, 305–325.

BLANK PAGE

Comparison of the LaCoste & Romberg gravimeter ET18 with the superconducting gravimeter CD-034 at the Geodynamic Observatory Moxa (Germany)

A. Hegewald, G. Jentzsch, Th. Jahr

Institute of Geosciences, Friedrich-Schiller-University Jena, Germany

Abstract

Superconducting gravimeters were developed to overcome mechanical deficiencies of spring gravimeters. They are well known for their long-term stability. But what about the information contents in the other period ranges (short period and Earth tidal bands) compared to spring gravimeters?

For comparative analyses the well calibrated superconducting gravimeter CD-034 (SG) and the LaCoste and Romberg (L&R) Earth tide gravimeter ET18 record next to each other at the broadband Geodynamic Observatory Moxa (Germany). The processing and analyses of the one year long time series were carried out in three frequency ranges: the low frequency band ($< 1.5 \cdot 10^{-3}$ cph), the high frequency band (> 0.125 cph) and the Earth tide frequency intervals in between. Results are: same information content of both records in the high frequency band and the Earth tide frequency intervals, although the ET18 shows a higher noise level than the SG data. As expected, the ET18 time series contain a stronger instrumental long-term drift than the SG record.

The aim of this work is to evaluate the differences between the two data sets in the three frequency bands, and to calibrate the L&R with regard to the SG in order to prepare future measurements of the ET18 in other places.

1. Introduction

The sensors of the LaCoste & Romberg gravimeter ET18 (L&R) and the superconducting gravimeter CD-034 (SG) are totally different: The ET18 has a classical system with a mass at the end of beam which is supported by the zero-length spring (Asch et al. 1986b), whereas the SG has a small ball floating on a magnetic field produced by a superconducting coil system. Consequently, the data sets contain different information, and resolution of small signals (e.g. seasonal hydrological effects) is also different.

The L&R gravimeter ET18 was completed in 1975. It was used at different places in Germany (Asch et al. 1986a), Denmark (Jahr 1989), Fennoscandia (Jentzsch 1986, Weise 1992, Weise et al. 1999) and Greenland (Jentzsch et al. 1995, Ramatschi 1998). Aims of the measurements were comparative analyses of different gravity observations with regard to Earth tides and ocean tidal loading, and the comparison with the modelled response of the elastic Earth's crust. The gravimeter was calibrated several times at the vertical base-line in Hanover between 1985 and 1997 (Melzer 1989, Ramatschi et al. 1993).

Since April 1999 the SG records at the Geodynamic Observatory Moxa (Germany). The gravity registration consists of a dual-sphere-sensor system with high long-term stability. Aims of previous measurements were investigations of polar motion, core modes, Slichter triplet, Earth tides and free modes of the Earth (Kroner et al. 2004). Furthermore, comparative analyses of gravity residuals from the gravimeter to modelled effects of different hydrological contributions from soil moisture, water level, meteorological observations and snow were carried out (Kroner et al. 2007). The calibration factors of the superconducting gravimeter were determined twice a year parallel recordings of 2-3 days of an absolute gravimeter. The calculations of the calibration factors were carried out using the least squares method (Kroner 2002).

In previous studies, comparative analyses between superconducting gravimeters and mechanical spring gravimeters were also performed by other authors. By Richter et al. (1995), a report about the comparison of the spectra of 57 day parallel records from the SG-102 and the ET19 at the Black Forest Observatory (BFO, Germany). Another study concerned the differences between the L&R gravimeter ET19 at BFO, an identical instrument at the South Pole and the superconducting gravimeters at Brussels and Bad Homburg (Zürn et al. 1991).

New results in this paper are based on the following facts: The SG works with a dual-sphere-sensor system, and both gravimeters (the SG and the ET18) record next to each other in the Geodynamic Observatory Moxa, and for the comparison in different frequency bands time series of one year were used. The aim of these investigations is to test and classify the "old" L&R gravimeter ET18 for future use in other stations.

2. Fundamentals and techniques

At the broadband Geodynamic Observatory Moxa both gravimeters are operating under very stable conditions in a separate room. Moxa is located about 30 km south of Jena. The observatory is built in a narrow valley and contains of rooms converted by soil to reduce environmental noise. The galleries inside the hill are used for strain measurements and seismic observations. The Observatory Moxa is well known for its low noise level compared to other stations of the Global Geodynamic Project all over the world. The scale is the New Low Noise Model of Peterson (1993), from the seismic to the tidal frequency bands (Rosat et al. 2004). Both gravimeters record next to each other (distance about 5 m) on their own pillars. To correct for barometric pressure effects (Warburton and Goodkind 1977, Scherneck 1985, Zürn and Widmer 1995), air pressure is recorded in parallel next to each gravimeter.

The superconducting gravimeter CD-034 is based on a dual-sphere-sensor system. Both spheres are located on top of each other in constant magnetic fields, generated by two superconducting coils each. The feedback system is realised by a non-superconducting inductor. Gravity changes are recorded with a 1 sec sampling interval. For the comparative analyses only the data set of the lower sensor was used.

The L&R gravimeter ET18 consists of a damped spring-mass system with electrostatical feedback installed by Larson (1968). All 1 sec samples are recorded and numerically filtered to 10 sec samples.

For the analyses, the time series of the two gravimeters and barometric pressure sensors include 374 days (July 11, 2007 until July 17, 2008; Fig. 1). The following steps were part of the data preprocessing: numerical filtering to 1 min samples and calibration of the time series with calibration factors of -0.6065 (nm/s²)/mV for the SG and 0.8079 (nm/s²)/mV for the ET18. After that, theoretical tides were subtracted using tidal parameters derived from tidal analyses of 100 day records of the ET18 and the SG (August 4, 2007 until November 12, 2007). The theoretical tides include ter-diurnal, semi-diurnal, diurnal, fortnightly and monthly tidal wave groups. For the tidal analyses and the calculation of the theoretical tides, the program package ETERNA34 was used (Wenzel 1996). Furthermore, barometric pressure was corrected based on the approximated air pressure regression parameters, resulting from the tidal analyses. Regression factors β are (-3.40 ± 0.02) (nm/s²)/hPa for the SG and (-3.40 ± 0.09) (nm/s²)/hPa for the ET18 gravimeters. In short the data processing contains of:

$$\text{residuals} = \text{observations} - \text{theoretical tides} + \beta \cdot \text{air pressure}$$

Processing of the residuals was carried out with the program PreAnalyse (Gebauer et al. 2007). Working steps contained the elimination of spikes and strong earthquakes, correction of offsets and linear interpolation of gaps until 8 hours (in the residual curve). The analyses of the edited time series were accomplished in three different frequency bands: the low frequency band (less than $1.5 \cdot 10^{-3}$ cph), the high frequency band (higher than 0.125 cph) and the Earth tidal frequency intervals in between.

In the three frequency bands tidal analyses, calculation of spectra and regressions were accomplished. One working step was the calculation of a transfer function from the ET18 to the SG. For this, the spectrum of the SG was divided by the spectrum of the ET18 over the whole frequency range from 0 cph until the Nyquist Frequency of 0.5 cph (Fig. 2 and 3). The transfer function has an average of nearly one in the Earth tide frequency bands and the high frequency band, and an average less than one at low frequencies. These results point to the larger drift of the ET18 and they confirm the published results from the other authors (Richter et al. 1995 and Zürn et al. 1991).

3. Comparative analyses in the low frequency band (long-term drifts)

To quantify the long-term drift of both gravimeters the residuals of the 374 days data sets (Fig. 4) were analysed. These residuals contain waves with periods longer than 28 days (equivalent to frequency $< 1.5 \cdot 10^{-3}$ cph = 0.0144 cpd). The residual curve of the ET18 varies in a gravity range of 1447 nm/s², whereas the curve of the SG varies in an interval of 100 nm/s², only.

Linear regression lines were fitted on the residual curves of both gravimeters. The equations for the regression lines are (comp. Fig. 4):

$$\text{ET18:} \quad g = 0.13295 \ (\text{nm/s}^2)/\text{h} \cdot t + 2725.663 \ \text{nm/s}^2$$
$$\text{SG:} \quad g = -0.00015 \ (\text{nm/s}^2)/\text{h} \cdot t + 3063.593 \ \text{nm/s}^2$$

with g: gravity value and t: time span in hours. The comparison of the slopes of both regression lines shows the long-term stability of the SG gravimeter (slope nearly zero) and the long-term drift of the L&R gravimeter.

After subtraction of the linear drift, the variation of the residuals of the ET18 is in the range of 759 nm/s², and the variation interval of the SG is still 100 nm/s².
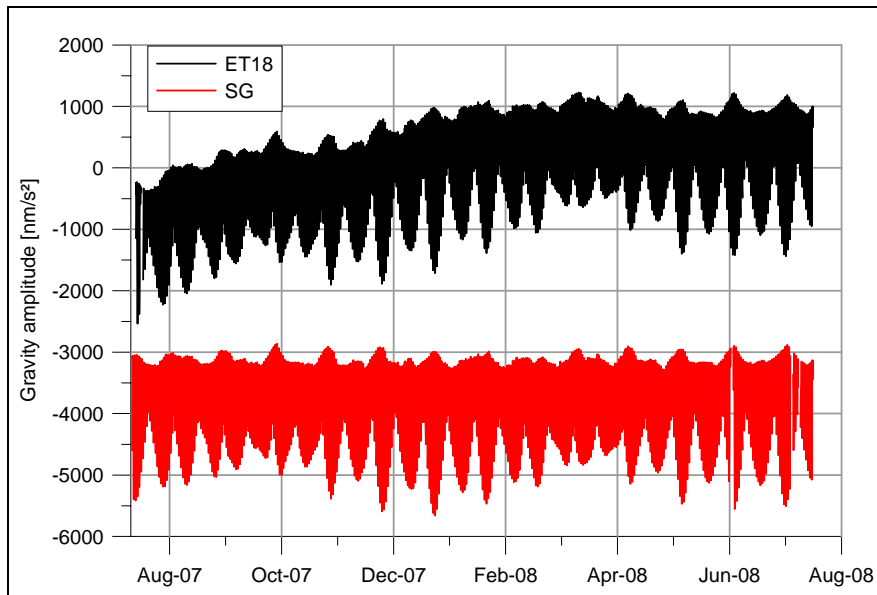
Fig. 1: Time series of the ET18 gravimeter and the SG gravimeter over 374 days (July 11, 2007 until July 17, 2008).
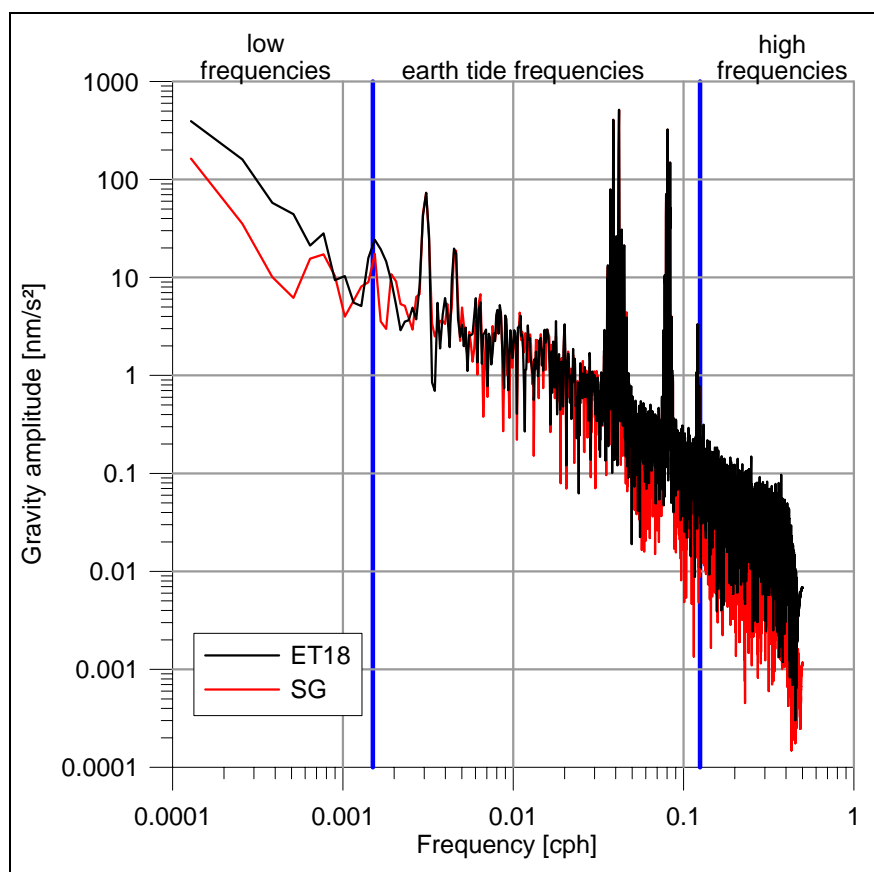

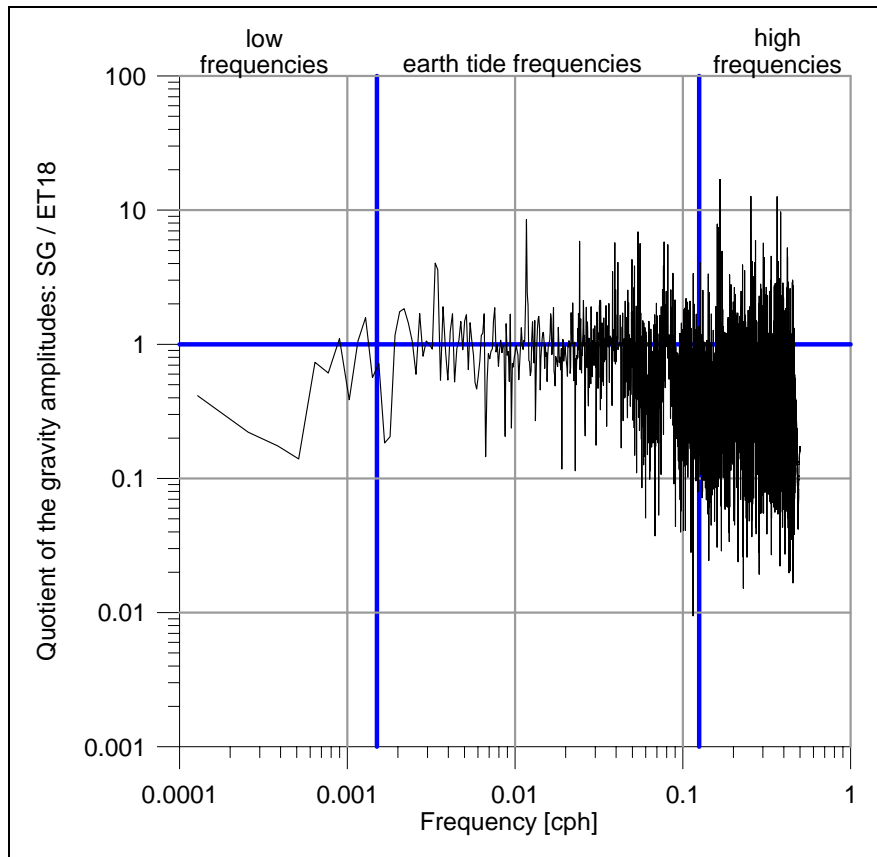**Fig. 2**: Spectra of the ET18 gravimeter and the SG gravimeter over the whole frequency range.

Fig. 3: Transfer function between the ET18 gravimeter and the SG gravimeter over the whole frequency range.
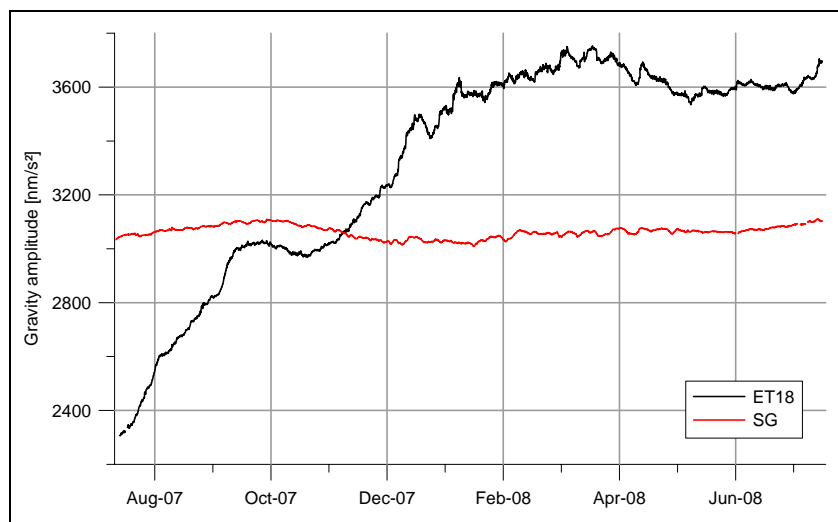

Fig. 4: Long-term drift of the ET18 gravimeter and the SG gravimeter. Both records contain waves with periods longer than 28 days.

4. Analysis of the Earth tide frequency ranges

The Earth tide bands include waves with periods between 8 hours and 28 days. With the Earth tide data processing package ETERNA34, the preprocessing and analysis of Earth tide observations, the prediction of Earth tide signals and the computation of ocean tide loading are possible. The adjustment of the tidal parameters is based on the least squares method. Results are the amplitude factors δ and phase differences α. The amplitude factors δ for the tidal wave groups are calculated by the equation:

$$\delta = h / H$$

with h: amplitude of the tidal wave group of the gravity record, which is analysed; H: amplitude of the tidal wave group from the tidal potential catalogue according to Hartmann and Wenzel (1995; HW95). The phase differences α are results of the equation:

$$\alpha = \varphi - \Phi$$

with φ: phase of the tidal wave group of the gravity record, which is analysed; Φ: phase of the tidal wave group from the tidal potential catalogue HW95.

After the correction of both records as mentioned above, theoretical tides and barometric pressure were added to the computed residuals of the gravity records. In short the data processing covers:

edited observations = edited residuals + theoretical tides - β • air pressure

with β: estimated air pressure regression parameter, resulting from the tidal analyses with ETERNA34 of the 100 day data sets from the ET18 and SG. Then, the edited observations were filtered to one hour samples.

The tidal analyses of the two time series were carried out in two steps: first, for the ter-diurnal, semi-diurnal and diurnal tidal wave groups and second, for the fortnightly and monthly tidal wave groups. The reason for the two step calculation is to get the best fitted results for the ter-diurnal, semi-diurnal and diurnal tidal parameters. In the first analysis step the gravity and barometric pressure data were filtered by a low pass filter with 167 supporting points and a cut-off frequency of 0.0333 cph (equivalent to a period of 30 hours). In the second step, the edited observations were used without any filter.

The results of the tidal analyses are the tidal parameters (which still contain the ocean loading effect, Tab. 2 and 3) and the averages of noise levels at the different frequency bands (Tab. 4). Furthermore, the signal-to-noise ratios for the analysed tidal wave groups were calculated (Tab. 2 and 3). These signal-to-noise ratios of the ter-diurnal, semi-diurnal and diurnal tidal wave groups from the ET18 are a factor of 6 lower than these of the SG. Ratios of the fortnightly and monthly tidal wave groups from the ET18 are a factor of 3 lower than of the SG. The big differences in the tidal parameters for the fortnightly and monthly tidal wave groups are caused by the long-term drift in the ET18 record and the long-term stability of the SG data set.

Another result of the analyses is given by the comparison of the spectra of the residuals. The residuals are the difference between the observed data and the fitted theoretical tides by the least squares method. In the spectra of the residuals from the ET18 and SG analyses (Fig. 5), no significant information at the known tidal frequencies is found. Thus, the calculated tidal parameters are a good fit to the recorded Earth tides. The residual amplitudes in the spectra from the ET18 are a factor 10 higher than of the SG.

Tab. 2: Tidal parameters and the signal-to-noise ratios for the ET18 gravimeter record.

wave group	δ-factor	phase delay [°]	s/n ratio
MM	1.24644 0.26448	6.3987 12.0211	11
MF	1.13596 0.04633	3.0390 2.3782	19
O1	1.14907 0.00058	0.1236 0.0289	1389
K1	1.13701 0.00045	0.1438 0.0227	1932
M2	1.18582 0.00034	1.5707 0.0165	2899
S2	1.18245 0.00068	0.1716 0.0333	1345
M3	1.07147 0.01755	-0.3132 0.9384	48

Tab. 3: Tidal parameters and the signal-to-noise ratios for the SG record.

wave group	δ-factor	phase delay [°]	s/n ratio
MM	1.14555 0.09422	5.4032 4.6392	29
MF	1.12844 0.01635	-0.5810 0.8508	54
O1	1.14880 0.00010	0.0760 0.0047	8480
K1	1.13653 0.00007	0.1851 0.0038	11794
M2	1.18551 0.00006	1.4858 0.0028	17342
S2	1.18428 0.00011	0.2485 0.0056	8059
M3	1.07135 0.00249	0.0071 0.1334	339

Tab. 4: Averages of noise levels at the different frequency bands for the analysed ET18 and SG data sets.

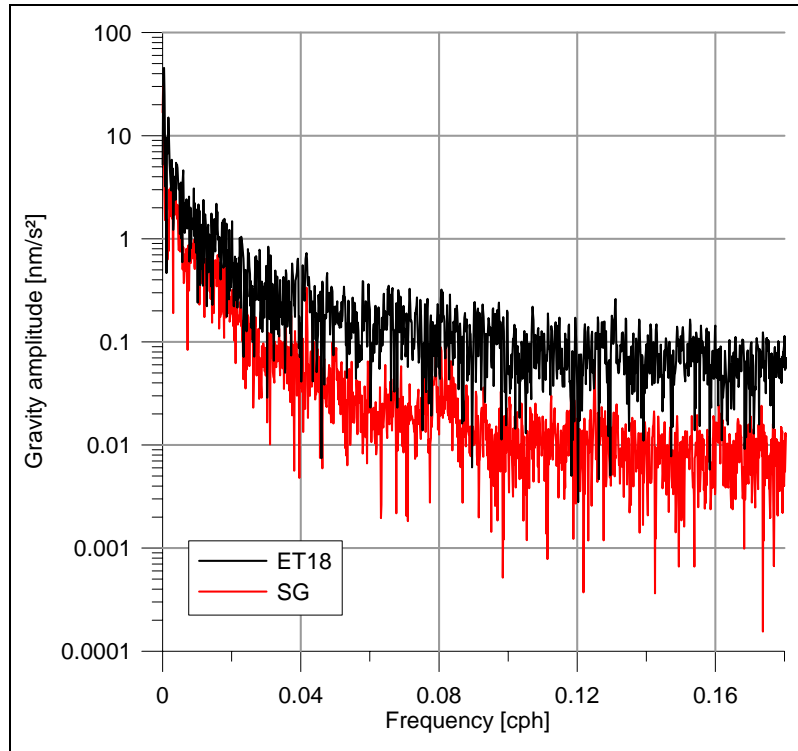|	4.17 • 10⁻³ cph	0.0417 cph	0.0833 cph	0.125 cph
ET18 [nm/s²]	2.992	0.252	0.124	0.085
SG [nm/s²]	1.060	0.041	0.021	0.012

Fig. 5: Frequency spectra of the residuals from tidal analyses for the ET18 gravimeter and SG gravimeter.

5. Comparative analyses in the high frequency band (free modes of the Earth)

After strong earthquakes the Earth oscillates with a sum of discrete spheroidal and toroidal modes. Spheroidal modes are affected by the gravitational field of the Earth and can be measured using gravimeters. For the determination of the free modes three strong earthquakes were cut out of the gravity records of the ET18 and the SG (source: earthquake catalogue USGS NEIC):

1. August 15, 2007 near the coast of central Peru with a magnitude of 8.0
2. September 13, 2007 southern Sumatra with magnitudes of 8.5
3. May 12, 2008 eastern Sichuan, China with a magnitude of 7.9

Each of the three data sets has a length of 49 hours. Figure 6 shows the residuals of the time series (detided and depressed) of the ET18 and SG for the earthquake in eastern Sichuan, China. For all records discrete Fourier spectra between 0.25 mHz and 4 mHz (periods between 67 min and 4 min) were calculated. Furthermore, the spectra were stacked for each gravimeter to increase the signal-to-noise ratios. Results are 28 spheroidal free modes (frequencies of the modes after Masters and Widmer 1995) in the stacked spectra (Fig. 7). As can be seen, the noise level of the ET18 is slightly higher than the one of the SG until a frequency of 1.5 mHz. Moreover, the amplitude values of the frequency peaks in the ET18 spectrum are a bit lower than the peak values of the SG spectrum. From these two facts follows, that the signal-to-noise ratios of the ET18 are smaller than those of the SG. Nevertheless, the information content in both spectra is the same.
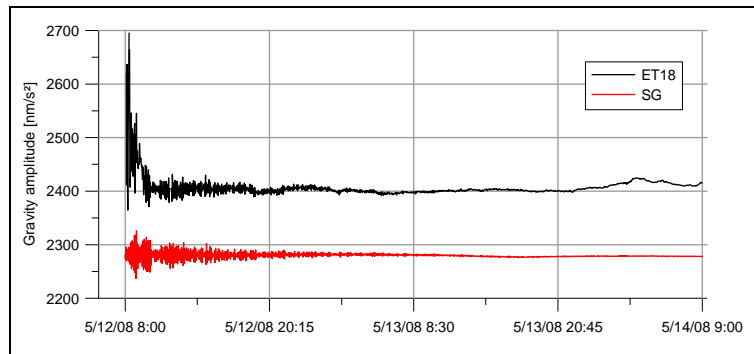
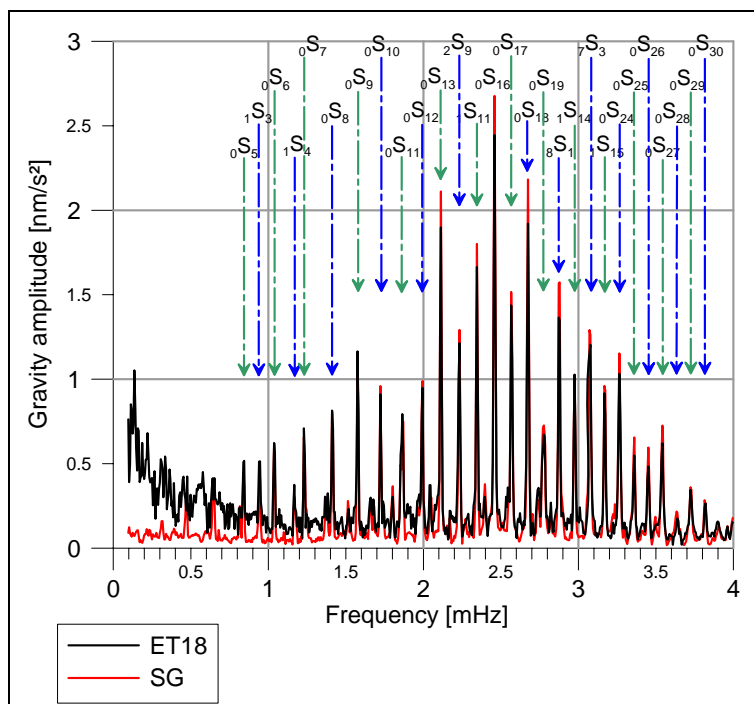**Fig. 6**: Reduced time series from the China earthquake (May 12, 2007).

Fig. 7: Stacked spectra of three earthquakes of the ET18 and
the SG gravimeter with 28 spheroidal free modes of the Earth.

6. Conclusions

With one year parallel records of the L&R gravimeter ET18 and the superconducting gravimeter CD-034 at the Geodynamic Observatory Moxa it was possible to carry out a comparison between these different gravity measuring systems. The analyses of the time series were conducted in three frequency ranges: the low frequency band ($< 1.5 \cdot 10^{-3}$ cph), the high frequency band (> 0.125 cph) and the Earth tide frequency intervals in between.

The results show in the low frequency band a long-term drift in the ET18 record and a long-term stability in the SG time series, in the high frequency range (free modes of the Earth) nearly identical information content in the data sets of both gravimeters, although higher noise level in the ET18 record up to a frequency of 1.5mHz and lower peak values in the spectrum compared to the SG data. Furthermore, in the Earth tide frequency intervals the information content in both time series for the ter-diurnal, semi-diurnal, diurnal and fortnightly tidal wave groups is also identical, although a higher noise level by a factor of 6 in the ET18 record compared to the SG. For the monthly tidal wave groups, the tidal parameters from the ET18 data set are higher than these of the SG. The reason may be the energy provided by the long-term drift in the ET18 time series.

These investigations show that one of the best spring gravimeters, the L&R Earth tide gravimeter ET18 is comparable to the superconducting gravimeter for periods of 14 days and shorter. The advantage of the L&R gravimeter is the mobility. Therewith, the newly calibrated and tested ET18 is ready to be used for recording of gravity changes at different stations.

References

Asch, G., Elstner, C., Jentzsch, G., Plag, H. P. (1986a): *On the estimation of significant periodic and aperiodic gravity variations in the time series of neighbouring stations – Part 1: Tidal Signals*. Proceedings of the 10th International Symposium on Earth Tides, Madrid, Spain, 239 – 250

Asch, G., Elstner, C., Jentzsch, G., Plag, H. P. (1986b): *On the estimation of significant periodic and aperiodic gravity variations in the time series of neighbouring stations – Part 2: Non-Tidal Signals*. Proceedings of the 10th International Symposium on Earth Tides, Madrid, Spain, 251 – 262

Gebauer, A., Jahr, Th., Jentzsch, G. (2007): *Recording and interpretation/analysis of tilt signals with five ASKANIA borehole tiltmeters at the KTB*. Review of Scientific Instruments 78, 054501-1 - 054501-6

Hartmann, T., Wenzel, H. G. (1995): *Catalogue HW95 of the tide generating potential*. Marees Terrestres Bulletin d'Informations 123, 9278 – 9301

Jahr, Th. (1989): *Tidal loading in the shelf area around Denmark*. Marees Terrestres Bulletin d'Informations 105, 7485 – 7494

Jentzsch, G. (1986): *Auflastgezeiten in Fennoskandien*. Habilitationsschrift, Berliner Geowiss. Abh., Reihe B, 13, Verlag von Dietrich Reimer, Berlin, 184 S.

Jentzsch, G., Ramatschi, M., Madsen, F. (1995): *Tidal gravity measurements on Greenland*. Marees Terrestres Bulletin d'Informations 122, 9239 - 9248

Kroner, C. (2002): *Zeitliche Variationen des Erdschwerefeldes und ihre Beobachtungen mit einem supraleitenden Gravimeter im Geodynamischen Observatorium Moxa*. Habilitationsschrift, Jenaer Geowissenschaftliche Schriften Heft 2 (Germany)

Kroner, C., Jahr, Th., Jentzsch, G. (2004): *Results from 44 months of observations with a superconducting gravimeter at Moxa/Germany*. Journal of Geodynamics 38, 263 – 280

Kroner, C., Jahr, Th., Naujoks, M., Weise, A. (2007): *Hydrological signals in gravity – foe or friend?*. International Association of Geodesy Symposia, Vol. 130, Dynamic Planet , Ed. P. Tregoning and C. Rizos, Cairns, Australia, 504 - 510

Larson, J. V. (1968): *A cross correlation study of the noise performance of electrostatically controlled LaCoste and Romberg gravimeters*. Dissertation University of Maryland (USA)

Masters, T. G., Widmer, R. (1995): *Free oscillations: Frequencies and attenuations*. Global Earth Physics, A Handbook of Physical Constants, Ed. T. J. Ahrens, AGU, Washington DC (USA), 104 – 125

Melzer, J. (1989): *Analyse und Vergleich des hochfrequenten Signalanteils in den Gezeitenregistrierungen des Gravimeters LCR ET18*. Diploma thesis University Berlin (Germany)

Peterson, J. (1993): *Observations and modelling of seismic background noise*. Open-File Report 93 – 332, U.S. Department of Interior, Geological Survey, Albuquerque, New Mexico

Ramatschi, M., Liebing, M. and Jentzsch, G. (1993): *Instrumental tests and calibration of the gravimeter LCR ET18*. Marees Terrestres Bulletin d'Informations 115, 8472 – 8477

Ramatschi, M. (1998): *Untersuchungen von Vertikalbewegungen durch Meeresgezeitenauflasten an Referenz-stationen auf Grönland*. Dissertation TU Clausthal (Germany)

Richter, B., Wenzel, H. G., Zürn, W., Klopping, F. (1995): *From Chandler wobble to free oscillations: comparison of cryogenic gravimeters and other instruments in a wide period range*. Physics of the Earth and Planetary Interiors 91, 131 - 148

Rosat, S., Hinderer, J., Crossley, D., Boy, J. P. (2004): *Performance of superconducting gravimeters from long-period seismology to tides*. Journal of Geodynamics 38, 461 – 476

Scherneck, H. G. (1985): *Tidal gravimeters: environmental effects, response and data acquisition*. Marees Terrestres Bulletin d'Informations 94, 6269 – 6278

Warburton, R. J., Goodkind, J. M. (1977): *The influence of barometric-pressure variations on gravity*. Geophys. J. R. astr. Soc. 48, 281 - 292

Weise, A. (1992): *Neigungsmessungen in der Geodynamik – Ergebnisse von der 3-Komponenten-Station Metsähovi*. Dissertation TU Clausthal (Germany)

Weise, A. Jentzsch, G., Kiviniemi, A., Kääriäinen, J. (1999): *Comparison of long-period tilt measurements: results from the two clinometric stations Metsähovi and Lohja, Finland*. Journal of Geodynamics 27, 237 - 257

Wenzel, H. G. (1996): *The nanogal software: Earth tide data processing package ETERNA 3.30*. Marees Terrestres Bulletin d'Informations 124, 9425 – 9439

Zürn, W., Wenzel, H. G., Laske, G. (1991): *High quality data from LaCoste-Romberg gravimeters with electrostatical feedback: a challenge for superconducting gravimeters*. Marees Terrestres Bulletin d'Informations 110, 7940 – 7952

Zürn, W., Widmer, R. (1995): *On noise reduction in vertical seismic records below 2 mHz using local barometric pressure*. Geophysical Research Letters, Vol. 22, No. 24, AGU, Washington DC (USA), 3537 – 3540

APPLICATION OF WAVELET TECHNIQUE TO THE EARTH TIDES OBSERVATIONS ANALYSES

Andrzej Araszkiewicz[1), 2)]
Janusz Bogusz[1)]

[1)] *Department of Geodesy and Geodetic Astronomy, Warsaw University of Technology*
[2)] *Institute of Geodesy and Cartography, Warsaw*

1. INTRODUCTION

Wavelet analysis is a powerful and popular tool for the analysis of non-stationary signals. The wavelet transform is a joint function of the time series of interest *x(t)* and an analysing wavelet *ψ(t)*. This transform isolates signal variability both in time *t*, and also in scale *s*, by rescalling and shifting the analysing wavelet. The wavelet itself can be said to pay the role of a lens through which a signal is observed, and therefore, it is important to understand how the wavelet transform depends upon the wavelet properties. Such understanding would permit the identification of optimal wavelets which most accurately represent signal characteristics in the properties of the transform. This paper presents the results of the diploma thesis based on the application of the wavelet transform to the analyses of the Earth tides observations recorded in the Astro-Geodetic Observatory at Jozefoslaw.

2. METHOD

Wavelet transform is derived from Fourier Transform, but it is much more flexible. The FT could not be used to the non-stationary time series, in which stochastic characteristics change in time. If we assume that non-stationary signal consists of several stationary signals the STFT (Short-Time Fourier Transform) could be applied. The signal is divided into small segments which are assumed to be stationary. The main role in such analysis plays "window", which is used to divide the signal. But in this case we act with indeterminacy. If narrow window is chosen the accurate information about time is obtained, less accurate about frequency. In case of wide window just the other way about.
Continuous Wavelet Transform (CWT) assumes that the signal is a composition of a several functions (wavelets in this case). CWT of a signal $x(t) \in L^2(\Re)$ is a sequence of projections onto rescaled and translated versions of an analysing functions of wavelets *ψ(t)* (Mallat, 1989):

$$CWT_x^{\psi}(s,\tau) = \int_{-\infty}^{\infty} x(t)\psi_{s,\tau}(t)dt \qquad (1)$$

where:

$$\psi_{s,\tau}(t) = \frac{1}{\sqrt{|s|}}\psi\left(\frac{t-\tau}{s}\right), \quad s,\tau \in R, \quad s \neq 0 \qquad (2)$$

The equation presents wavelet function, which depends on two parameters:

    s - scale coefficient,
    τ - time shift.

Using this equation we can derive the family of the functions from *ψ* - mother wavelet using scale factor and shift. The wavelet has finite length and is concentrated around *t*=0 point and its mean value is equal to zero:

$$\int_{-\infty}^{+\infty} \psi(t)dt = 0 \qquad (3)$$

The $1/\sqrt{s}$ part is also worth mentioned. It is a kind of normalization of the signal to keep the same energy for all scales.

The algorithm of CWT contains:

- comparison of the wavelet with the beginning of the signal. The factor C is calculated which could be interpreted as the correlation between wavelet and the part of the signal;
- using shift factor τ the next part of the signal is chosen and the subsequent comparison is done. This step is repeated until the whole signal is compared.
- using scale factor we extend the wavelet and make the comparison once again.

3.   DATA

The data analysed in this project was collected at Astro-Geodetic Observatory in Jozefoslaw. The Observatory belongs to the Warsaw University of Technology and is placed at the suburb of Warsaw, 15 km from the city centre, but the vicinity is rather quiet. The data had been collected by the ET-26 LaCoste&Romberg gravimeter since January 2002. To these analyses the data from 2006 to 2008 were used because of the highest consistency. The data was only despiked and degapped using TSoft software (Van Camp and Vauterin, 2005).
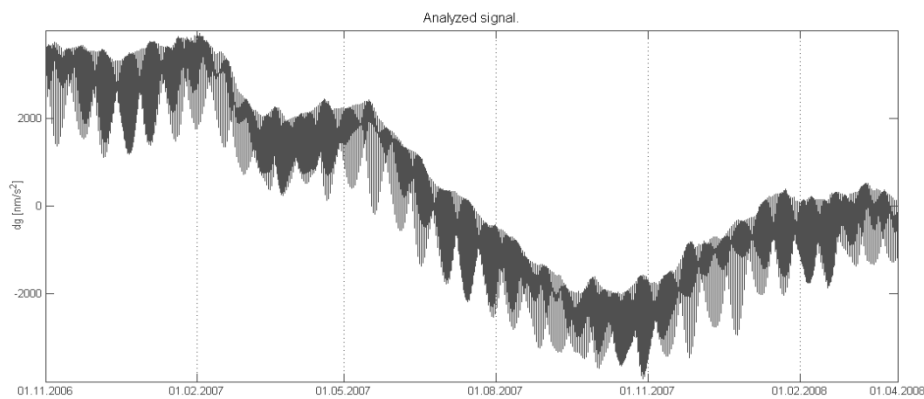

Fig. 1. Tidal data from LC&R ET-26 gravimeter.

4.   TOOL

For the calculations Matlab software was used with help of additional library - Wavelet Toolbox and complex Morlet wavelet (Goupillaud et al.,1984):

$$\psi(x) = \frac{1}{\sqrt{\pi \cdot f_b}} e^{2i\pi f_c x} e^{-\frac{x^2}{f_b}} \qquad (4)$$

In Matlab this wavelet is described as cmor"f_b-f_c" and depends on two parameters:

f_b - bandwidth parameter;

f_c - centre frequency.

and different modifications of Morlet complex wavelet are possible, presented in figure 2 (solid and dashed lines represent real and imaginary part respectively).
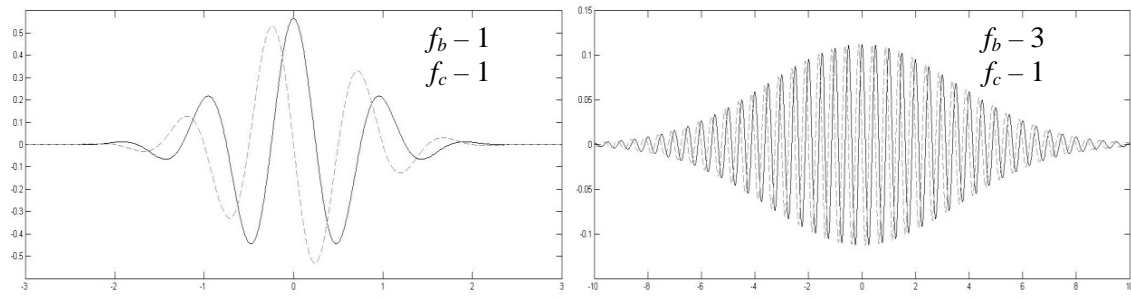
Fig. 2. Modification of complex Morlet wavelet.

Base on Nyquist rule Matlab allows to determine wavelet coefficients C for periods from 0 to f_n, where f_n is equal to half of the signal's length. On these conditions maximum determinable scale is:

$$S = \frac{1}{2} \cdot \left(2^n\right)$$

(5)

where n is the highest power of 2 to be comprised in the original signal's length.

5.   RESULTS

The analyses have been started with complex Morlet wavelet f_b=3 and f_c=1 (cmor3-1) obtaining spectrogram describing power spectrum (C-coefficients) in the particular frequencies occurred in the original gravity signal (fig. 3).
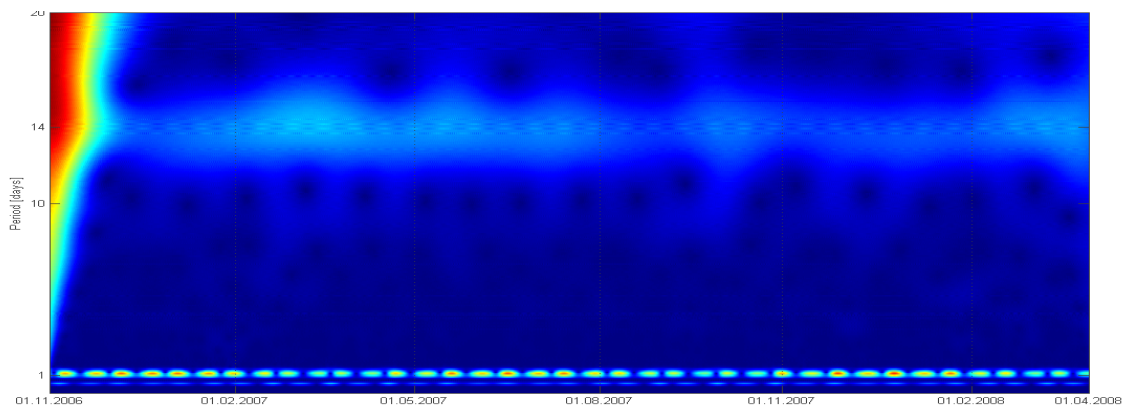

Fig. 3. Morlet Wavelet Spectrum, cmor3-1.

Application of cmor3-1 wavelet did not allowed to separate particular diurnal and semi-diurnal tidal waves (left figure below). Better solution was obtained using cmor25-8 wavelet (right figure below).
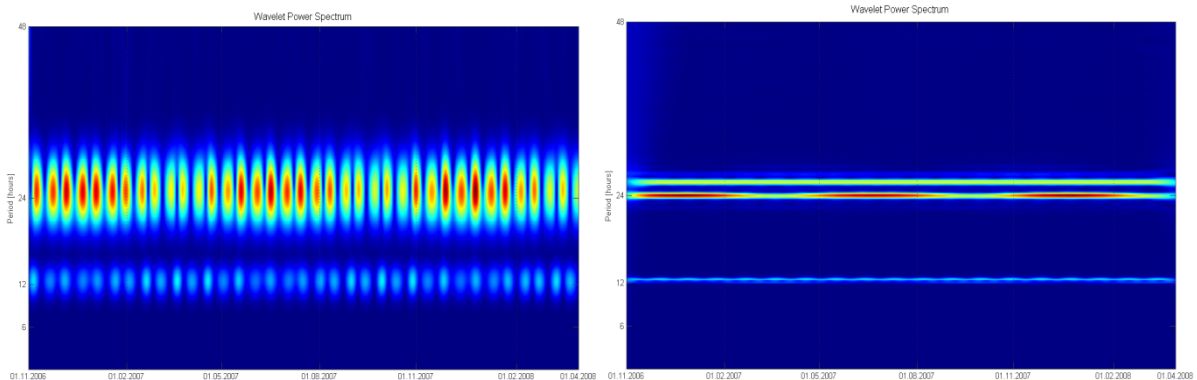

Fig. 4. Comparison of Morlet Wavelet Spectrum (cmor3-1 – left, cmor25-8 – right).

As it was mentioned before the results of the CWT is the matrix of *C*-coefficients, which are the amounts of the energy in particular periods. To recalculate it into amplitude the linear relationship was used (Kalarus, 2007):

$$A = \frac{1}{C_n} \cdot C \qquad (6)$$

where:

    A is the amplitude,

    C - wavelet coefficient,

    C_n - integral from the envelope of the wavelet function used for calculations.

In practice, C_n is calculated by making wavelet transform of the artificial signal of amplitude 1 and period determined by the transform of the original signal. The C_n coefficients obtained by this method are different for different frequencies (Fig. 5).
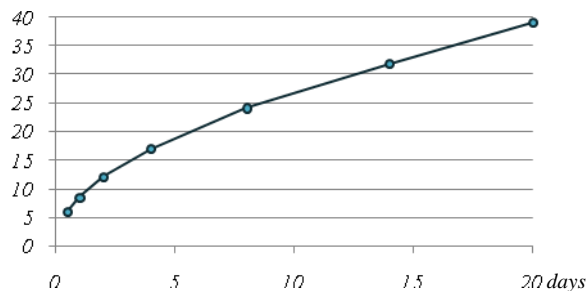

Fig. 5. Calculated values of C_n factors.

6. COMPARISON

The amplitudes obtained by this method were compared to those determined using classical least square manner (Chojnicki, 1977) calculated using Eterna 3.4 (Wenzel, 1996) with the same original signal of gravity changes (see table 1).

Table 1. Frequencies of the tidal waves.

Frequency [cycle/day] from	to	Name	Amplitude [nm/s^2]	Std. dev. [nm/s^2]	Frequency [cycle/day] from	to	Name	Amplitude [nm/s^2]	Std. dev. [nm/s^2]
0.501370	0.842147	SGQ1	2,76	0,143	1.035251	1.054820	J1	27,45	0,124
0.842148	0.860293	2Q1	8,83	0,135	1.054821	1.071833	SO1	4,61	0,128
0.860294	0.878674	SGM1	10,45	0,137	1.071834	1.090052	OO1	14,85	0,089
0.878675	0.896968	Q1	66,09	0,127	1.090053	1.470243	NU1	2,85	0,087
0.896969	0.911390	RO1	12,53	0,131	1.470244	1.845944	EPS2	2,43	0,058
0.911391	0.931206	O1	346,55	0,124	1.845945	1.863026	2N2	8,44	0,061
0.931207	0.949286	TAU1	4,61	0,165	1.863027	1.880264	MU2	10,21	0,067
0.949287	0.967660	M1	27,19	0,109	1.880265	1.897351	N2	64,11	0,065
0.967661	0.981854	CHI1	5,37	0,122	1.897352	1.915114	NU2	12,23	0,068
0.981855	0.996055	PI1	9,15	0,149	1.915115	1.950493	M2	335,38	0,068
0.996056	0.998631	P1	161,06	0,156	1.950493	1.970390	L2	9,60	0,102
0.998632	1.001369	S1	3,49	0,227	1.970391	1.998996	T2	9,15	0,065
1.001370	1.004107	K1	480,85	0,140	1.998997	2.001678	S2	155,54	0,066
1.004108	1.006845	PSI1	4,49	0,150	2.001679	2.468043	K2	42,40	0,049
1.006846	1.023622	PHI1	7,07	0,156	2.468044	7.000000	M3M6	3,64	0,037
1.023623	1.035250	TET1	5,21	0,132					

From the comparison we can notice that there is a big discrepancy in K1 frequency. We can claim that classical manner based on the least squares method better separate P1, K1 and S1 waves. The same conclusion could be pointed out: wavelet transform of this signal did not separated correctly S2 and K2 waves (see fig. 6).
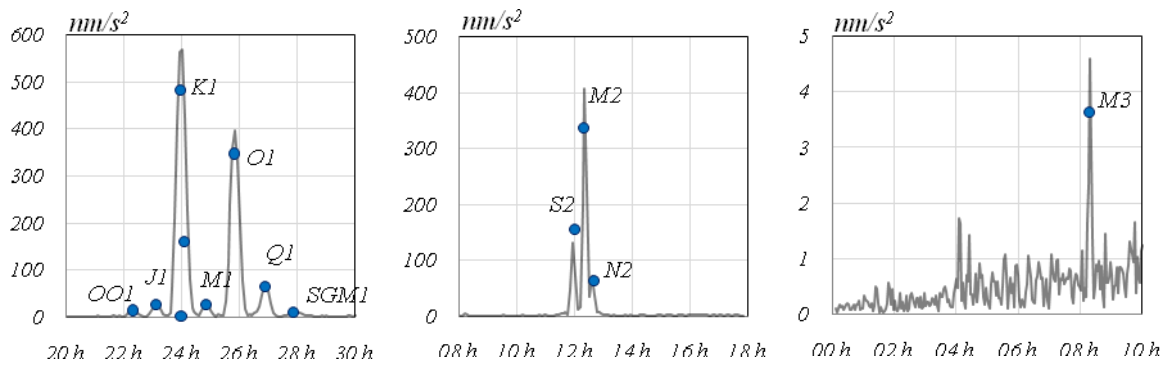
Fig. 6. Tidal waves amplitudes (solid line – CWT, 1st July 2007, ● ETERNA).

7. DIURNAL AND SUB-DIURNAL WAVES

To investigate frequency of the diurnal and sub-diurnal waves Morlet wavelet cmor25-8 was used, the results are presented in fig. 7 to 9.
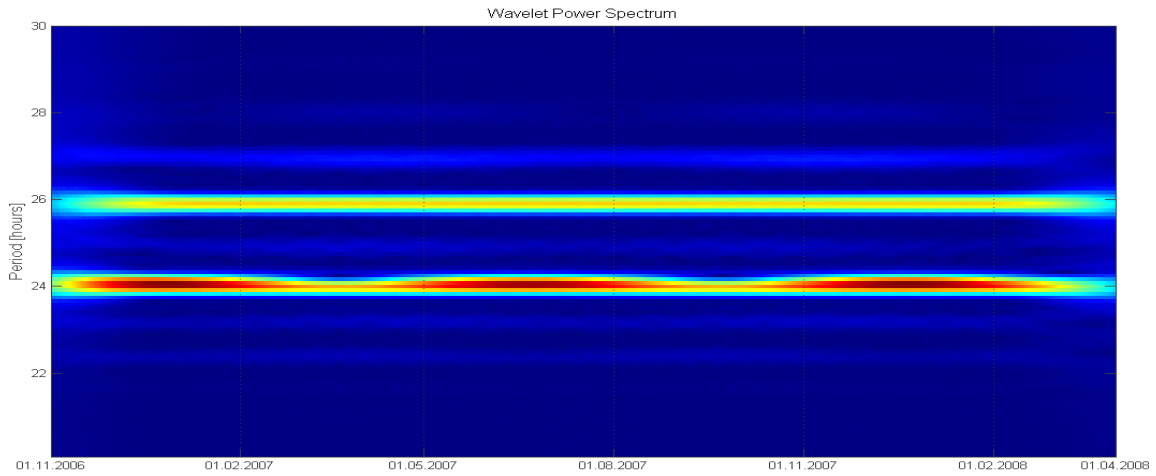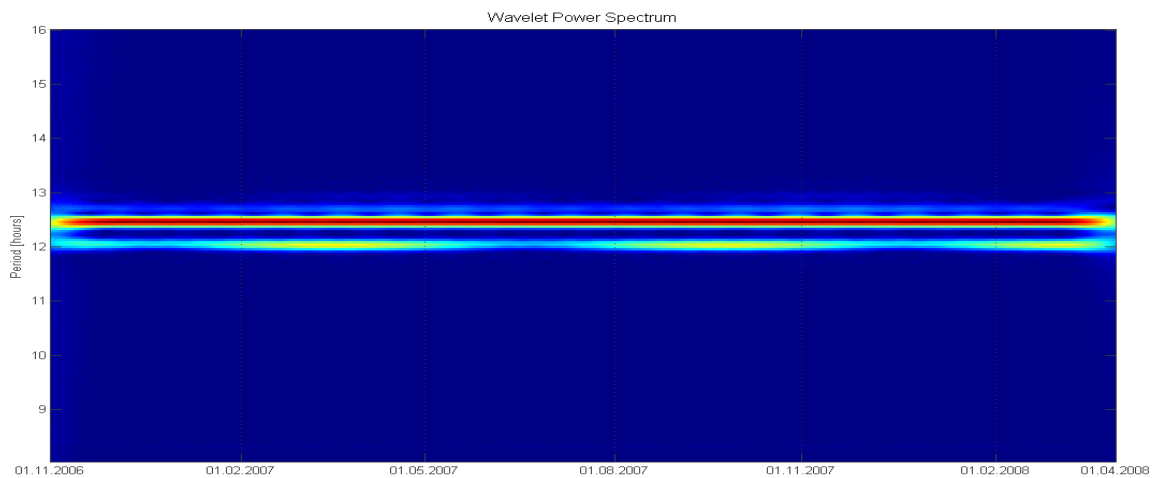

Fig. 7. Morlet Wavelet Spectrum, diurnal.

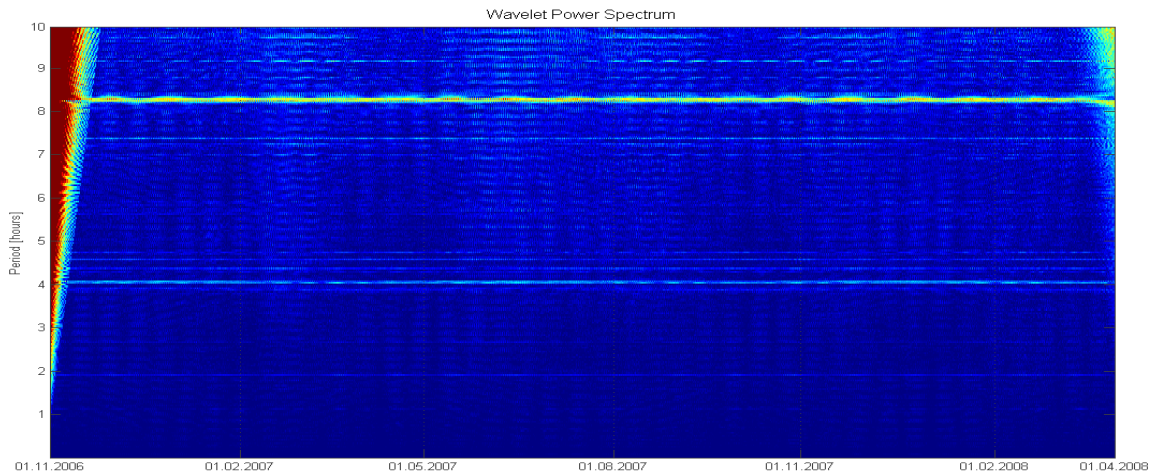Fig. 8. Morlet Wavelet Spectrum, semi-diurnal.

Fig. 9. Morlet Wavelet Spectrum, sub-diurnal.

The considered time span allowed to identify 7 diurnal waves and 4 sub-diurnal waves . They are:
- PSK1, O1, Q1, J1, M1, OO1, SIG1,
- M2, S2K2, N2, M3.

Table 2 presents differences between theoretical and obtained periods, the maximum difference did not exceed 5 minutes.

Table 2. Comparison of the waves period.

Name	Period [h]			Differences [min]
	theoretic	determined		
		range	mean value	
SGM1	27.848388	27.8333 – 28.0000	27.91667	4.1
Q1	26.868357	26.7500 – 26.9167	26.83333	2.1
O1	25.819342	25.7500 – 25.9167	25.83333	0.8
M1	24.833248	24.7500 – 24.9167	24.83333	0.0
PSK1	23.934469	23.9167 – 24.0000	23.95833	1.4
J1	23.098477	23.0833 – 23.1667	23.12500	1.6
OO1	22.306074	22.2500 – 22.3333	22.29167	0.9
N2	12.658348	12.5833 – 12.7500	12.66667	0.8
M2	12.420601	12.3333 – 12.5000	12.41667	0.2
S2K2	12.000000	11.9167 – 12.0833	12.00000	0.0
M3	8.280401	8.2500 – 8.3333	8.29167	0.7

8. MODULATION

At this stage changes of the wave's amplitudes were investigated.

Changes of the PSK1 wave's amplitude ranged from 450 to 630 nm/s^2 and are periodical. Major period is 180.5 days, minor 24-hours, 14- and 28-days, but they are of range 1 to 5 nm/s^2. O1 wave is much more stable. Changes of the amplitude are mainly half-yearly and oscillate from 398 to 408 nm/s^2. M1 wave arises from the Earth-Moon motion, so the main modulation is 27.5 days, but the amplitude is rather small: 5 to 7 nm/s^2. Conclusions from the modulation of J1, OO1 and SIG1 amplitudes are very similar. 28- and 14-day changes, but also 9- and 7-day, rather unexpected, but very small and at the level of the accuracy of the measurements. Chart of Q1's amplitude changes show strong 3-month modulation (30 nm/s^2) and 9-days, but less of importance.

M2 wave is the most stable from sub-diurnal waves. Changes of the amplitude are about 8 nm/s^2, which amount 2%. 14- and 180-days modulations could be clearly seen. The highest modulation was investigated in S2K2 wave. These oscillations are related to the thermal activity of the Sun and reach up 120 nm/s^2. Using CWT the N2 wave was also identified as the weakest possible. The amplitude varies from 55 to 90 nm/s^2 and changes with 28-days and half of the year. The last from sub-diurnal waves that were determined is M3. This is relatively weak wave, modulation of the amplitude seem to be non-regular.

The wavelet transform allows also for determination of the long-period tides and investigate its properties. As the example declinational wave Mf was taken. The amplitude is about 100 nm/s^2, but changes from 63 to 118 nm/s^2. The range of the observations was relatively short so only 60-day period of changes was found.

The wave's modulation are results from drumming near frequency's waves, that's the reason why modulation are periodic (tidal period).

But from previous results (Chojnicki, 1996; Bogusz and Klek, 2008) we can claim that some part of this modulation is not artificial and represents real, geophysical effect.
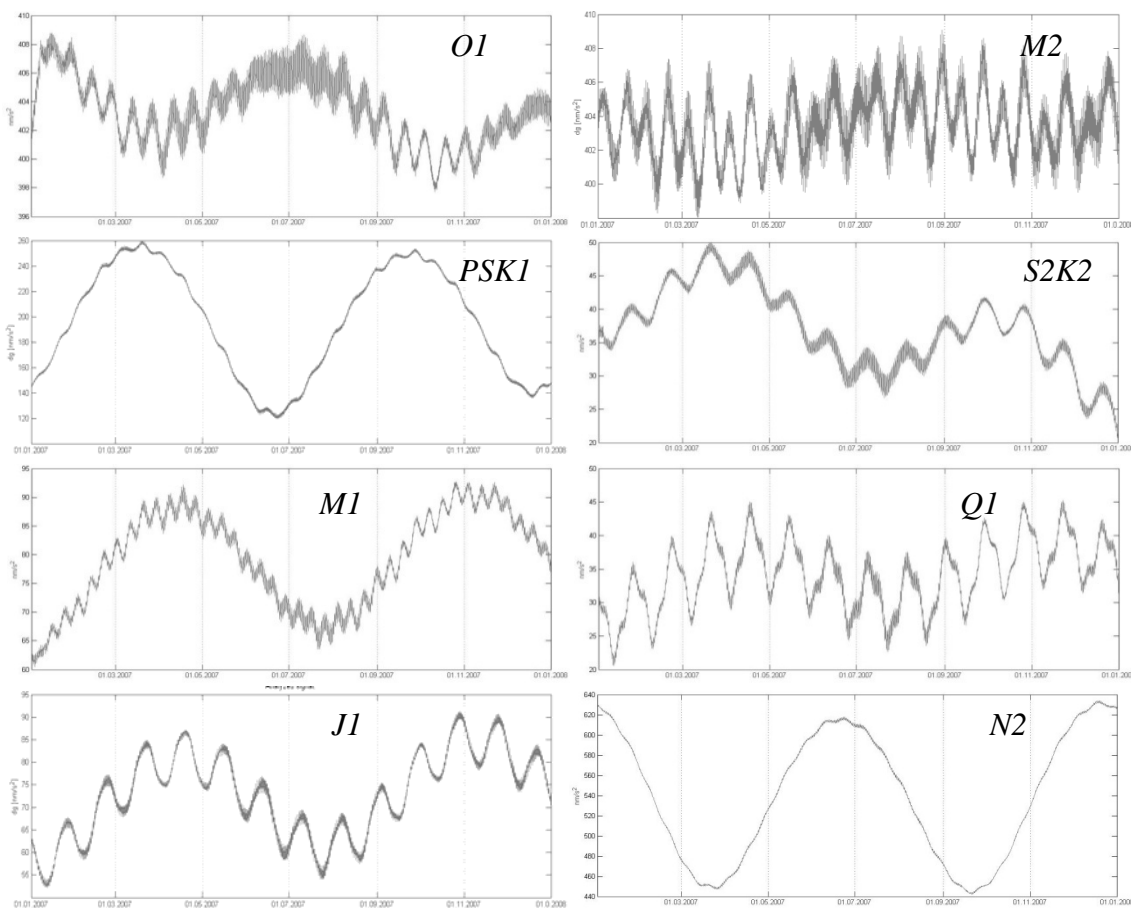

Fig. 10. Amplitude's seasonal modulation.

9. CONCLUSIONS

This investigation was aimed at application of the wavelet transform to the Earth tides observations analyses. It was done upon the data collected in Astro-Geodetic Observatory at Jozefoslaw by LC&R Et-26 gravimeter. Wavelet transform was made using Morlet functions with different parameters to recognise its usefulness to this type of data. Calculations were made in the Matlab environment. The results were compared to the previously obtained by different method. Good consistence was found in frequencies (with theoretical) and amplitudes (compared to Eterna) as well. A big advantage of WT is the ability of amplitude's seasonal modulation investigation. Seasonal changes of the main diurnal and sub-diurnal tidal waves were presented. Disadvantage is lack of phase determination, obtainable in least square method. WT could be also implemented to investigation of the long-period tides. Wavelet analysis is now a very popular tool for the analysis of non-stationary signals and after careful setup can be implemented to the selected analyses of the Earth tides observations.

BIBLIOGRAPHY

1. Bogusz J., Klek M. (2008): "Seasonal Modulation of the Tidal Waves". Proceedings of the European Geosciences Union General Assembly 2008 session G10 "Geodetic and Geodynamic Programmes of the CEI (Central European Initiative)", Vienna, Austria, 13 – 18 April 2008. Reports on Geodesy No. 1(84), 2008, pp. 79-86.
2. Chojnicki T. (1996): "Seasonable modulation of the tidal waves 1993". Publications of the Institute of Geophysics Polish Academy of Sciences. F-20 (270), 1996.
3. Chojnicki, T. (1977): "Sur l'analyse des observations de marees terrestres". Ann. Geophys., 33, 1/2, Edition du CNRS, Paris, pp.157-160.
4. Goupillaud P., Grossman A. and Morlet J. (1984): "Cycle-Octave and Related Transforms in Seismic Signal Analysis". Geoexploration, 23:85-102, 1984.
5. Kalarus M. (2007): "Analiza metod prognozowania parametrów orientacji przestrzennej Ziemi". PhD Thesis. Warsaw University of Technology Printing Office. Warsaw, 2007.
6. Mallat S. (1989). "A theory for multiresolution signal decomposition: the wavelet representation". IEEE Pattern Anal. and Machine Intell. no. 7, 11, 674693.
7. Matlab (2006). The Mathworks, inc. - site help. http://www.mathworks.com.
8. Van Camp. M., Vauterin P. (2005): "TSoft: graphical and interactive software for the analysis of time series and Earth tides". Computer&Geosciences, 31(5), pp. 631-640.
9. Wenzel H.-G. (1996): "The nanogal software: Earth tide processing package ETERNA 3.30". Bulletin d'Information des Marées Terrestres (BIM), No. 124, pp. 9425-9439, Bruxelles, 1996.

Gravimetric Tide observation at Lake Nasser Region, Aswan, Egypt

R.M. Hassan, E.M. Abdelrahman, A. Tealeb, K.H. Zahran and G. Jentzsch

ABSTRACT

The LaCoste and Romberg gravimeter D-218 of the National Research Institute of Astronomy and Geophysics (NRIAG) was installed in the tidal gravity station in the ground floor of the main building of the Seismological Centre at Sahari, close to Lake Nasser, Aswan, Egypt. Two years of continuous gravity observations (from October 2002 to December 2004) were available to conduct the current study. The main objectives of this study are to determine the real response of the crust to the tidal forces and, in consequence, to increase the accuracy of the geodetic observations, which were initiated due to the continuous seismological activities in this region, and, in addition, to shed more light on the effect of variation of the Lake level to the surrounding crust. The analysis of tidal gravity observations at Aswan tidal station shows discrepancies between the observed tidal parameters and the synthetic tidal parameters. These discrepancies may be due to variations of lake level, which are seen in the variable load of the lake and the change of underground water level. The residuals are generally quite high: They cover about 300 nm/s². The amplitude spectrum shows a noise level in the diurnal band of 16 nm/s² and 9 nm/s² in the semidiurnal band, but no distinct tidal lines.

1. Introduction

The main objective of geodetic and geophysical activities, which have been initiated in Lake Nasser region after the occurrence of November 1981 earthquake and the continued seismic activities, is to understand the seismic mechanism in this region, to study recent crustal movements around active faults responsible for the seismological activities and to evaluate a possible relation between variation of water level in the lake and seismicity. The results of gravity and GPS observations around Lake Nasser showed that the annual gravity variation around the lake is in the order of tens of microgals; on the other hand, the crustal deformation around the lake is in the order of few millimetres. Thus, to study such small phenomena, higher accuracy in both gravity and GPS are needed. Consequently, accurate determination of gravity variations and local site deformations due to Earth tides are necessary. A tidal gravity station was decided to be installed close to Lake Nasser to determine the response of the crust to tidal forces, to study the effect of the loading of the lake, and to increase the accuracy of geodetic and geophysical observations in the area. Beside gravity also tilt measurements are suitable for monitoring effects of lake level changes to the crust: Jentzsch and Koß (1997) used borehole tilt measurements to observe tilts associated with the change of the level of the artificial reservoir Blå Sjø in southern Norway. This monitoring was conducted to evaluate both the tidal parameters and the long-term drift and to test the correlation of temporal variations to water level variations. In addition, a comparison of long-period measurements was carried out in southern Finland. The results from the two clinometric stations Metsähovi and Lohja, Finland (Weise et al., 1999), showed that continuous tilt measurements are suitable not only for the investigation of small-scale but also for regional-scale crustal dynamics. However, to benefit from the high sensitivity of tilt and strain measurements, observations have to be carried out inside deep tunnels or boreholes. Thus, because gravity measurements can be carried out on or near the surface, it was decided to install a tidal gravity station at Lake Nasser (Hassan et al., 2007).

2. Objectives of Aswan Tidal Gravity Station

Recent crustal deformation studies around Lake Nasser area demand accurate corrections for tidal forces. Zahran (2005) showed that even when using high accurate Earth and ocean tide models, tidal observation is needed, if high precision observations are to be obtained. Moreover, variations of the water level of the lake deform the crust and as a result, affect the geodetic observations, which are mostly located very close to the lake. Thus, evaluation of the effect of the water level variation of the lake is strongly needed. Finally, continuous gravity observations can also shed some light on the response of Lake Nasser to seismic activities in this region. Generally, the objectives of Aswan tidal gravity station can be summarized in the following points:

a. Continuous gravity observations to determine the elastic parameters of the Earth's crust and, thus, to increase the accuracy of geodetic observations in the region;
b. Determination of the variation of the elastic response of the Earth's crust as a result of the variable load of the lake;
c. Evaluation of the effect of the load of the lake, as seen from continuous gravity observations.

3. Description of the Station

The tidal gravity station is located at the ground floor of the main building of the Seismological Centre at Sahari, Aswan, which is a few tens of meters away from Lake Nasser. The station coordinates are 24.100° N and 32.600° E, and elevation is 117.00m. The Aswan tidal gravity station consists of two rooms: one for the gravimeter (measuring room), and the other one for recording (registration room). In the measuring room (Fig. 1), a wooden box chamber was designed that consists of double walls of wood and an insulation material between the double walls to keep the sensor (gravimeter) isolated from the surroundings. A pillar of the size 0.5 m x 0.5 m, connected to the bedrock, was established inside the measuring room, which is separated from the construction of the building. The gravimeter used is the LaCoste-Romberg meter D-218 with electrostatic feedback. Test of temperature stability in the sensor room shows that acceptable stability exists; the change is less than 1°C per day. The recording room contains a multi-channel A/D-converter to provide the feedback output to the computer (Fig. 2). Data are logged at high resolution with sampling interval of 5 seconds.

The recording room contains a multi-channel A/D-converter to provide the feedback output to the computer (Fig. 2). Data are logged at high resolution with sampling interval of 5 seconds. The quartz clock in the computer was compared to a GPS clock. A drift of 1.5 minutes per month was found in the quartz clock. Thus, this deviation was corrected every two weeks. The digital multimeter provides ten channels, of which only three are used, two of them for the cross and long levels of the gravimeter to monitor the stability of the meter, and the third one for the feedback output voltage, which reflects the changes of gravity. The resolution of this multimeter is based on a 28 bit A/D converter, that provides the resolution and the dynamic range (1µV to 20 V) needed to cover smaller changes as well as the drift. All data are stored on the hard disk, using a program that was designed under Q basic.

4. Calibration of the Gravimeter D-218

The calibration factors for both the spring of the sensor and the feedback plays an important role for the accuracy of the analysis of tidal records and consequently the accuracy of the separated tidal parameters. Spring calibration of the gravimeter has been carried out by comparing the gravity difference between two gravity stations with known absolute values located close to the Aswan tidal station. The used stations, Sahari and Aswan have a distance of about 15 km and a gravity difference of about 42 mGal.

Figure 1: Gravimeter D-218 in the measuring room of Aswan station.

Figure 2: Registration room of Aswan tidal gravity station.

The calibration factor of the gravimeter has been determined by comparing the observed gravity difference of the gravimeter and the difference between the absolute gravity values. The optimum calibration factor was estimated by a linear fit between the observed calibration factor and the number of readings. The optimum calibration factor is 0.72560±0.01280. The comparison of the observed calibration factor with the one provided by the manufacturer of 0.72815 shows that the disagreement of both factors is not significant. Thus, as this factor of the manufacturer lies well inside the error bars, it has been decided to keep this value. Calibration of the feedback was done by comparing the fine dial reading of the gravimeter with the feedback output. The calibration factor for feedback was found to be -0.887±0.01309 mvolt /dial. This factor converts the output voltage to reading dial.

5. Recording of Data

The data logged were stored in a computer using software developed by the first author, which was designed under Q-basic. Data were logged in a high resolution sampling interval of 5 seconds. The data were stored in files, each of one hour capacity. The ETERNA format used was described by Wenzel (1994). It was adopted for the exchange of high precision and high rate Earth tide data by the working group on High Precision Tidal Data Processing at its meeting in Bonn 1994 (comp. Jentzsch, 1995). This format was used in the tidal analysis. The recording of tidal gravity data started at the end of 2002 and is still going on. The feedback of the D–218 gravimeter returns the beam of the gravimeter to the reading line continuously, also after the occurrence of any earthquake. The changes in air pressure and temperature affect the quality of the recorded data. Besides, the data contain some gaps due to power failure. The raw data, with all noise and local perturbations, are shown in Fig. 3. The data contain, in general, a high drift of about 1,500 nm/s^2 per month in average. The high drift is probably due to the high noise level in the station, and the environmental effects. Because the station is located in a region of seismic activity, therefore, any seismic activity is clearly observed in the raw data. However, a period of two years (from 2003 to 2004) was selected for the tidal analysis, because in this period no big gaps in the data occurred and the noise in the raw data is not so high. Because of the response time of the feedback system there was no additional anti-aliasing filter.
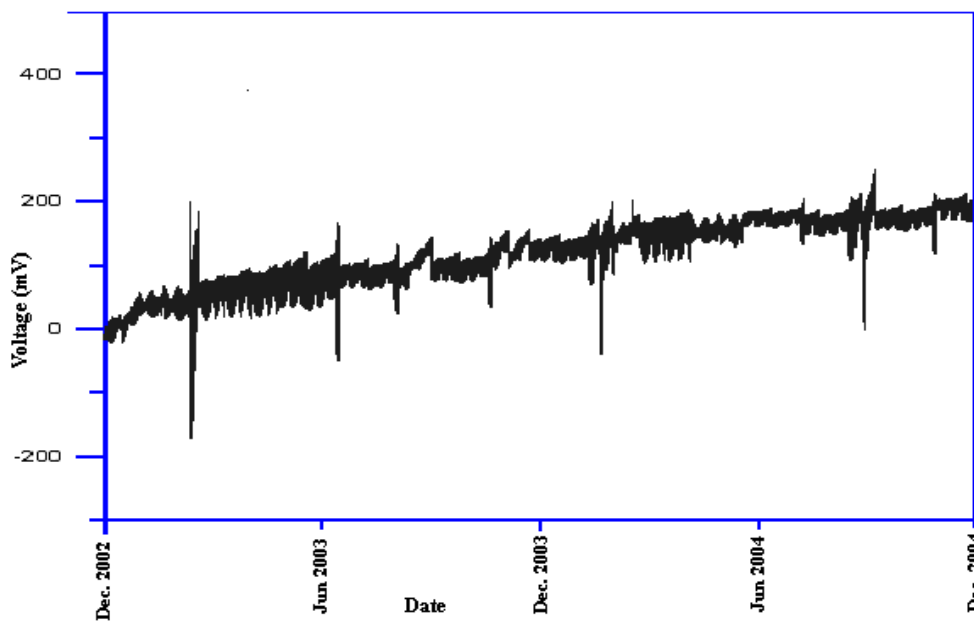

Figure 3: Raw data recorded by D-218 LaCoste & Romberg gravimeter at Aswan station during the period of study (from 2002 to 2004).

6. Analysis of Aswan Tidal Gravity data

The period of two years from October 2002 to December 2004 was selected for the tidal analysis. The analysis of data consisted of two main steps, the pre-processing and analysis. In the first step the 5 second data files for each day were combined into one single file per day, and then, all files were combined into one file. The data were numerically filtered and sampled at 1 min interval. Afterwards, the 1 min data were calibrated and de-tided (synthetic tidal gravity, computed using a-priori tidal parameters). Fig. 4 shows the synthetic tide gravity variation at Aswan station through the studied period. For the pre-processing of high rate Earth tide data the programs DECIMATE,

DETIDE, DESPIKE and PREGRED of Wenzel's package were used. The data pre-processing was carried out using a remove-restore technique. At first, all well-known signals were removed with program DETIDE. With program DESPIKE, the residual signal (the Earth tide sensor drift) was automatically cleaned (de-stepped, de-spiked, and de-gapped) and the known signals were added back to the cleaned residual signal. The interrupted data, such as earthquakes or micro-seismic waves, were deleted, gaps filled and steps corrected automatically. The corrected one minute samples were finally numerically filtered and decimated to 5 min sampling interval and again decimated to one hour sampling interval, using the program DECIMATE. The hourly samples have been used for tidal analysis. Fig.5 shows the pre-processed hourly samples of the recording period. It can be noticed that there is a non-linear drift in the observed hourly data, the linear drift being removed by the processing.

The analysis was carried out using the program ANALYZE of the ETERNA 3.3 package (Wenzel, 1996a, 1997), where the Hartmann and Wenzel (1995a, b) tidal potential catalogue was used. In addition a numerical digital high-pass filtering was applied in order to eliminate the long periodic drift of the instrument.
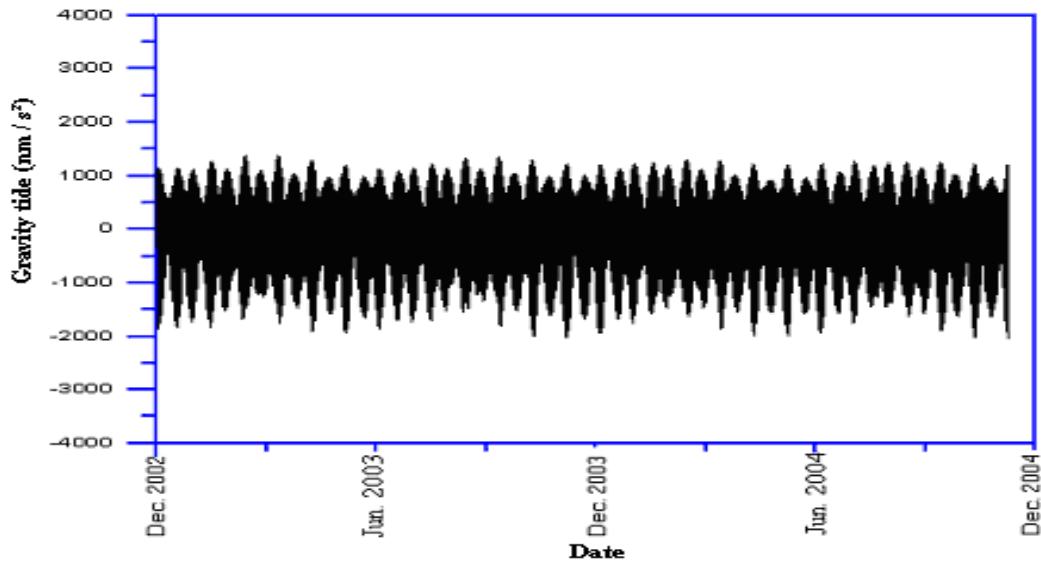

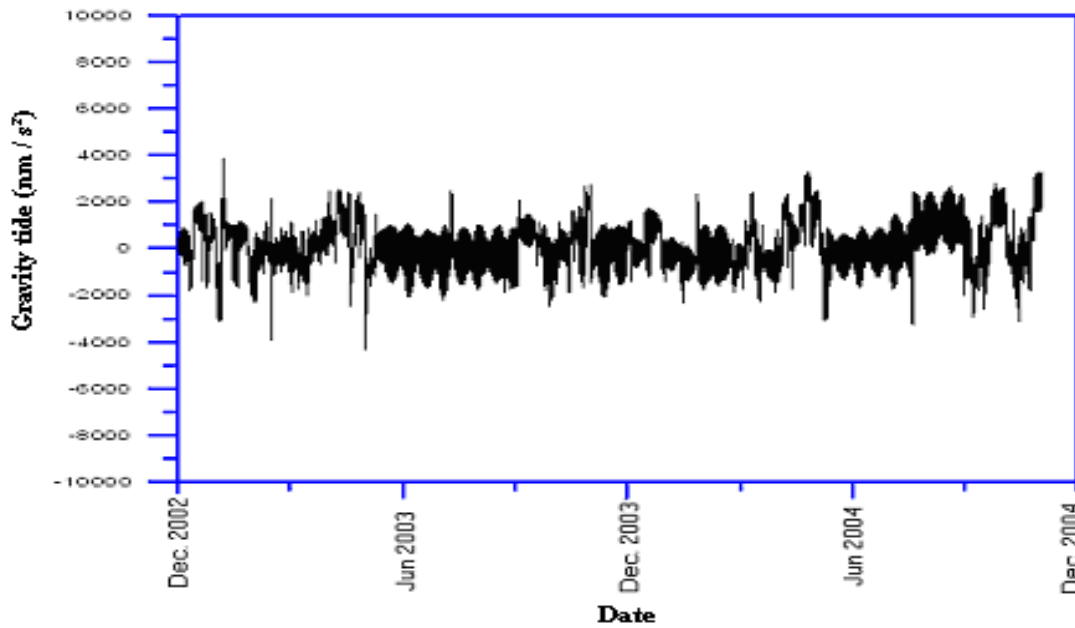Figure 4: Synthetic tidal gravity for a rigid Earth model computed at Aswan station (from 2002 to 2004).

Figure 5: Pre-processed hourly data of gravity tide, observed at Aswan.

7. Results of Tidal Gravity Data

The adjusted tidal parameters, using ETERNA 3.3, are given in Tab. 1. It can be noticed from the table that most waves of the diurnal wave group show an amplification factor close to one and much less than the global amplification factor, i. e., 1.16. In contrary, most of the semidiurnal wave group amplification factors are close to the global value. Almost all wave groups have a phase shift close to zero. Generally, smaller standard deviations in the amplification factors are accompanied by small standard deviations in the phase shift, with smaller standard deviations in the semidiurnal band, especially for wave groups of large amplitudes as M2, both in amplification factor and phase shift.

The highest standard deviation has been obtained for K1 and S2, in phase shift. This could be due to the strong air pressure variation and the high solar variation in a tropic area like Aswan during the day. On the other hand, the high standard deviation of the phase shift may be due to an error in the quartz clock.

Table 1: Adjusted tidal parameters of Aswan tidal gravity station.

Wave	from (cpd)	to (cpd)	Amplitude nm / s²	Amplif. factor	Stand. dev.	Phase shift (degree)	Stand. dev. (degree)
Mf	0.054748	0.501690	38.7448	1.0611	0.0152	0.536	0.378
Q1	0.501370	0.911390	41.8379	1.1070	0.0138	-0.187	0.089
O1	0.911391	0.947991	232.1882	1.1498	0.0115	-0.376	0.119
M1	0.947992	0.981854	5.2569	1.1601	0.0225	-0.724	0.853
K1	0.981855	1.880264	297.5135	0.9906	0.0395	-2.886	1.987
N2	1.880265	1.914128	72.5071	1.1620	0.0215	-1.136	1.158
M2	1.914129	1.950419	476.7849	1.1647	0.0102	2.065	0.023
S2	1.984283	2.451943	227.3244	1.0256	0.0410	2.809	2.854
M3	2.451944	7.000000	9.5189	1.1205	0.0342	0.312	1.538

8. Discussion of Tidal Analysis Results

Evaluation of the quality of observed tidal gravity data was conducted by comparing the observed with theoretical tidal parameters. Thus, the gravity tide parameters were calculated using synthetic tide gravity parameters (Zahran et al., 2005). The synthetic tidal parameters were estimated using the Dehant (1987) rigid Earth model and CSR3.0 ocean tide model (Eanes, 1994). The computations were carried out using the SPOTL-program (Agnew, 1996) at the coordinates of Aswan tidal station. The comparison between observed and predicted tidal parameters at Aswan station is shown in Tab. 2. The analysis of tidal gravity observations at Aswan tidal station shows discrepancies between the observed and synthetic tidal parameters. As can be seen from Tab. 2, there is a low agreement in K1 and M3, whereas O1 and M1 show a good agreement, and a better agreement in N2 and M2. It can be seen also from Tab. 2 that a very low agreement in phase shift is obtained in K1, N2, M3 and S2, whereas Mf, O1 and M1 show little agreement. A better agreement in phase shift can be only obtained in M2 and Q1. The high discrepancies cannot be related to ocean tidal loading, as the large distance between Aswan tidal station and the shore provides a very small ocean loading effect, only. However, these high discrepancies may be due to the variable loading of the lake level variation or the atmospheric loading, which were not considered during the analysis of data. The high phase standard deviations could be due to the error in quartz clock during recording the data.

Table 2: Comparison between observed and predicted tidal parameters at Aswan station.

Wave	Ampl. fact. (predicted)	Ampl. fact (observed)	Ampl. fact (discrepancies)	Pha. Shif. (predicted)	Pha. Shif. (observed)	Pha. Shif. (discrepancies)
Mf	1.1411	1.0611	0.0800	0.210	0.536	-0.033
Q1	1.1564	1.1070	0.0494	-0.247	-0.187	0.061
O1	1.1562	1.1498	0.0064	0.080	- 0.376	0.456
M1	1.1507	1.1601	-0.0194	0.343	0.724	-0.381
K1	1.1352	0.9906	0.1446	-0.207	-2.885	2.678
N2	1.1599	1.1620	-0.0021	2.543	-1.136	3.679
M2	1.1599	1.1647	-0.0048	2.033	2.065	-0.032
S2	1.1599	1.0256	0.1343	0.627	2.809	-2.182
M3	1.1019	1.1205	0.1414	1.700	0.312	1.388

9. Gravity Residuals and Conclusions

The tidal gravity residuals are given in Fig. 6. The residuals have a general range of about 300 nm/s². In some periods, this range reaches 500 nm/s², and in other periods reaches to 750 nm/s². Significant anomalies can be recognized in some periods in the residual gravity. There is a modulation in time, indicating that the tidal gravity factors are not stable, that can be associated to instrumental or environmental factors. The residual gravity signals observed at Aswan show seasonal periods. The amplitude spectrum of residual gravity is very important to prove if the tidal waves are completely separated or not. The ANALYZE program allows the computations of the Fourier amplitude spectrum of the residuals. The Fourier amplitude spectrum of the residuals can be seen in Fig. 7. It shows a noise level in the diurnal band of 16 nm/s² and in the semidiurnal band of 9 nm/s². The significant energy in the residual spectrum may be due to the timing problem of the quartz clock, and air pressure variation, which were not considered during registration and analysis. Besides, the high energy in the diurnal band may be due to the variation of water level in the lake.
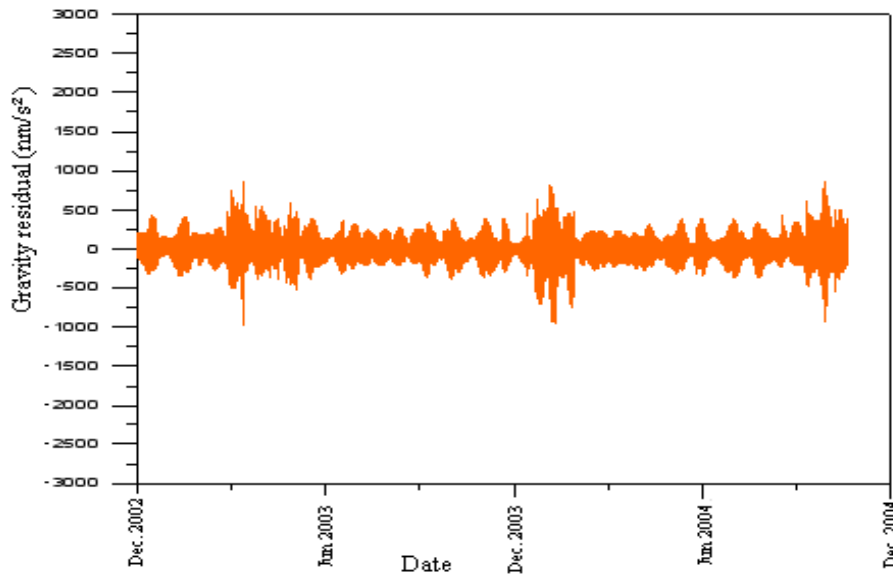
Figure 6: Residuals of gravity tides, observed with gravimeter D-218 at Aswan station (from 2002 to 2004).
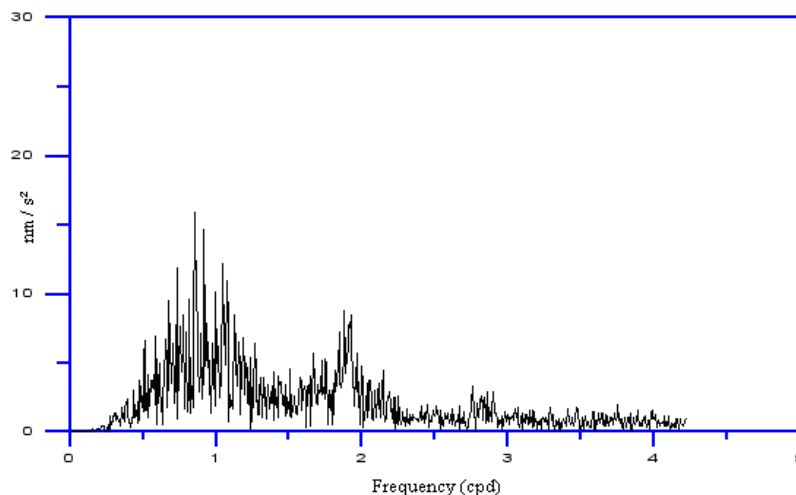
Figure 7: Fourier amplitude spectrum of residual gravity tide at Aswan station.

References

Agnew, D. C., 1996. SPOTL: Some programs for ocean - tide loading. Scripps Institution of Oceanography. SIO Reference Series 96-8.

Dehant, V., 1987. Tidal parameters for an inelastic Earth. PEPI, Vol. pp. 97-116.

Eanes, J., 1994. Diurnal and semidiurnal tides from TOPEX/POSEIDON altimetry (Abstract). Eos Trans. AGU, vol. 75(No. 16), Spring Meet. Suppl., 108p.

Hartmann, T. and Wenzel, H. G., 1995a. The HW95 tidal potential catalogue. Geophys. Res. Lett., vol. 22, pp. 3553-3556.

Hartmann, T. and Wenzel, H. G., 1995b. Catalogue HW95 of the tidal potential Bull. Inf. Marèes Terrestres, vol. 123, pp. 9278-9301.

Hassan, R. M., 2007. Tidal gravity observations at Nasser Lake area, Aswan, Egypt. Dissertation, Geophysics Department, Faculty of Science, Cairo University, 147 pp**.**

Jentzsch, G., 1995. Report of the Working Group on 'High Precision Tidal Data Processing'. Proc. 12th Int. Symp. Earth Tides, Beijing, August 1993, Science Press, Beijing, 1924.

Jentzsch, G. and Koß, S., 1997. Interpretation of long-period tilt records at Blå Sjǿ, Southern Norway, with respect to the variations of the lake level. Phys. Chem. Earth, vol. 22, pp. 25 – 31.

Weise, A., Jentzsch, G., Kiviniemi, A. and Kääriäinen, J., 1999. Comparison of long period tilt measurements: Results from the two clinomatic stations Metsähovi and Lohjia / Finland. J. of Geodynamics, vol. 27, pp. 237 – 257.

Wenzel, H. G., 1994. PRETERNA a preprocessor for digitally recorded tidal data. Bull. d'Inf. Marèes Terr., vol. 118, pp. 8722 – 8734.

Wenzel, H. G., 1996a. The nanogals software: Earth tide data processing package ETERNA 3.30. Bulletin d'Inf. Marèes Terr., vol. 124, pp. 9425 9439.

Wenzel, H. G., 1997. Analysis of the Earth tide observations In: Wilhelm, H.,W. Zürn and H. -G. Wenzel (Eds),Tidal Phenomena. Lecture Notes in Earth Sciences, Springer Verlag, Berlin, Germany, pp. 59-75.

Zahran, K. H., Jentzsch, G. and Seeber, G., 2005. World – wide synthetic tide parameters for gravity and vertical and horizontal displacements. J. Geod., vol. 79, pp. 293-299.

Zahran, K. H., 2005. Benefit of tidal observations to gravity and GPS networks. Egyptian Geophys. Soc. Journal, vol. 3, No. 1, pp 89-98.

Hydrological Signals due to the Seasonal Variation of Lake Nasser and its Effect to the Surrounding Crust as Deduced from the Tidal Gravity Observations

Hassan, R. M., E.M. Abdelrahman, A. Tealeb, K.H. Zahran and G. Jentzsch

Abstract

Impounding of Lake Nasser started in 1964 and reached the highest water level so far in 1978 with a capacity of 133.8 km^3. It is extending 500 km in southern Egypt and northern Sudan, thus forming the second largest man-made lake in the world. The water level fluctuates between 168m and 178m, the cycle being divided into four different periods of inflow, stability, discharge, and stability again. The variation of the mass of the water of the reservoir changes the potential field either by loading or by change of the ground water level. To detect these signals two years of continuous gravity measurements (from the year 2002 to the year 2004) have been used from a tidal station installed very close to the Lake. A combined plot of water level variation and residual gravity shows that the residual gravity follows water level variations with a time delay. Two methods have been used in the current study to evaluate the gravity variations in the tidal records due to variations of water level at Lake Nasser. In the first method, the data were divided into blocks, each block represents an epoch of a certain water level in the lake. These blocks reflect the situation in the lake during the decrease, stability, and increase of water level. The tidal parameters at different blocks with different water levels show some changes. These changes reach up to 4% in amplitude factors, and 0.5° in phase shifts. The variations in the elastic parameters follow to some extent the variations of water level in the lake. In the second method, cross-correlation was applied between residual gravity and change of water level in the lake. Generally, a moderate correlation coefficient (0.556) between residual gravity variation and water level variation, and a weak correlation coefficient (0.480) between residual gravity and ground water variation were recognized. Correlation coefficients of selected blocks follow to some extent the values of water level variation on one side and ground water variation on the other side. The study shows that variations of the Lake level affect the surrounding crust significantly. Variation of the lake has to be modelled and considered in the geodetic and gravity observations in this region if higher accuracy is to be achieved.

1.   Introduction

The filling of large reservoirs changes the stress regime, either by increasing vertical stress (compression) by loading or increasing pore pressure through the decrease of effective normal stress (Snow, 1972; Bell and Nur, 1978; Simpson, 1986; Roeloffs, 1988). At Lake Nasser, water level fluctuates four times during the year, according to the cycle of charge (inflow) and discharge (outflow), followed each by a period of stabilisation. The variations of water level in the lake affect the dynamic stability of the area, either by variable induced loading or variation in the underground water level. On the other hand, the analysis of tidal gravity observations at Aswan tidal station, which is very close to Lake Nasser, shows discrepancies between the observed and synthetic tidal parameters. These discrepancies may be due to variations in water lake level. In the region of Lake Nasser, the Nubian sandstones cover a large area, with a porosity of about 25%. So, any change in water level in the lake changes the underground water level. Seepage of water of the lake into the underground depends on the types of rocks in the underground, their state of weathering and tectonic influences (formation of clefts and cavities of different sizes). The run-off depends on the properties of superficial material, the evaporation on meteorological parameters (air temperature, humidity of air, and wind) and plant cover, etc. In hydrologic modelling, generalized input data and parameters are commonly used, which are representative for a certain area or a certain period of

time. In addition, models for gravimetric purposes should describe with high accuracy the actual hydrologic situation in the area under consideration and its variation with time. At Lake Nasser area, in the epochs of recharge the increase of the water level of the lake leads to outflow from lake to underground, increasing the ground water level. On the other hand, in the epochs of decreasing water level the inflow from underground water to the lake leads consequently to decreasing ground water level. Thus, ground water level should follow to a great extent the lake level variation. However, structural setting of the area of Lake Nasser indicates that:

a. The number of faulting systems at the north western part of the lake causes a complicated hydro-dynamical behaviour.
b. Decrease of the sediment thickness towards the east leads to a decrease of this effect in eastern direction.

2.   General Geology

The area of Lake Nasser belongs to the so-called Arabo-Nubian Massif. The area is characterized by four main geomorphological and geological units. These are: Aswan Hills, old Nile Valley and High Dam Reservoir, Lake Nasser, Nubian Plain, and Sinn El-Kaddab Plateau (Fig. 1). The Aswan Hills extend along the eastern bank of Lake Nasser and are characterized by their rugged topography. Precambrian basement rocks are exposed within the hills along the crust of the uplifts (Issawi, 1968).The old Nile valley and the High Dam reservoir are located along the western edge of Aswan hills. Lake Nasser extends mostly over the low lands in the west of the old Nile valley. Embayments were formed covering low lands to the west, the greatest one covers the former "Wadi Kalabsha". The Nubian Plain covers most of the low lands west of the old Nile valley. It has a relatively flat surface covered by Foreland sediments, ranging in age from Late Cretaceous to Eocene. These sediments overlie unconformably the Pre-Cambrian rock unit. The Nubian formation is composed of fine- to coarse-grained sandstone, with some shale and siltstone intercalations. It thins towards the High Dam and Lake Nasser. In some places, sandstone hills, composed of resistant beds, interrupt to the flat surface of the Nubian plain. The Sinn El–Kaddab Plateau is a vast limestone capped table land that extends westwards. The eastern margin is a steep east-facing escarpment called "Sinn El-Kaddab Escarpment". Lake Nasser area is characterized by three main features (Issawi, 1968; 1978). The most important one is faulting. The largest of which are Kalabsha and Seiyal Faults, trending mainly in an E-W direction. Faults in the N-S direction are also predominant. Two other systems of subordinate faults, the NW-SW and the NE-SW also exist. The area is affected by up-arching due to uplifting of basement rocks. Folding is less predominant structure in the study area. Small domes and several basins were created according to the up-arching of the basement.

3.   Geophysical Studies

On November 14th, 1981, a moderate earthquake with magnitude 5.6 occurred in the unpopulated area of Kalabsha, along the Kalabsha Fault, 70 km southwest of Aswan City (Kebeasy et al., 1982; 1987). Since then, seismicity continued to occur in the area, but with different magnitudes. The epicentres of these earthquakes were located near the epicentre of the main earthquake of November, 1981, along the eastern part of Kalabsha Fault, mainly near to the wide area of the lake (Kebeasy et al., 1987). Several study programs were initiated at Lake Nasser region. These programs include: monitoring of seismicity, underground water behaviour, strong motion effects on important structures, geological as well as geophysical investigations and monitoring of co-seismic crustal deformation by means of geodetic methods (Vyskočil and Tealeb, 1985; Vyskočil, 1987). Other programs for geophysical measurements were initiated by NRIAG, since 1986. These programs include mapping of the subsurface structures using seismic reflection and refraction techniques (Kebeasy and Ghareib, 1991) as well as magnetic and geoelectric measurements (Vyskočil and Tealeb, 1995).The November 14th, 1981, earthquake is located in Kalabsha area,

about 70 km to the south of the High Dam site. The spatial distribution of the earthquakes forming the seismicity map of Aswan area (Fig. 2) shows that the seismicity is concentrated in five main clusters (Fat-Helbary, 1995). These five cluster are: Gabel Marawa, east of Gabel Marawa, Khor El-Ramla, Abu-Derwa, and Old Stream. Most of these zones are attributed to Lake Nasser and can be strongly affected by environmental changes of the lake.
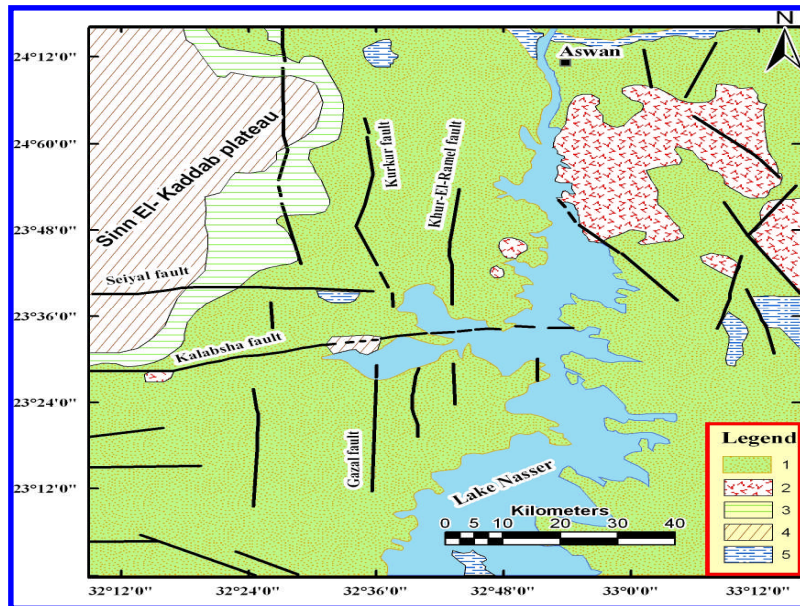

Figure 1: Geological map of Lake Nasser region modified by WC (Woodward-Clyde Consultants, 1985). Legend: 1- Latest Cretaceous sandstones and shale of Nubian Formation.
                        2- Precambrian metamorphic and plutonic rocks.
                        3- Latest Cretaceous rocks, mainly shale of the Dakhla Formation.
                         4- Paleocene to Eocene-age marine limestone.
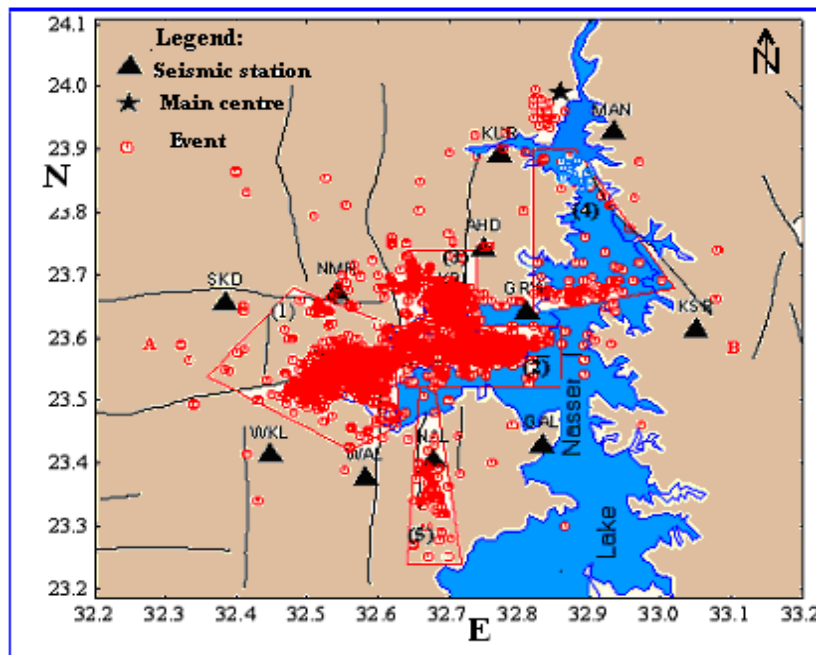   5- Undivided Quaternary sediment.

Figure 2: Seismicity map of the Aswan area around Lake Nasser (Fat-Helbary, 1995).

Gravity observations were carried out and repeated at different epochs along the points of the regional network to study the temporal gravity variations around the northern part of Lake Nasser.

11809

Fig. 3 (Zahran, 2005) shows gravity variations along the network at the period from November 2001 to November 2002. The Figure indicates the gravity variations around the lake over a period of one year. This variation is in the order of tens of microgals. Temporal gravity variations along the regional network around Lake Nasser obey to a great extent to water level variations of the lake. It shows significant mass redistribution around the active faults, which can contribute to the seismological activities. Seasonal variations of the level of Lake Nasser modify the stress regime of the area and, thus, variations of the gravity field and crustal deformations are to be expected (Zahran, 2005).

Figure 3: Gravity variations around Lake Nasser from Nov. 2001 to Nov. 2002; difference of contour lines is 20 µGal (Zahran, 2005).

4. Gravity Residuals and Water Level Variations at Lake Nasser

Fig. 4 gives a combined plot of the water level variations at Lake Nasser and residual gravity due to the tidal analysis of data from Aswan tidal station, Hassan et al., 2009. Fluctuations in gravity residues indicate that the tidal factors are not stable. It can be easily noticed that there is a significant change in residual gravity related to water level variation. It can be also noticed that the peak of maximum water level does not coincide with the peak of the maximum residual. This indicates that the response of the crust around the lake to water level variation is not instantaneous. The delay of the residual gravity regarding to water level variation may be due to slowly migrating water in the permeable sandstone. The available data about the variation of underground water level were obtained from March to December 2004 from a well in the area of Nubian sandstones. Fig. 5 shows the variations of Lake water level, underground water level, and residual gravity during the year 2004. From this figure, it can be seen that a steep change in underground water level led to an increase in residual gravity. Clear correlations between residual gravity and change of water level at Lake Nasser can be recognized, and also with change in the underground water level. Moreover, it can be noticed that high residual gravity is obtained at the periods of high underground water level, and low gravity residuals are obtained at periods of low underground water level.

5. Induced Loading Effect

Two methods have been used to evaluate the gravity variation in the tidal record due to the variable load of the lake. In the first method, the data were divided into blocks; each block corresponds to one of the four meteorological seasons (comp. Tab. 1). These blocks reflect more or less the

situation in the lake during periods of decrease, stability and increase of the water level. Comparison of some of the selected tidal waves, accurately separated at different blocks could reflect the response of the

Figure 4: Fluctuation of water level and residual gravity from 2002   to 2004, Lake Nasser area, Aswan, Egypt.
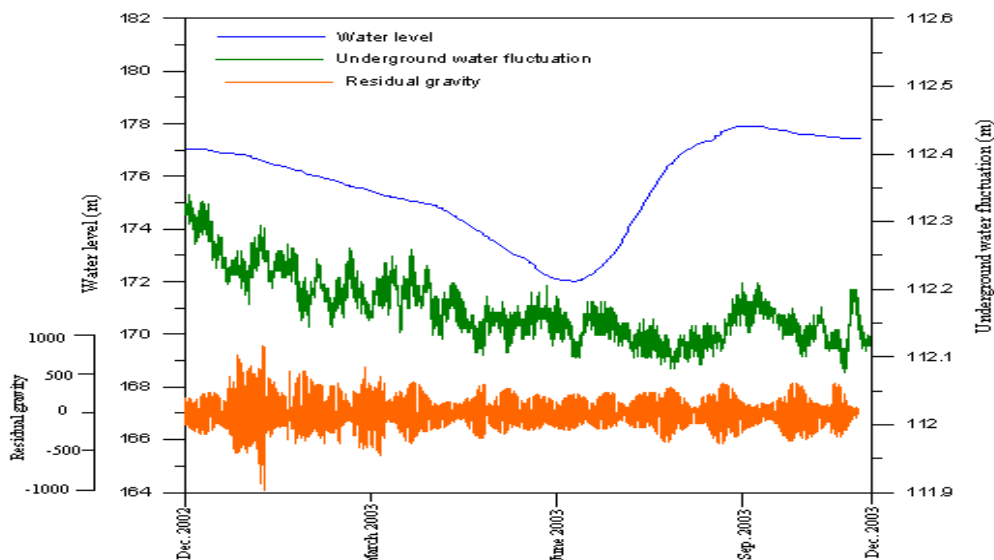

Figure 5: Residuals gravity, water level fluctuations and underground water fluctuations from 2002 to 2003, Lake Nasser area, Aswan, Egypt.

behavior of the crust to the variable load of the lake. In the second method, a quantitative evaluation to the relation between residual gravity and water level will be numerically evaluated by applying the cross-correlation between the residual gravity and the change of water level in the lake during the period of observations (from 2002 to 2004).

Block analysis method

Three main wave groups (Q1, O1, and M2) were chosen because of their large amplitudes which can be easily separated from tidal gravity observations. The observed amplitude factors for the different blocks were compared using the program ANALYZE of the ETERNA 3.3 package (Wenzel, 1996a; 1997). Tables. 1 and 2 show the observed amplitude factors of different blocks

11811

during the years 2003 and 2004. It has been noticed that there is a change in the amplitude factors from block to block, in which there is a change in water level. The variations in amplitude factor after block analysis during 2003 are shown in Fig. 6. It can be noticed that the wave O1 shows higher sensitivity to water level changes than Q1. This may be due to the daily variation of the

Table 1: Variation of the observed amplitude factors, after block analysis, during the year 2003, Lake Nasser area, Aswan, Egypt.

Tidal wave / Period	Q1	O1	M2	Water level fluctuation (m)
January to March 2003	1.086 ± 0.031	1.036 ±0.027	1.094 ±0.011	-1.04
April to June 2003	1.045 ± 0.031	0.998 ±0.029	1.059 ±0.010	-1.68
July to September 2003	1.048 ± 0.037	0.985 ±0.019	1.048 ±0.013	-2.64
October to December 2003	1.096 ± 0.029	1.029 ±0.018	1.103 ±0.011	+4.16

Table 2: Variation of the observed amplitude factors, after block analysis, during the year 2004, Lake Nasser area, Aswan, Egypt.

Tidal Wave / Period	Q1	O1	M2	Water level fluctuation (m)
January to March 2004	1.081 ± 0.029	1.029 ±0.019	1.098 ±0.013	-1.09
April to Jun, 2004	1.052 ± 0.025	0.993 ±0.017	1.066 ±0.013	-2.18
July to September, 2004	1.049 ± 0.030	0.984 ±0.016	1.055 ±0.013	-2.60
October to December, 2004	1.075 ± 0.028	1.017 ±0.018	1.090 ±0.013	+3.52
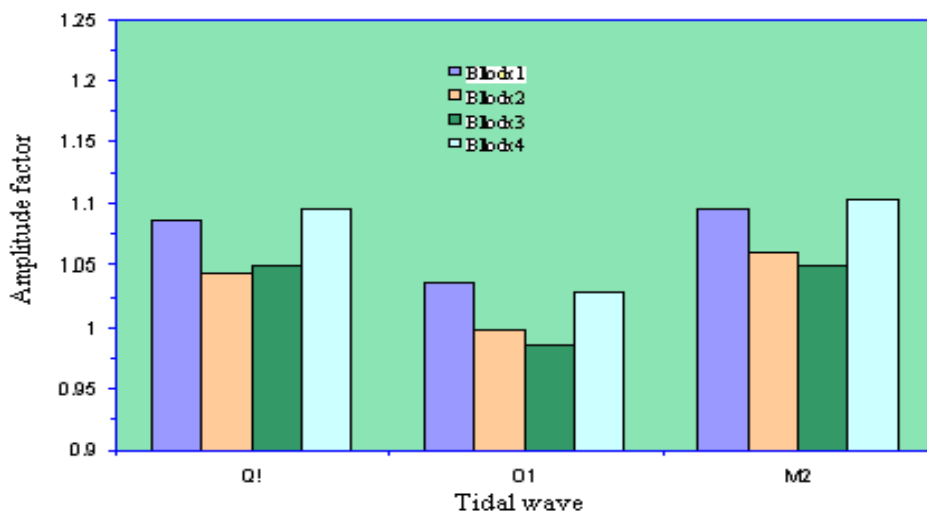
Figure 6: Variation of the observed amplitude factors, after block analysis, during the year 2003, Lake Nasser area, Aswan, Egypt.

11812

variable load of the lake, which has a frequency close to O1 band rather than Q1 band. However, this assumption needs some more verification and study.

Besides, the phase shift for different blocks was compared. Tabs. 3 and 4 show the observed phase shift after block analysis during the years 2003 and 2004. It has been found that there is a change in phase shift from period to period. Variations in phase shift are shown in Fig. 7. As a result of the block analysis, the effect of the variable load of Lake Nasser is obvious in the changes of both amplitude factor and phase shift. With regard to the accuracy of the separated waves, the observed changes in the amplitude factor and phase shift are significant for O1 and M2.

The Amplitude factors are higher in autumn and spring i.e. during the period of charge and stabilisation of the Lake. This effect reaches 0.4%. There exists a tendency to observe a decrease of 0.5° of the phase differences at the same time.

Table 3: Variation of phase shift, after block analysis during the year 2003, Lake Nasser area, Aswan, Egypt.

Tidal wave / Period	Q1	O1	M2	Water level fluctuation (m)
January to March	1.05 ± 0.50	-0.35 ±0.33	1.96 ±0.30	-1.04
April to June	1.45 ± 0.46	-0.24 ±0.44	2.53 ±0.28	-1.68
July to September	1.46 ± 0.48	-0.24 ±0.33	2.40 ±0.21	-2.64
October to December	1.06 ± 0.47	-0.42 ±0.43	1.99 ±0.29	+4.16

Table 4: Variation of phase shift, after block analysis during the year 2004, Lake Nasser area, Aswan, Egypt.

Tidal wave / Period	Q1	O1	M2	Water level fluctuation (m)
January to March	1.07 ± 0.47	-0.36 ±0.39	1.88 ±0.28	-1.09
April to June	1.51 ± 0.35	-0.24 ±0.31	2.39 ±0.28	-2.18
July to September	1.42 ± 0.47	-0.25 ±0.31	2.41 ±0.30	-2.60
October to December	1.09 ± 0.33	-0.37 ±0.30	1.89 ±0.29	+3.52
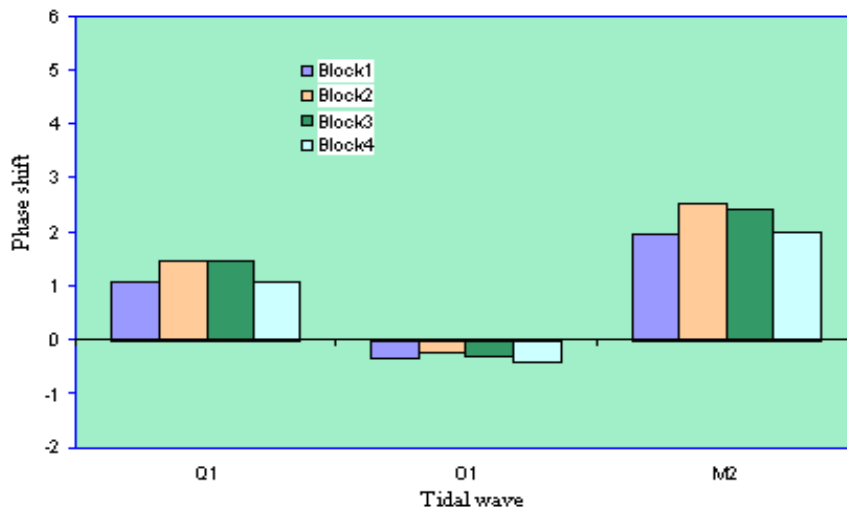
Figure 7: Variation of phase shift, after block analysis during the year 2003, Lake Nasser area, Aswan, Egypt.

Cross-Correlation method

First, the correlation coefficient between the tidal residuals and the lake level changes was computed for the whole period of observations. Hereafter, the correlation coefficient has been computed separately for some selected blocks. The results obtained from these analyses are shown in Tab. 5. The correlation coefficient for the whole period was found to be +0.556. The best relationship between the water level fluctuation and change in gravity could be obtained for the period from October to December, 2003, where the correlation coefficient attained +0.562. In this period, the water level reached its maximum value (177.91 m). The worst relationship could be obtained for the period from July to September, 2004, where the correlation coefficient dropped down to +0.432. In this period, the water level reached its minimum value of 172.02 m. So, it can be noticed from the results in Tab. 5 that there is a clear correlation between the fluctuation of water level and the change in gravity. To estimate the effect of underground water level variation on the residual gravity, again a cross-correlation was computed. The correlation coefficient was found to be +0.480, which means there is a weak relation between the variation of underground water level and residual gravity.

Table 5: Variation of cross correlation coefficient between residual gravity and water level fluctuation, Lake Nasser area, Aswan, Egypt.

Period	Correlation coefficient	Water level Fluctuations (m)
from Jan., 2003, to Dec., 2004	+0.556	
from January to March 2003	+0.530	-1.04
from April to June 2003	+0.502	-1.68
from July to September 2003	+0.468	-2.64
from October to December 2003	+0.562	4.16
from January to March, 2004	+0.495	-1.09
from April to June 2004	+0.445	-2.18
from July to September 2004	+0.432	-2.16
from Oct., 2004, to Dec., 2004	+0.492	3.52

11814

Table 6: Variation of cross correlation coefficient between residual gravity and underground water level fluctuation, Lake Nasser area, Aswan, Egypt.

Period	Correlation coefficient	ground water level fluctuations (cm)
From Mar., 2003 to Dec., 2004	+0.480	
From Mar., 2003 to Jun., 2003	+0.352	10
From Jul., 2003 to Sep., 2003	+0.283	7
From Oct., 2003 to Dec., 2003	+0.336	8

6. Time Variation of the Earth's Gravity Field at Lake Nasser Area

Zhang et al. (1996) developed a method to predict time variations of the Earth's gravity field and crustal deformation due to mass loading caused by the impounding of the three Gorges reservoir. Zahran (2005, pers. communication) used Zhang's method to compute the effect of the induce loading on the gravity field during the period of study. Fig. 8 shows gravity field variations as induced by water level variations at Lake Nasser. It can be seen that the variation in gravity follows the variation of the water level in the lake. The maximum gravity variation is 500 nm /s^2 due to maximum water level variation. The range of induced load gravity variation is significant for tidal observations and also for repeated gravity variations for geodetic purposes. The high residuals were found to be associated with high water level variations. Moreover, the obtained phase shift between water level variation and residual gravity (Fig. 4) is not clear. This effect may be due to mass changes by water migrating through the rock around the lake in addition to the elastic behaviour.

7. Discussion

A combined plot of water level variation and residual gravity shows that the residual gravity follows water level variation with a time delay. This time shift may be due to the permeability of the rocks and migrating water masses. On the other hand, the differences of the tidal parameters in different blocks under different loading conditions may be due to pore pressure changes, and, thus, modifications of overall elasticity of the rock. There is a moderate correlation between residual gravity variation and lake water level variation, whereas the correlation between residual gravity and underground water variation is weak. Correlation coefficients of selected blocks show that their values follow to a great extent the values of water level variations on one side and on the other side groundwater variation. The effect of induced load in the lake on the gravity field was calculated at different water levels at Aswan tidal gravity station. The range of induced load gravity variation is significant for tidal observations and also for repeated gravity surveys for geodetic purposes.
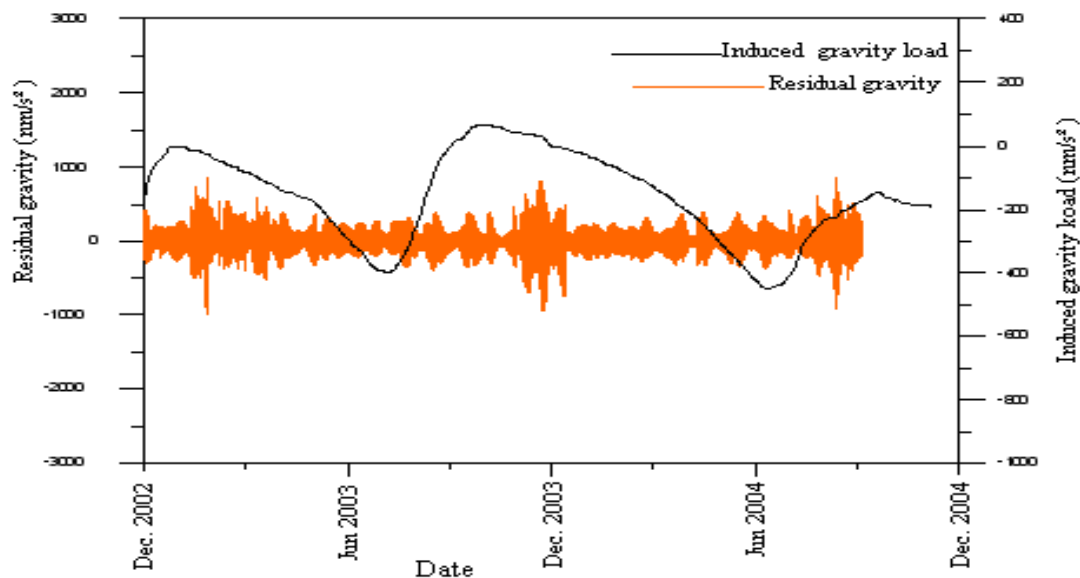
Figure 8: Induced gravity load and residual gravity, Lake Nasser Area, Aswan, Egypt (from 2002 to 2004).

References

Bell, M. L. and Nur, A., 1978. Strength changes due to reservoir - induced pressure and stress and application to Lake Oroville. J. Geophys. Res., vol. 83, pp. 4469 - 4483.

Fat-Helbary, R. E., 1995. Assessment of seismic hazard and risk in Aswan area, Egypt. Ph. D. Thesis. Architectural Engineering Department Tokyo Univ., Japan, 182p.

Hassan R.M., Abdelrahman E.M., Tealeb A., Zahran K.H., Jentzsch G., 2009. Gravimetric tide observation at Lake Nasser Region, Aswan, Egypt: a preliminary investigation, Bull. Inf. Marées Terrestres , 146, 11797-11806.

Issawi, B., 1968. The geology of Kurkur - Dungle area. General Egyptian Organization for Geological Research and Mining, Geol. Surv. Cairo, Egypt. Paper No. 46, 102P.

Issawi, B., 1978. Geology o f Nubia west area , Western Desert, Egypt. Annals Geo. Surv., Egypt, vol. 8, PP. 237 – 253.

Kebeasy, R. M. Maamoun, M. and Ibrahim, E., 1982. Aswan Lake induced earthquakes. Bull. Int. Inst. Seismology & Earthquake Engineering, Tokyo, Japan, vol. 19.

Kebeasy, R. M., Maamoun, M., Ibrahim, E. M., Meghahed, A., Simpson, D. and Leith, W., 1987. Earthquake studies at Aswan reservoir. J. of Geodynamics, Vol. 7, pp. 173–197.

Roeloffs, E. A., 1988. Fault stability changes induced beneath a reservoir with cyclic variations in water level. J. Geophys. Res., vol. 93, pp. 2107-2124.

Snow, D. T., 1972. Geodynamic of seismic reservoirs, symposium on percolation through fissured rocks. Proceedings, Deutsche Gesellschaft für Erd- und Grundbau, Germany, T2- J, pp. 1-14.

Simpson, D. W., 1986. Triggered Earthquakes. Ann. Rev. Earth plant Sci. 14, 21- 42.

Vyskočil, P. and Tealeb, A., 1985. Report on activity by monitoring recent crustal movement at Aswan period 1983-1985. Bull. Helwan Inst. of Astronomy and Geoph., vol. II, Ser. B, pp. 33-41.

Vyskočil, P., 1987. Recommendations on the project of monitoring recent crustal movements   in the western part of the Aswan region in Egypt. J. of Geodynamics, vol.7, pp. 257-259.

Vyskočil, P. and Tealeb, A., 1995. The present stage and prospect for recent crustal movement studies around seismo-active areas in Egypt. Bull. Helwan Inst. of Astronomy and Geophysics, vol. xi, pp. 105-138.

Wenzel, H. G., 1996a. The nanogal software: Earth tide data processing package ETERNA 3.30. Bulletin d'Inf. Marèes Terr., vol. 124, pp. 9425-9439.

Wenzel, H. G., 1997. Analysis of the Earth tide observations In: Wilhelm, H., W. Zürn and H.-G. Wenzel (Eds), Tidal Phenomena. Lecture Notes in Earth Sciences, Springer Verlag, Berlin, Germany, pp. 59-75.

WCC (Woodward - Clyde Consultants), 1985. Identification of earthquake sources and estimation of magnitudes and recurrence intervals, Internal Report, High and Aswan Dams Authority, Aswan, Egypt, 135p.

Zhang, K. F., Featherstone, W. E. , Bian, S. F., and Tao, B. Z., 1996. Time variation of the Earth's gravity field and crustal deformation due to the establishment of the Three Gorges reservoir, J. Geod., vol. 70, pp. 440-449.

Zahran, K. H., Jentzsch, G. and Seeber, G., 2005. World – wide synthetic tide parameters for gravity and vertical and horizontal displacements. J. Geod., vol. 79, pp. 293-299.

Zahran, K. H., 2005. Benefit of tidal observations to gravity and GPS networks. Egyptian Geophys. Soc. Journal, vol. 3, No. 1, pp 89-98.

Superconducting Gravimeter OSG-050 at the Station Pecný, Czech Republic

Vojtech Pálinkás, Jakub Kostelecký

Research Institute of Geodesy, Topography and Cartography, Geodetic Observatory Pecný, CZ – 251 65 Ondrejov 244, vojtech.palinkas@pecny.cz

Abstract

The Pecný station is equipped by first-rate instrumentations in the field of terrestrial gravimetry thanks to the absolute gravimeter (AG) FG5#215 and superconducting gravimeter (SG) OSG-050. Repeated AG observations at the Pecný station allowed to determine the two important parameters of the SG, its scale and drift. The repeatability of the FG5#215 has been also computed from combined time series.

One year of SG observations showed the sizeable improvement of earth tides observations respect to the existing observations with spring gravimeters and necessity to improve the method of air pressure effect correction by the single admittance. The noise of OSG-050 in the normal mode band is higher than it would be expected. Small improvement of the noise characteristic was achieved by careful setting of dewar pressure.

1. Introduction

Continuous tidal observations by spring gravimeters have been carried out at the station Pecný since early seventies of the last century (Broz et al. 2005). Different type of spring gravimeters (Askania Gs11, Gs15, L&R, ZLS) has been used for observations . Of course, during this long period, the gravimeters and registration was dramatically improved. Methods of calibration, digital registration, and feedback system development were milestones of observation improvements (Brož et al., 2002; Pálinkáš, 2006). These improvements allowed to increase the measurement accuracy more than 10 times during 30 years. The standard deviation of the observed hourly ordinate on the level of 0.1 μGal was achieved which is comparable with older type of SGs (Ducarme et al., 2002). Unfortunately this high accuracy is relevant only for the short-period tides due to the instrumental drift. The drift of spring gravimeters at Pecný can be considered as linear for the period below one week in spite of the temperature and humidity control at the station with precision of 0.1^{o}C and 1%, respectively.

Fig. 1. The absolute gravimeter FG5#215 and the superconducting gravimeter OSG-050 at the Pecný station

The instrumentation of the tidal station has improved significantly thanks to the superconducting gravimeter (SG) OSG-050, installed in February 2007. The Pecný station as the core station of ECGN (European Combined Geodetic Network) is equipped with permanent GNSS station, absolute gravimeter (AG) FG5#215 and the superconducting gravimeter OSG-050. These high quality instrumentations in the field of gravimetry allow to monitor wide range of gravity variations of geophysical origin from Earth's free oscillations to secular gravity variations. Possibility of frequent simultaneous AG and SG observations at the station allow to solve main problems of both instruments: drift and calibration of the OSG-050 and the offset variations of the FG5#215.

2. Calibration and drift

The calibration factor and drift of the SG has been determined using simultaneous observations with the AG (Hinderer et al. 1998). Altogether 15, typically one-day absolute measurements with FG5#215 has been carried out from April 2007 to June 2008. For the purpose of SG calibration, five AG campaigns has been extended to three-days observations. These extended observations were carried out during tidal variations at least 230 μGal. The precision of all individual determination of scale factor was better than 0.07%. However, the final calibration factor and corresponding accuracy should be computed from results of repeated calibrations. The dispersion of individual results with corresponding error bars in Fig. 2 show necessity of such repeated measurements. The final calibration factor of the OSG-050 has been determined as average of all calibrations . From dispersion of individual result we can assume that accuracy of the final calibration factor is of about 0.06%.
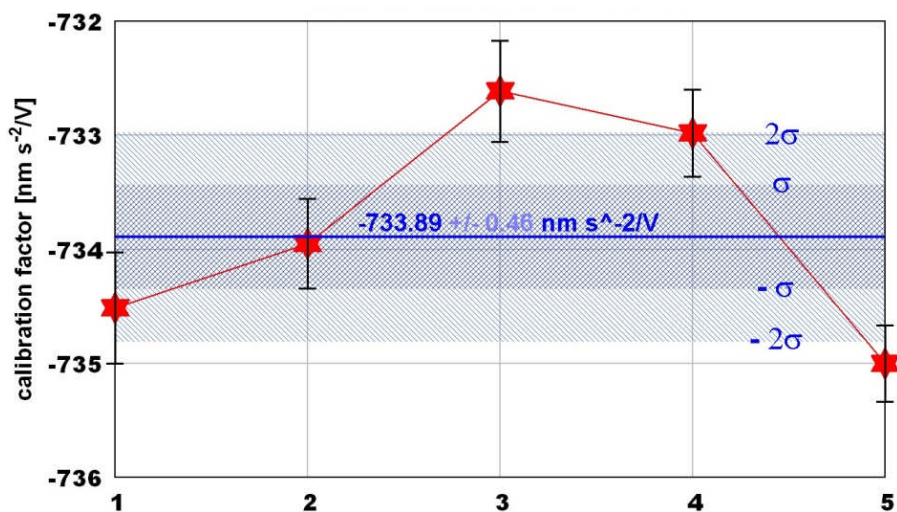
Fig. 2. Calibration factor of the OSG-050 determined from 5 simultaneous three-days observations with FG5#215. Error bars represents precision of individual calibrations.

The SG drift has been determined from the comparison between SG and AG observations (see, Fig. 3 and Fig. 4) and described by linear term 1.7 ± 0.4 μGal/year. We can assume, that after removing drift from SG time-series, the rest of differences between AG and SG is caused mainly by random and systematic errors of the AG. This approach can help to detect variations in AG offsets. In our case (see, Fig. 4) all differences are within expected error bars of the AG (1.1 μGal, Niebauer et al. 1995). Comparison of both techniques has been used for the evaluation of FG5#215 repeatability (precision) by such experimental way. The standard deviation of individual absolute gravity measurements of 0.6 μGal respect to the OSG-50 observations describe the precision of the FG5#215. It is necessary to say that the FG5#215 is not installed permanently at the Pecný station and the precision of 0.6 μGal includes error of instrumental set-up, meter alignments etc.
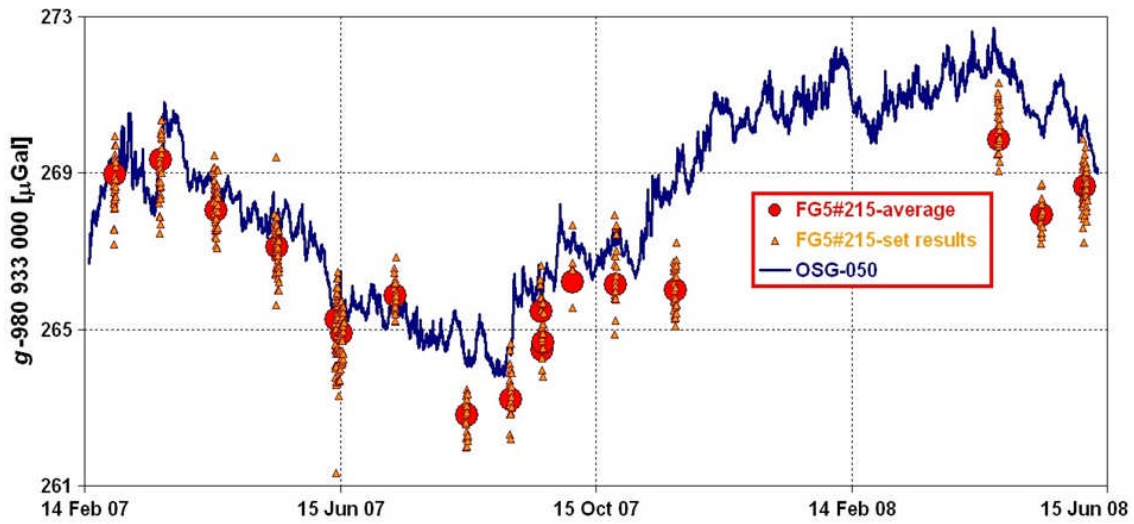
Fig. 3. Gravity series of the FG5#215 and OSG-050, corrected for earth tides, air pressure variations by single admittance and effect of polar motion.
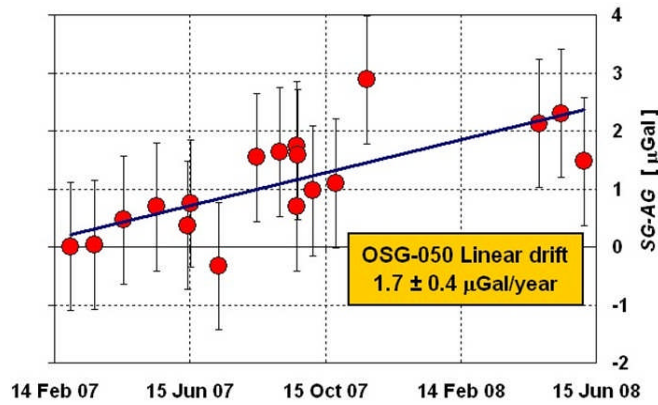

Fig. 4. Differences between gravity series for determination of SG drift and AG repeatability.

3. Time delay

The time delay of the OSG-050 in tidal frequency band was evaluated from the transfer function of the meter, experimentally determined by injection step voltage into the feedback (Van Camp et al. 2000). Altogether 34 injections have been carried out for three different size of steps (15V, 10V and 5V). For the processing the TSOFT (Vauterin and Van Camp, 2001) and ETSTEP (Wenzel, 1995) software were used. Both processing method and also three-different size of steps gave results within 0.03 sec (see, Tab. 1). Specially the results from ETSTEP software show high consistency and precision. Utilization of ETSTEP seems to be more efficient but it need careful and correct evaluation of initial and final step values. On the other hand the method using TSOFT is more user-friendly.

Table 1. Time delay of the OSG-050 for three different size of steps (15V, 10V and 5V) and computed with two different software (TSOFT and ETSTEP), θ - time delay, n - number of steps

	TSOFT	ETSTEP
	$\theta \pm \sigma_\theta$ *(n)* [sec]	$\theta \pm \sigma_\theta$ *(n)* [sec]
15 Volt	8.873 ± 0.012 (10)	8.856 ± 0.003 (4)
10 Volt	8.860 ± 0.010 (10)	8.853 ± 0.005 (4)
5 Volt	8.884 ± 0.019 (14)	8.853 ± 0.021 (4)
Average	**8.868 ± 0.009**	**8.855 ± 0.002**

4. Tidal analysis

The tidal analysis was carried out by the program ETERNA 3.4 (Wenzel, 1996) for the period April 2007 – June 2008. The tidal parameters of main tidal waves determined from the OSG-050 record show the agreement better than 0.05% in amplitude and 0.04 deg in phase with results of spring gravimeters during last 6 years. The very good agreement in amplitude demonstrates the accurate calibration of gravimeters by simultaneous measurements with FG5#215 (Pálinkás, 2006), when the spring meters and OSG-050 have been calibrated over 60 and 15 days, respectively.

Table 2. Comparison of the results of tidal measurements with Askania, LaCoste & Romberg and superconducting gravimeter at the station Pecný. The results were computed by ETERNA 3.4 (Wenzel, 1996), δ - amplitude factor, κ - phase lag [deg].

Gravimeter	ASKANIA Gs15 #228 electromag. feedback		L&R G #137 MVR feedback		OSG-050	
Period Days	2000 04 – 2005 04 1568		2002 09 – 2004 04 522		2007 04 – 2008 06 435	
Wave	$\delta \pm \sigma_\delta$	$\kappa \pm \sigma_\kappa$	$\delta \pm \sigma_\delta$	$\kappa \pm \sigma_\kappa$	$\delta \pm \sigma_\delta$	$\kappa \pm \sigma_\kappa$
O_1	1.1503 1	0.122 0.004	1.1500 1	0.102 0.004	**1.1505 1**	**0.122 0.004**
K_1	1.1373 1	0.185 0.003	1.1370 1	0.155 0.003	**1.1374 1**	**0.196 0.003**
M_2	1.1851 1	1.229 0.003	1.1846 1	1.209 0.003	**1.1856 1**	**1.240 0.002**
S_2	1.1804 1	0.018 0.007	1.1820 1	0.104 0.006	**1.1826 1**	**0.156 0.005**
σ [nm·s^{-2}]	**1.61**		**0.63**		**0.59**	

The air pressure correction has been applied as component of the tidal analysis by ETERNA using regression coefficient with local air pressure. The regression coefficient of -3.3 nm s^{-2}/hPa as result of tidal analysis doesn't describe air pressure correction sufficiently due to frequency dependence of single admittance. This situation can be seen in Fig. 5 and confirm the necessity to improve the existing method of air pressure effect correction using single admittance. Implementation of corrections based on the 3D atmospheric models (Neumeyer et al., 2004) and local air pressure observations is necessary.
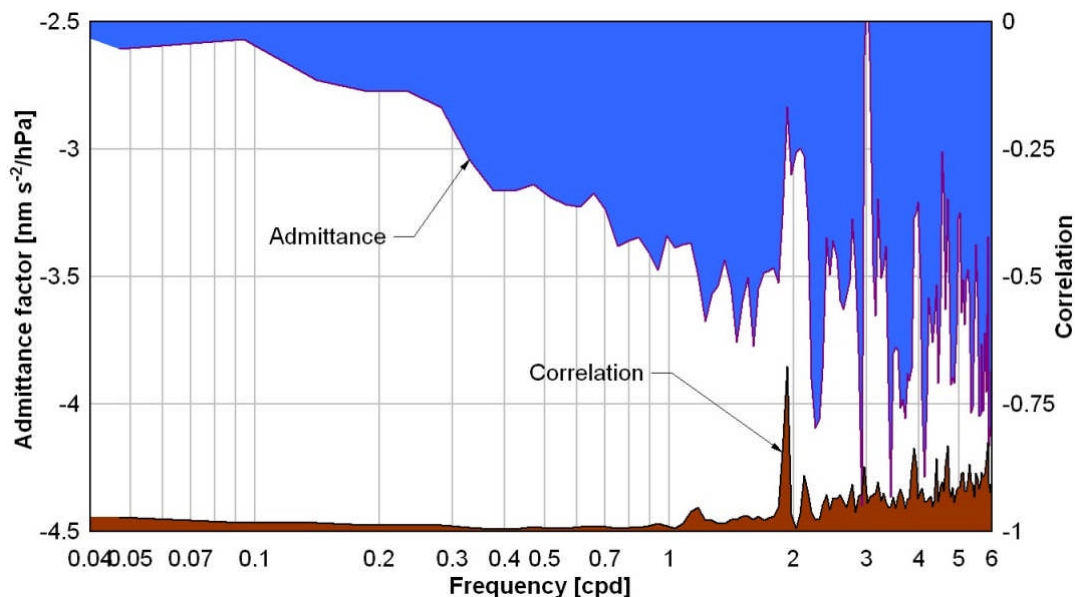
Fig. 5. Frequency dependence of the air pressure admittance

5. Noise in normal mode band

The Pecný station is located in a quiet place, far away from industrial noise and the SG pillar is founded on the quartzite bedrock. It should be expected, that noise in normal mode band (0.2 mHz – 10 mHz) will be low and thus the conditions for monitoring Earth's free oscillations excellent. Unfortunately, the comparison of power spectral densities with New Low Noise Model (NLNM, Peterson 1993) in Fig. 6 shows sizeable noise in this frequency band. The seismic noise magnitude(SNM, Banka and Crossley, 1999) of the OSG-050 is of about 1.4. To achieve best noise characteristic of the OSG-050, the influence of the dewar pressure setting has been experimentally studied by comparison of power spectrums under different pressure condition. Improvement less than 5 dB has been achieved by sensitive setting of the dewar pressure (see, Fig. 6).
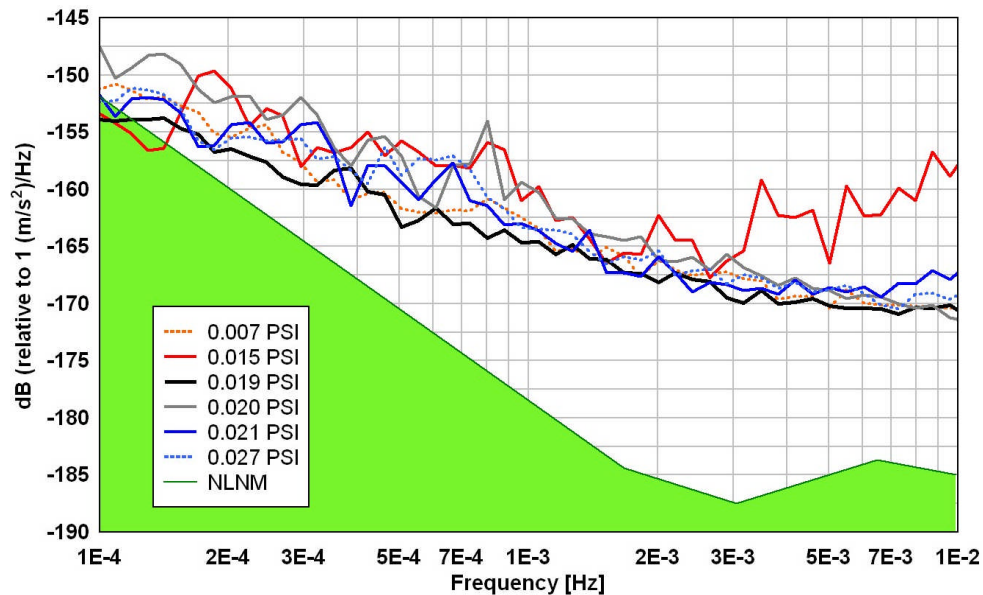
Fig. 6. Power spectral densities of the OSG-050 in normal mode band for different dewar pressures

6. Conclusions

During the first year of observation with the OSG-050 at Pecný the main parameters and characteristics of the meter has been determined. Calibration coefficient and the time delay were estimated with the accuracy of 0.06% and 0.01 sec, respectively. The comparison of SG and AG observations helped to determine the SG linear drift of 1.7 ± 0.4 µGal/year and the FG5#215 repeatability of 0.6 µGal. The analysis of recorded data showed the very good properties of the meter for monitoring gravity variations below 0.1 mHz (earth tides, hydrological effects etc.). On the other hand the observations in normal mode band (0.2 mHz – 10 mHz) are affected by sizeable noise of instrumental origin.

The superconducting gravimeter OSG-050 at the station Pecný represents dignified continuation of earth tide observation started in early seventies of the last century. Thanks to the good drift characteristics of the meter and regular repeated absolute gravity measurements, there is a good chance to determine valuable parameters of long-period tides and to monitor gravity variations of hydrologic and geodynamic origin. Moreover, the OSG-050 seems to be very important instrument for absolute gravimeter FG5#215 (national standard for acceleration due to gravity) to monitor variations of its systematic errors and consequently improve accuracy and credibility of our absolute measurements.

References

Banka, D., Crossley, D. (1999). Noise levels of superconducting gravimeters at seismic frequencies. Geophys. J. Int. 139, 87– 445.

Broz, J., Simon Z., Pálinkás V. (2005). The Gravimetric Tidal Station Pecný. 50 years of the RIGTC, Jubilee Proceedings 1994-2004, Zdiby, pp. 121-130.

Broz, J., Z. Simon, J. Dupac, A. Zeman. (2002). Two Feedback Systems to the Gs15 No.228 Gravimeter. Marees Terrestres Bulletin d'Informations. No. 137, pp. 10937-10951.

Ducarme, B., He-Ping Sun, Jian-Qiao Xu, (2002). New Investigation of Tidal Gravity Results from the GGP Network. Marees Terrestres Bulletin d'Informations. No. 136, pp. 10761-10776.

Hinderer, J., M. Amalvict, N. Florsch, O. Francis, J. Mäkinen. (1998). On the Calibration of Superconducting Gravimeters with the Help of Absolute Gravity Measurements. Proceedings of the 13th International Symposium on Earth Tides, Brussels, July 1997. Obs. Royal Belgique, Brussels, pp. 557-564.

Neumeyer, J., J. Hagedorn, J. Leitloff, T. Schmidt. (2004). Gravity reduction with three-dimensional atmospheric pressure data for precise ground gravity measurements. Journal of Geodynamics, Volume 38, Issues 3-5, pp. 437-450.

Niebauer, T., G. S. Sasagawa, J.E. Faller, R. Hilt, F. Klopping. (1995). A New Generation of Absolute Gravimeters. Metrologia, 32, pp. 159-180.

Pálinkás, V. (2006). Precise Tidal Measurements by Spring Gravimeters at the Station Pecný. Journal of Geodynamics, Volume 41, Issues 1-3, 2006, pp. 14-22.

Peterson, J., 1993. Observations and Modelling of Seismic Background Noise. Open-File Report 93U.S. Department of Interior, Geological Survey, Albuquerque, New Mexico.

Vauterin, P., Van Camp, M. (2001). Tsoft Manual.

Van Camp, M., Wenzel, H.-G., Schott, P., Vauterin, P. and Francis, O. (2000).Accurate transfer function determination for superconducting gravimeters. Geophys. Res. Let., 27, 1, 37-40.

Wenzel, H.G. (1995). Accurate instrumental phase lag determination for feedback gravimeters. Proc. 12th Int. Symp. Earth Tides, 191-198, H.T. Hsu (ed.), Science Press, Beijing, New-York.

Wenzel H. G. (1996). The Nanogal Software: Earth Tide Data Processing Package: ETERNA 3.3. Marees Terrestres Bulletin d'Informations. No. 124, pp. 9425-9439.

Assessment of atmospheric reductions for terrestrial gravity observations

M.Abe,[1] C.Kroner,[1] J.Neumeyer, X.D. Chen[2]

1) Deutsches GeoForschungsZentrum (GFZ), Gravity Field and Gravimetry
2) Institute of Geodesy and Geophysics, Chinese Academy of Sciences

Abstract

Atmospheric attraction and loading effects account for about 10% of all observed time-dependent gravity variations in which the dominant gravity signal is the tides of the solid Earth. The impact can be roughly estimated using barometric pressure from the observation site, but in that case only atmospheric variations which are correlated with local barometric pressure changes are taken into account. If e.g. geodynamic signals are to be investigated, the variations which are unconsidered have an amplitude of several µGal, therefore they are large enough to require consideration.

In this paper, three different procedures to remove the atmospheric effect are compared. Numerical results show that the atmospheric reduction using three-dimensional (3D) data from the European Center for Medium-Range Weather Forecasts (ECMWF) ought to be computed up to 5° around a station. A peak-to-peak amplitude of the differences between a reduction using 3D data and one using two-dimensional (2D) data from the ECMWF is 0.5 µGal including seasonal variations with an amplitude of 0.15 µGal, and it has a Root Mean Square (RMS) value of 0.1 µGal considering a time span of 4 years. The amplitude of reduction based on a regression coefficient/admittance factor differs from the two physical methods by approximately 3 µGal with a RMS value of 0.4 µGal in the same 4 year-long observation period.

From spectral analyses of the three reductions it emerges that the amplitudes of the more comprehensive methods are 11-12% smaller than the reduction using an admittance factor in the spectral range from 0.0 CPD (cycle per day) to 0.18 CPD on average. Investigation of the atmospheric reduction effects on the tidal analysis indicates that there are visible improvements in the tidal analysis using the reductions based on the physical approaches compared to the reduction using an admittance factor but not between the two physical approaches. Concerning the amplitude factor of the polar motion signal, there is 1.5% difference in the value of the factor after applying the two physical methods.

The differences between the physical approaches stem from the consideration of the air density distribution. A peak-to-peak amplitude is about 0.5 µGal when the attraction effect up to 5° around a station is computed. The omission of vertical variations in air density leads to inaccuracies which should be avoided, for instance, in the validation of non-tidal ocean loading effects or studies of tectonic phenomena.

11825

1. Introduction

The estimation of atmospheric attraction and loading effects are necessary for continuous and precise gravity observations, e.g., with superconducting gravimeters (SG), because gravity variations induced by shifts of air masses cover geodynamic signals of interest. Therefore, this atmospheric impact should be modeled as well as possible and be removed from the gravity observations.

A still widely used atmospheric reduction is based upon an admittance factor adjusted by least square fitting between barometric pressure and SG data from an observation site. By using this method, however, only effects which are correlated with local pressure are taken into account and effects uncorrelated are not considered.

During the recent past, several attempts were made (e.g. Merriam, 1992; Sun et al. 1995; Boy et al., 1998, 2002; Kroner & Jentsch, 1999; Guo et al., 2004) to improve reductions by means of Green's functions (Farrell, 1972) or using an empirical frequency-dependent method (Warburton & Goodkind, 1977; Crossley et.al., 1995; Neumeyer, 1995).

Merriam (1992) calculated atmospheric Green's functions (attraction and deformation), which are based on the ideal gas law, the hydrostatic assumption, and a temperature model of the COSPAR (Committee on Space Research) atmosphere. These are computed over a thin column from a height from 0 to 60 km. The attraction and loading effect can be computed from these functions and surface barometric pressure data for the whole Earth. As here only surface pressure is considered, surface pressure independent air mass movements are not taken into account.

Neumeyer et al. (2004) computed a physical reduction using three-dimensional (3D) meteorological model data from the European Center for Medium-Range Weather Forecasts (ECMWF). The attraction effect was calculated up to 1.5° distance from the SG station and for the deformation part using Green's function a distance up to 10° was considered. The amplitude of the attraction part which does not correlate with barometric pressure observed at the Earth's surface was about 2.0 µGal (Neumeyer et al., 2006).

The present investigation is based on the studies by Neumeyer et al. (2004, 2006) and the object of this paper is to derive an optimized atmospheric reduction suitable for ongoing research related to gravity changes of several days and longer (e.g. related polar motion or non-tidal ocean loading etc.). Thus, in this study the focus is atmospheric variations with spatial scales of tens of kilometers to global. Reductions for atmospheric effects are a means to an end, because gravity data interpretation begins after the atmospheric reduction. In this paper, we determine how large the zone needs to be for the computation of the attraction effect using 3D meteorological data and from which distance it is sufficient to use surface data and a standard atmosphere. We use spectral and tidal analyses to investigate and quantify the differences between the various reduction methods.

2. Data and method
2-1 The ECMWF data

7 data sets (surface geopotential, surface pressure, 2 m temperature, humidity with 60/90 height levels, temperature with 60/90 height levels, geopotential with 60/90 height levels, and barometric pressure with 60/90 height levels) from ECMWF Integrated Forecast System (IFS) daily analysis and error estimates are used in this investigation. The original data are re-sampled to a regular grid of 0.5° × 0.5° and the coverage is 89.5° to - 89.5° in latitude and 0° to 359.5° in longitude. The sampling rate is 6 h. Until 31.01.2006, ECMWF provided data for 60 height levels (about up to 64 km height), after this date the number of height levels was increased to 91 (about 80 km height). The gravity effects due to this modification amount to 8.42×10^{-4} µGal in a time span of 11 months. These effects are therefore small enough to be ignored in this study.

2-2 The air density distribution

For the estimation of the atmospheric attraction term, the air density distribution needs to be computed for each cell of air mass.

The atmosphere is considered as a mixture of dry air and water vapor. By using the ideal gas equation the air density ρ can be derived from

$$\rho = \frac{p}{RT(1 - q + \frac{q}{\varepsilon})} \quad (1),$$

where R is the gas constant for dry air ($287.05 \, Jkg^{-1}K^{-1}$), p, q, T are respectively barometric pressure, humidity, temperature taken from ECMWF data (from the Earth's surface to 80 km height) and ε is the ratio of the gas constants for dry air R and water vapour R_v ($\varepsilon = \frac{R}{R_v} = 0.62197$). Fig. 1a shows the air density distribution using (1) and ECMWF data for the example of Moxa station (Fig.3)(50.6447° N, 11.6156° E and a height of 455m) for the time span of one month and the vertical density distribution derived from the U.S. Standard Atmosphere 1976 (NASA,1976) and the well-known barometric formula (2)

$$\rho(z) = \frac{P_0}{RT_Z} \left(\frac{T_0 + \alpha z}{T_0} \right)^{-\frac{g_0}{R\alpha}} \quad (2)$$

with $T_Z = T_0 + \alpha z$ and α as the rate of temperature change with height from the US1976 standard atmosphere up to 84 km. P_0 and T_0 are respectively surface pressure and temperature from ECMWF, T_Z is temperature at height z, and g_0 is the mean surface gravity value 9.80665 m/s^2.
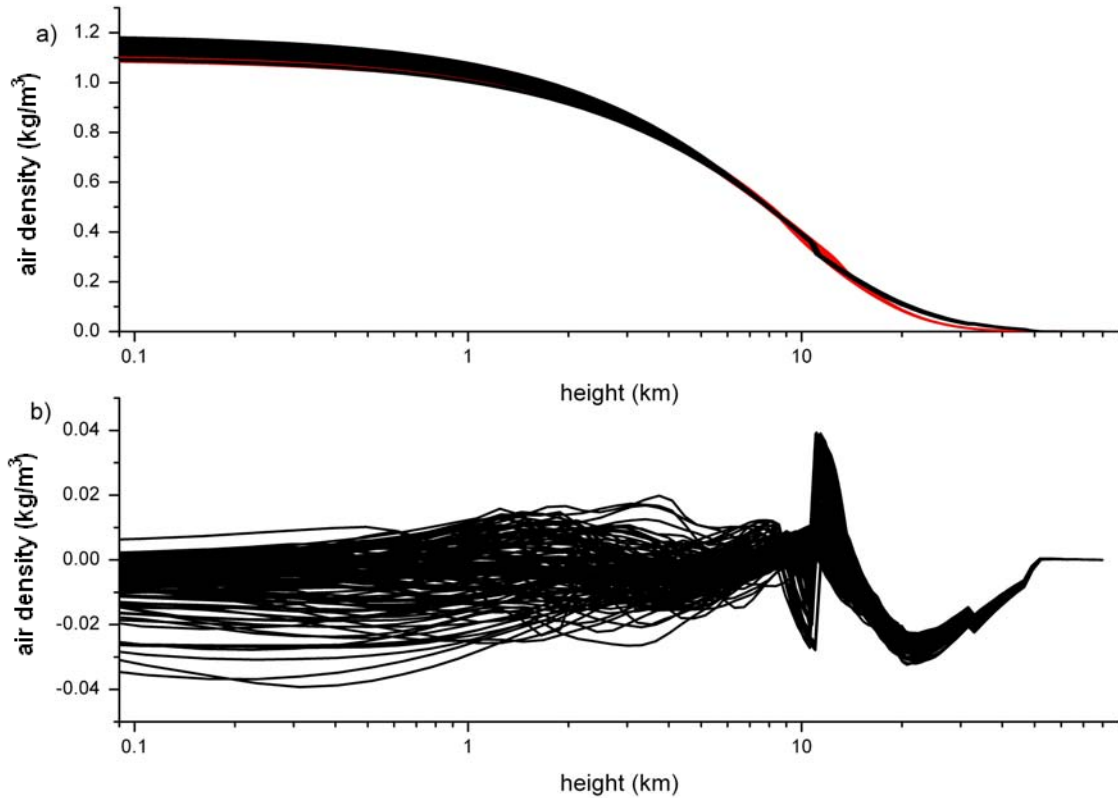
Figure 1
Air density distributions for Moxa station from 2007/07/01-2007/07/31
(a) red line : ECMWF data , black line : The US 1976 standard atmosphere
(b) difference (air density derived from ECMWF data – US standard atmosphere)

The air density distribution is computed from 1st of July, 2007 to 31st of July, 2007. In Fig.1b the difference between the air density distribution based on eq.(2) and 3D ECMWF data is shown. Random variations occur up to a height of 10 km with a deviation range of -0.04 to 0.02 kg/m^3. The differences become larger up to 0.04 kg/m^3 in a height of 11 km. Between 11 and 20 km distinct deviations are found. From the height of 20 km or more, the differences approach gradually 0. In Neumeyer et al. (2004), a test calculation was carried out to estimate how much the changes in the air density profiles affect the gravity reduction. Air density profiles were changed within the range of 0.02 kg/m^3 up to 16km height and during 5 h. From this test calculation, gravity changes of about 3 μGal were obtained.
Thus, the deviation range of -0.04 to 0.02 kg/m^3 induces non-negligible gravity variations.

2-3 Calculation of the attraction term using 3D data

The calculation of the attraction term using 3D data is based on the gravitational potential of the air masses. Using spherical coordinates (λ, ϑ, r) with origin at the centre of the Earth and the Z-axis coinciding with the observation station, the gravitational potential of the air mass Φ is given by

$$\Phi(0,0,R_{GS}) = -\gamma \int\limits_{R_{GS}}^{\infty} \int\limits_{0}^{\pi} \int\limits_{0}^{2\pi} \frac{\rho(\lambda,\vartheta,r) \cdot r^2 \sin\vartheta}{\sqrt{r^2 - 2rR_{GS}\cos\vartheta + R_{GS}^2}} \; d\lambda\, d\vartheta\, dr \quad (3),$$

where γ is the gravitational constant, R_{GS} is the radius of the Earth and ρ is the air density.

The gravitational potential of each air segment is changed to the gravitational acceleration caused by one spherical segment in the direction of the center of the mass

$$g_i^A(0,0,R_{GS}) = -\frac{\partial}{\partial R_{GS}}\Phi_i^A = \gamma \int\limits_{r}\int\limits_{\vartheta}\int\limits_{\lambda} \frac{\partial}{\partial R_{GS}}\left(\frac{\rho_i r^2 \sin\vartheta}{\sqrt{r^2 - 2rR_{GS}\cos\vartheta + R_{GS}^2}} \right) d\lambda\, d\vartheta\, dr \quad (4).$$

Equation (4) is differentiated, and becomes

$$g_i^A(0,0,R_{GS}) = -\gamma \int\limits_{r}\int\limits_{\vartheta}\int\limits_{\lambda} \frac{\rho_i r^2 \sin\vartheta (R_{GS} - r\cos\vartheta)}{(r^2 - 2rR_{GS}\cos\vartheta + R_{GS}^2)^{\frac{3}{2}}} d\lambda\, d\vartheta\, dr \quad (5).$$

The total acceleration of all spherical air segments is obtained by solving equation (5) and summing up all contributions. Detailed explanations can be found in Neumeyer et al. (2004, 2006).

As is well known, the atmospheric attraction effect is strongly dependent on the distance. Thus, in the vicinity of a station a large effect exists, so that it is not sufficient to use the 0.5° ×0.5° spacing of the ECMWF data. According to Neumeyer et al., (2004, 2006), therefore air density values are interpolated by means of bi-linear interpolation. 42 additional grid points are computed in the zone between 0 and 0.5°. This means the attraction effect can be calculated every 0.0119° in this zone.

2-4 Calculation of the attraction and deformation effect using 2D data and atmospheric Green's functions

The surface pressure data provided by ECMWF are also used for the calculation of the deformation and the attraction effect based on the formula given in Merriam (1992). The attraction part thus obtained is compared with the variation derived from 3D data.

The attraction and deformation terms at angular distance ϕ from the base of a column of air with an area A in steradians are given by

$$g(\phi)^{deformation} = \frac{GE(\phi)}{10^5 \phi(rad)} \frac{A}{2\pi[1 - \cos(1°)]} \mu Gal/hPa \quad (6)$$

$$g(\phi)^{attraction} = \frac{GN(\phi)}{10^5 \phi(rad)} \frac{A}{2\pi[1 - \cos(1°)]} \mu Gal/hPa \quad (7).$$

GE(ϕ) and GN(ϕ) are respectively the elastic deformation term and Newtonian attraction term from Merriam (1992, Table1 The atmospheric load gravity functions). For the oceans an inverted barometer response is assumed.

We investigate also effects of temperature variations for the calculation of the attraction effect using 2D data. According to the Merriam (1992), when the

temperature effect is considered, the tabular expression for $GN(\phi)$ should be modified in the following way:

$$GN(\phi) = GN(\phi)_{table} + \frac{\partial GN}{\partial T}(T_0 - 15°C) \quad (8)$$

T_0 is the surface temperature. Fig.2 shows the difference between the atmospheric reduction using 2D data with and without temperature variations.
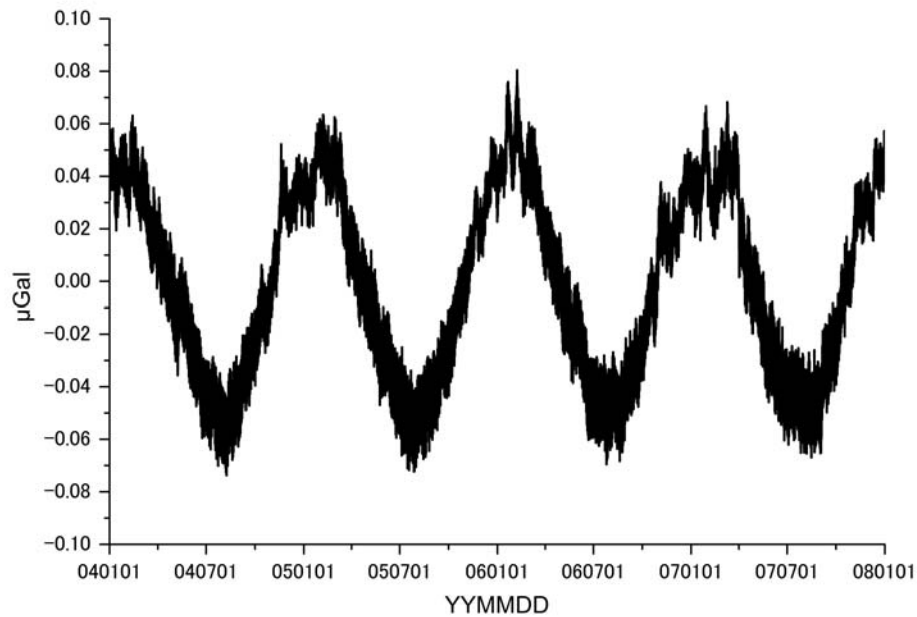
Figure 2
Differences between the attraction effects with and without temperature variation for the reduction using 2D data in Moxa from 2004/01/01 to 2007/12/31 (reduction using (2D with temperature)data – reduction using 2D data)

The peak-to-peak amplitude of the difference between both 2D reductions is 0.14 µGal with a dominant seasonal component and it has a RMS value of 0.036 µGal considering a time span of 4 years.

3. Results
3-1 Comparison between the reductions based on 2D and 3D data

To develop an optimized barometric pressure reduction suitable for current research related to gravity changes of several days and longer, we investigate how spatially extensive the zone needs to be for which the attraction effect should be computed using 3D data sets. This is done by computing the 3D atmospheric attraction effect around the Moxa station up to 15 ° for 6 zones (Fig.3), respectively the zone from the station to 0.5°, and the ring-shape zone from 0.5° to 1.5°, from 1.5° to 3°, from 3° to 5°, from 5° to 10°, and from 10° to 15°.
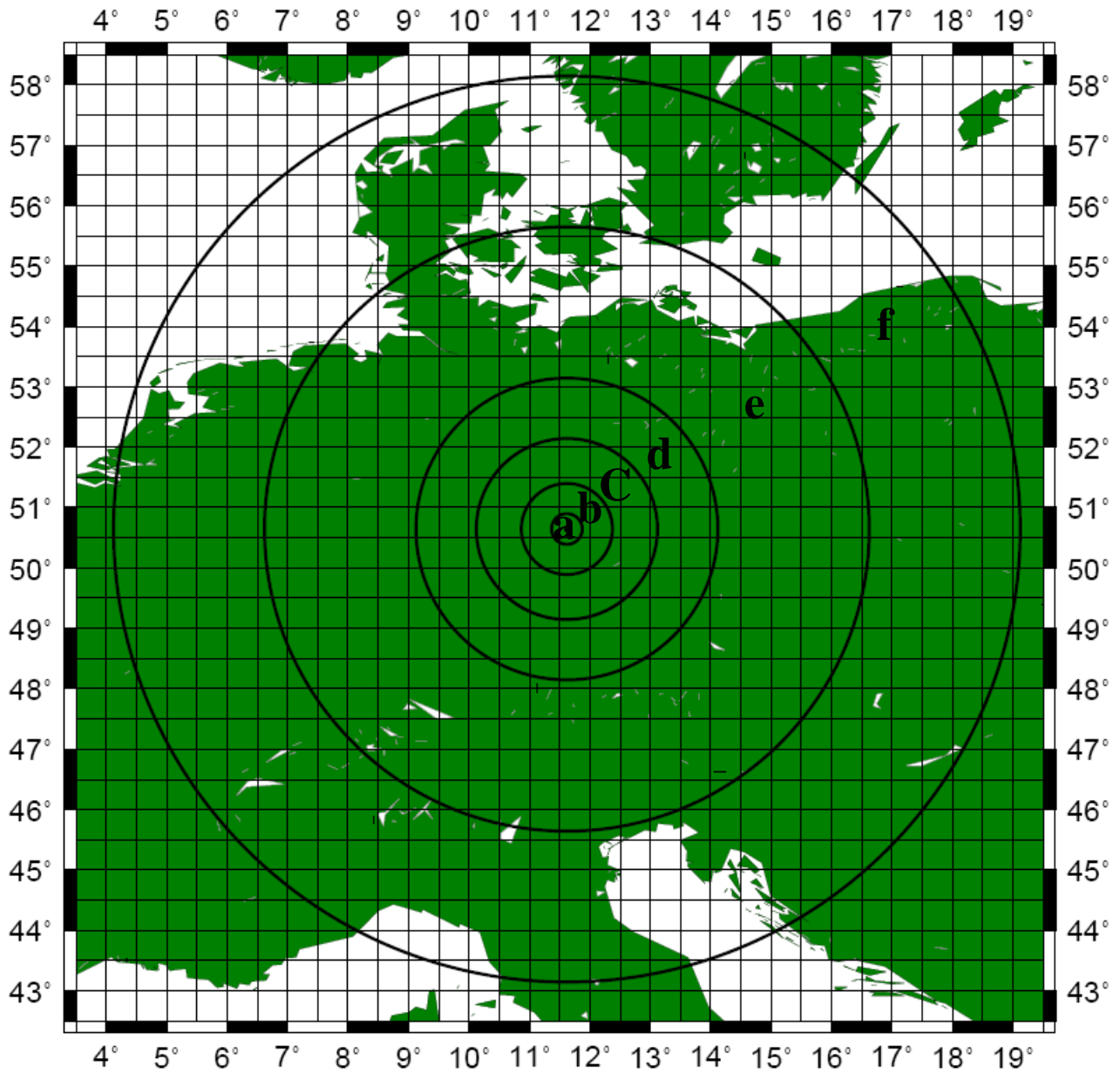
Figure 3
Location of Moxa station and considered zones
a) up to 0.5° , b) 0.5° - 1.5°, c) 1.5°-3°, d) 3°-5°, e) 5°-10°, f) 10°-15°

Fig.4 shows the atmospheric attraction using 3D data for one year from each zone.
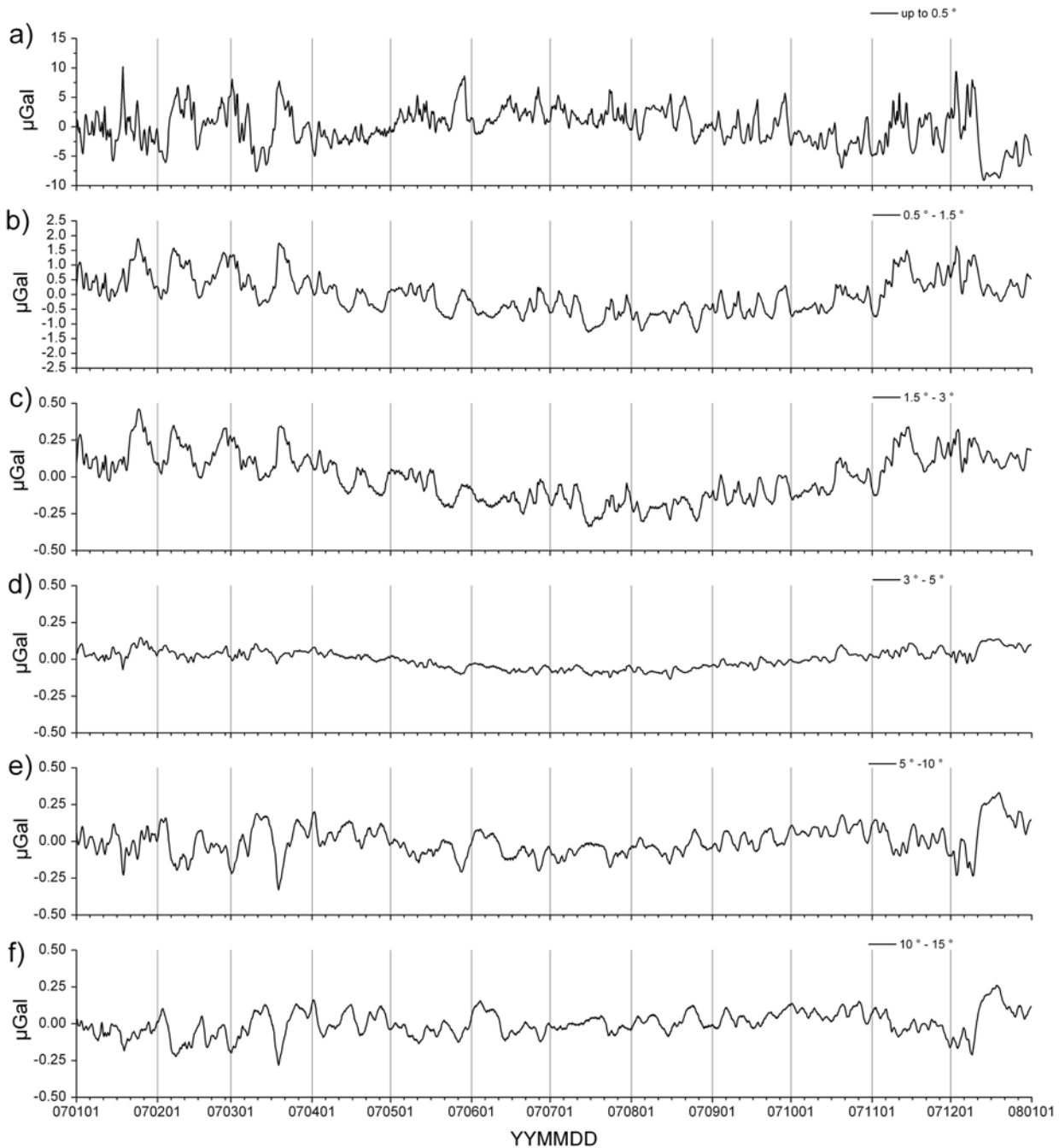
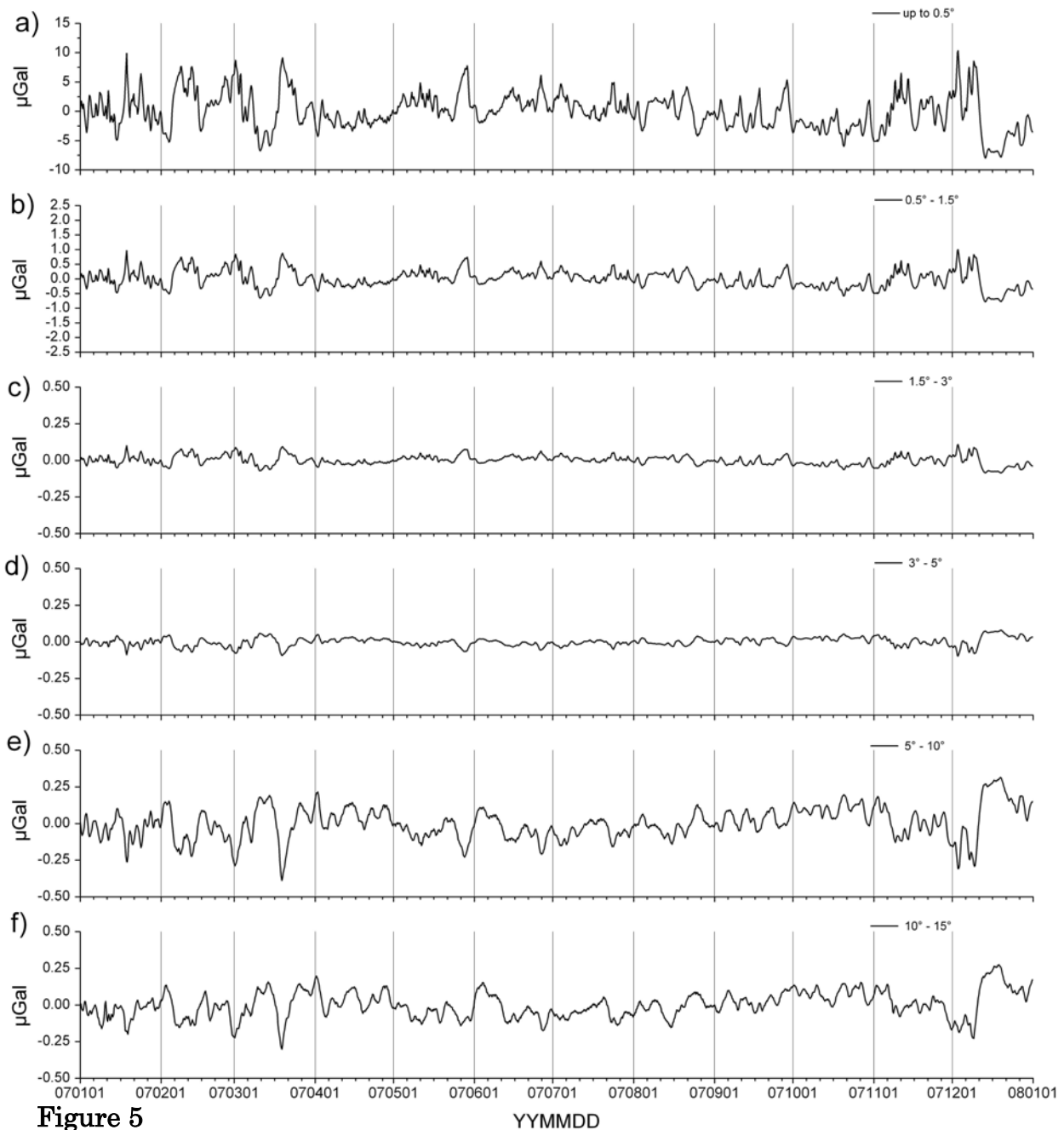**Figure 4**
Attraction effect from the zones indicated in Fig.2 computed with 3D data from 2007/01/01 to 2007/12/31 (different scaling)
a) up to 0.5° , b) 0.5°- 1.5° , c) 1.5°- 3.0° , d) 3.0°- 5.0° , e) 5.0° - 10.0° , e) 10.0°- 15.0°

For the innermost zone the maximal amplitude of attraction effect is around 20 µGal and the Root Mean Square (RMS) value is 3.19 µGal. The peak-to-peak effect from the zone of 0.5° - 1.5° is roughly 1/7 of the innermost zone and the contribution from the zone of 1.5° - 3° reaches 1/30 of the innermost zone. The amplitude of the attraction effect from the zone of 3° - 5° has a peak-to-peak amplitude of 0.3 µGal (Fig.6d), a RMS value of 0.06 µGal and the effect from this zone is the smallest one. The variations from the zone of 5° - 10° and 10° - 15°

revert in sign. The reason for this is that due to the Earth's curvature, the attraction effect around the zone of 3° - 5° is nearly at the same height level as the gravity meter. The attraction from the zone which is more than 5° from the gravity station is already below the height level of the gravity meter. Thus, the direction of the attraction effect changes in sign. These characteristics are also visible in the tabulated Green's functions in Merriam (1992).

In order to estimate for which area the attraction effect using 3D data should be computed, a reduction based on 2D surface data (pressure and temperature) from ECMWF and a standard atmosphere is calculated for comparison (Fig.5).

Figure 5

Attraction effect from the zones indicated in Fig.2 computed with 2D with temperature data from 2007/01/01 to 2007/12/31 (different scaling)

a) up to 0.5° , b) 0.5°- 1.5° , c) 1.5°- 3.0° , d) 3.0°- 5.0° , e) 5.0° - 10.0° , e) 10.0°-
15.0°

The attraction effect using 2D data from the innermost zone has an amplitude
of 18 µGal and a RMS value of 3.0 µGal. The attraction effect from the zone of
0.5° - 1.5° is 10 times smaller than that of the innermost zone. Moreover the
impact of the zone of 1.5° - 3° is 100 times smaller than the innermost zone and
this variation is 3 times smaller than the variation calculated using 3D data. The
variations from the remaining zones have similar features as the effect based on
3D data.

The differences between the gravity reductions using 3D data and 2D data are
given for one year in Fig. 6.
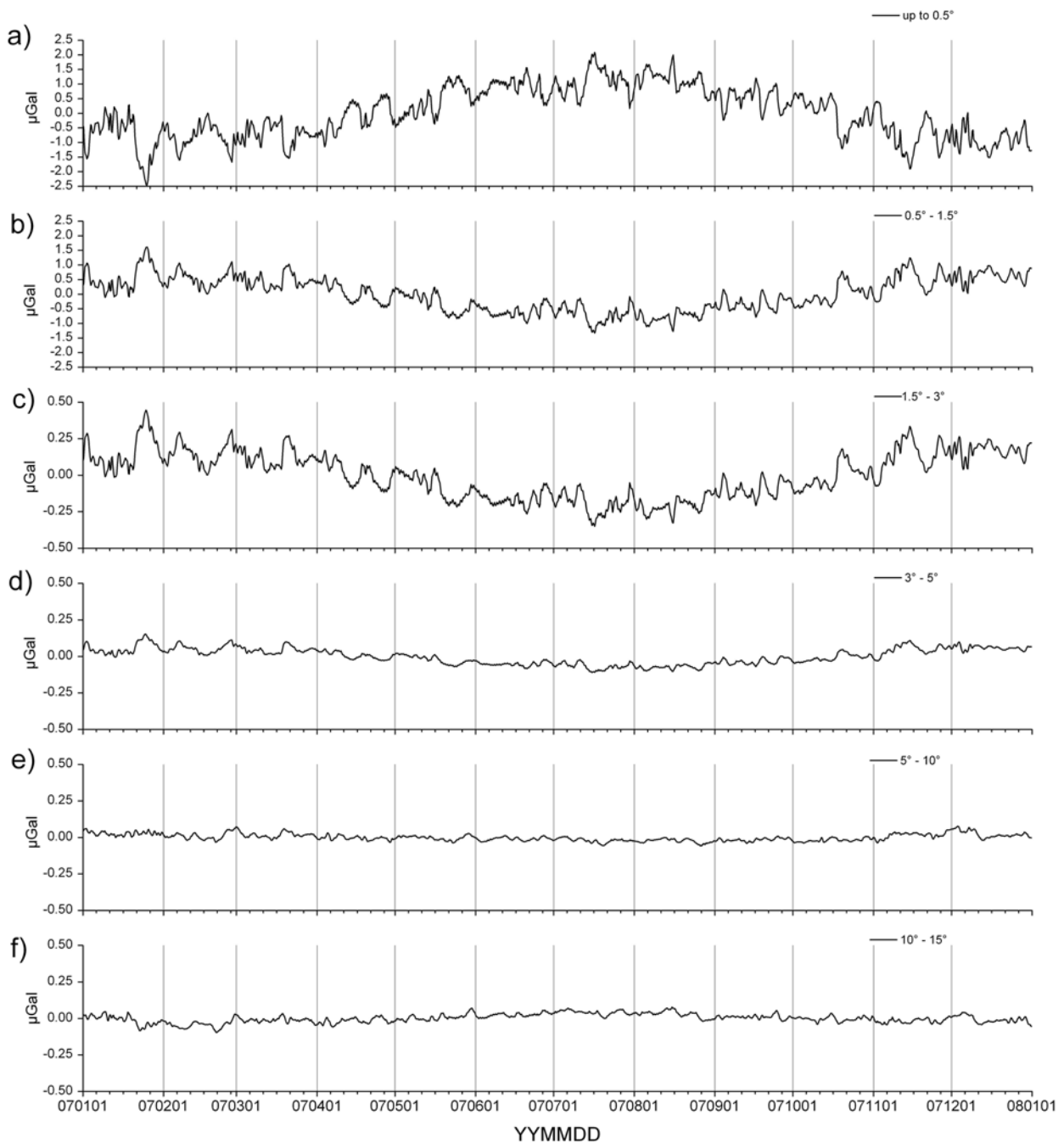
Figure 6
Differences between the attraction effects derived from 3D data and 2D with temperature data for zones of
a) up to 0.5° , b) 0.5° - 1.5°, c) 1.5°-3°, d) 3°-5°, e) 5°-10°, f) 10°-15° from 2007/01/01 to 2007/12/31 (different scaling)

It shows also the gravity effect of the surface pressure independent (SPI) part caused by the mass redistribution within the atmosphere from each zone. For the zone up to 0.5° (Fig.6a), the differences are in the range of 4.5 µGal with a maximum in summer and have a RMS value of 0.88 µGal. The differences for the zones 0.5° - 1.5° and 1.5° - 3° have a peak-to-peak amplitude of 3 µGal and 0.8 µGal (Fig.6b, c) and a minimum in summer. RMS values are 0.58 µGal and 0.16 µGal. As mentioned before, in these areas, the amplitude of the attraction effect using 3D data is 2-3 times larger than the effect obtained from 2D data. Thus, the differences show variations similar to the attraction effect using 3D data. The differences for the zone of 3° - 5° , 5° - 10° and 10°- 15° (Fig.6d,e,f) reach a peak-to-peak amplitude of 0.26 µGal, 0.14 µGal, and 0.18 µGal and RMS values are 0.05 µGal, 0.02 µGal and 0.03 µGal. The differences for the zone larger than 5° are below 0.2 µGal. This is two orders of magnitude smaller values than the total atmospheric effect. Therefore it is concluded that it is sufficient to use 3D data up to 5° and to compute the attraction effect for the remaining earth's surface from 2D data and atmospheric Green's functions. Up to the zone of 5°, there is a peak-to-peak difference of 0.5 µGal including seasonal variations with an amplitude of 0.15 µGal. The RMS value is 0.1 µGal considering a time span of 4 years (Fig.8a). The difference between the 3D and 2D data sets becomes smaller if we sum up the atmospheric attraction effect from each zone.

3-2 Comparison with 3 different atmospheric reductions

In order to gain insight on where the various pressure reductions differ, the three reductions are compared again for the example of Moxa station. Reductions comprise a) 3D data for an area up to 5° to calculate the atmospheric attraction effect, 2D data (pressure and temperature) for the rest of the Earth to calculate the atmospheric attraction effect and 2D data for the whole Earth to calculate the atmospheric loading effect (physical approach), b) 2D data (pressure and temperature) for the whole Earth for the calculation of the atmospheric attraction and loading effect (physical approach), c) an admittance factor (-0.3649 µGal/hPa) which is estimated from the regression analysis between observed barometric pressure data and SG data (standard method). Fig.7 shows these reductions for a time span of 4 years.
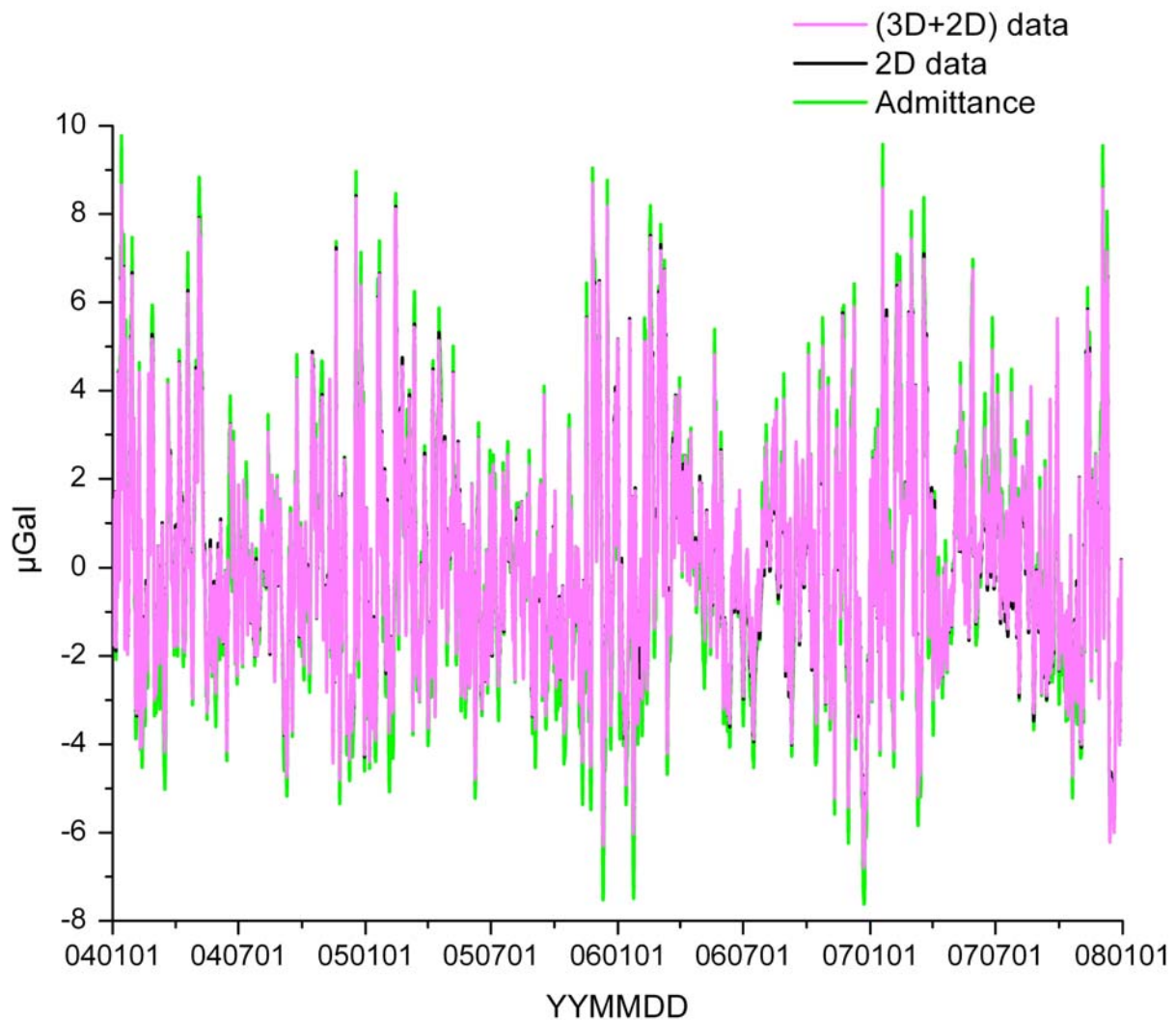
Figure 7
Atmospheric reductions for Moxa observatory from 2004/01/01 to 2007/12/31
(3D+2D) data =
attraction effect : based on 3D data up to 5 degree around station + 2D data are used for the calculation of the rest of the Earth
deformation effect : based on 2D data
2D data = attraction and deformation effect : based on 2D data
Admittance = the reduction based on admittance factor

The reduction using an admittance factor is larger than the others. The difference between the reductions is given in Fig.8 for the same 4 year-long data set.
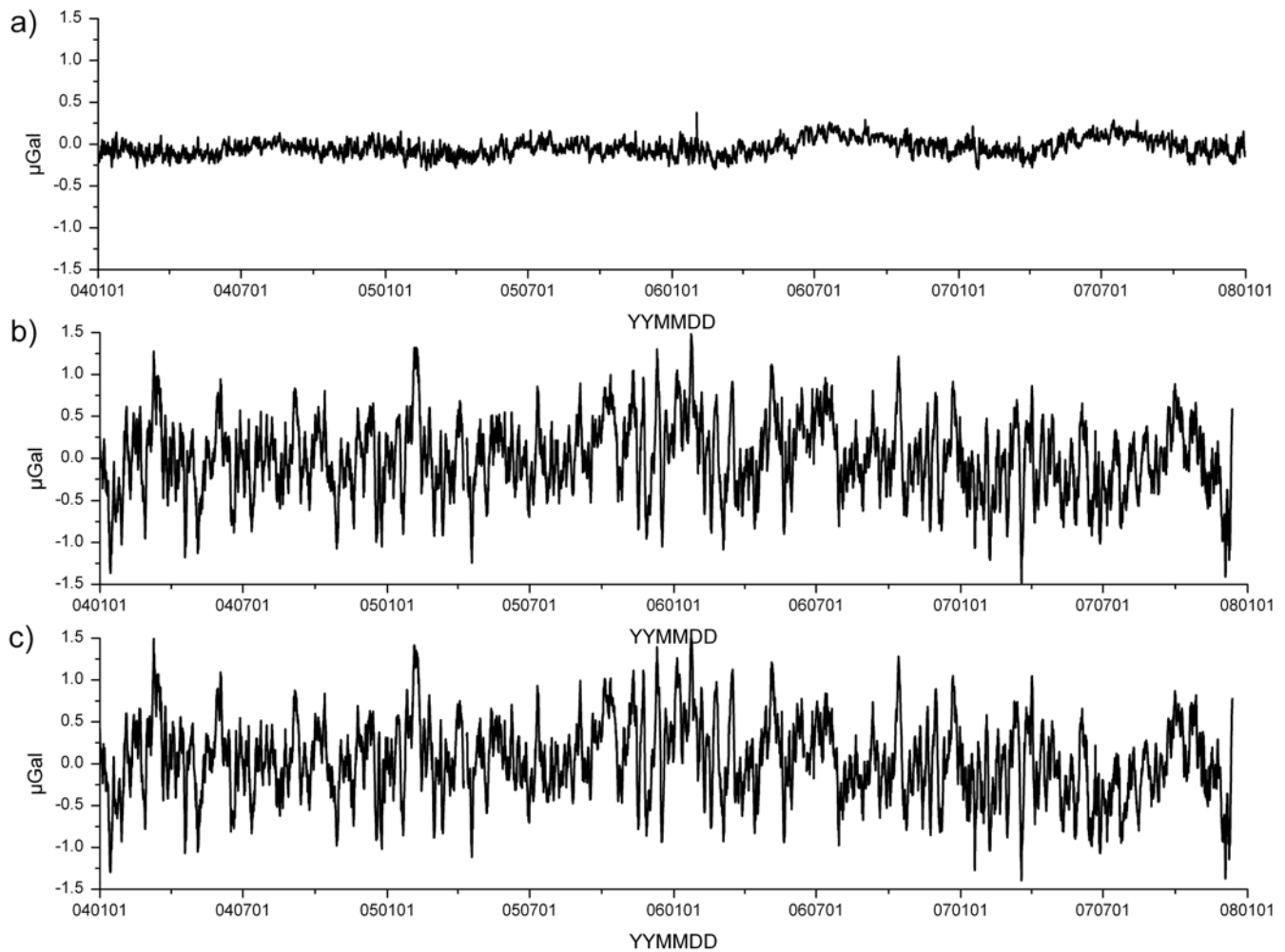
Figure 8
Differences between atmospheric reductions from 2004/01/01 to 2007/12/31
a) based on 3D+2D data - 2D data
b) based on 3D+2D - admittance factor
c) based on 2D data - admittance factor

The difference between the two reductions based on a physical approach (Fig.8a) has a peak-to-peak amplitude of 0.5 µGal including seasonal variations with an amplitude of 0.15 µGal as mentioned previously with a maximum in summer. The RMS value amounts to 0.1 µGal. Fig.8b, c show respectively the differences between the reductions derived from the two physical approaches and an admittance factor. They have similar variations and a peak-to-peak amplitude of 3 µGal with a RMS value of 0.4 µGal.

In order to determine, in which spectral ranges the differences occur, spectral analyses are computed (Fig.9).
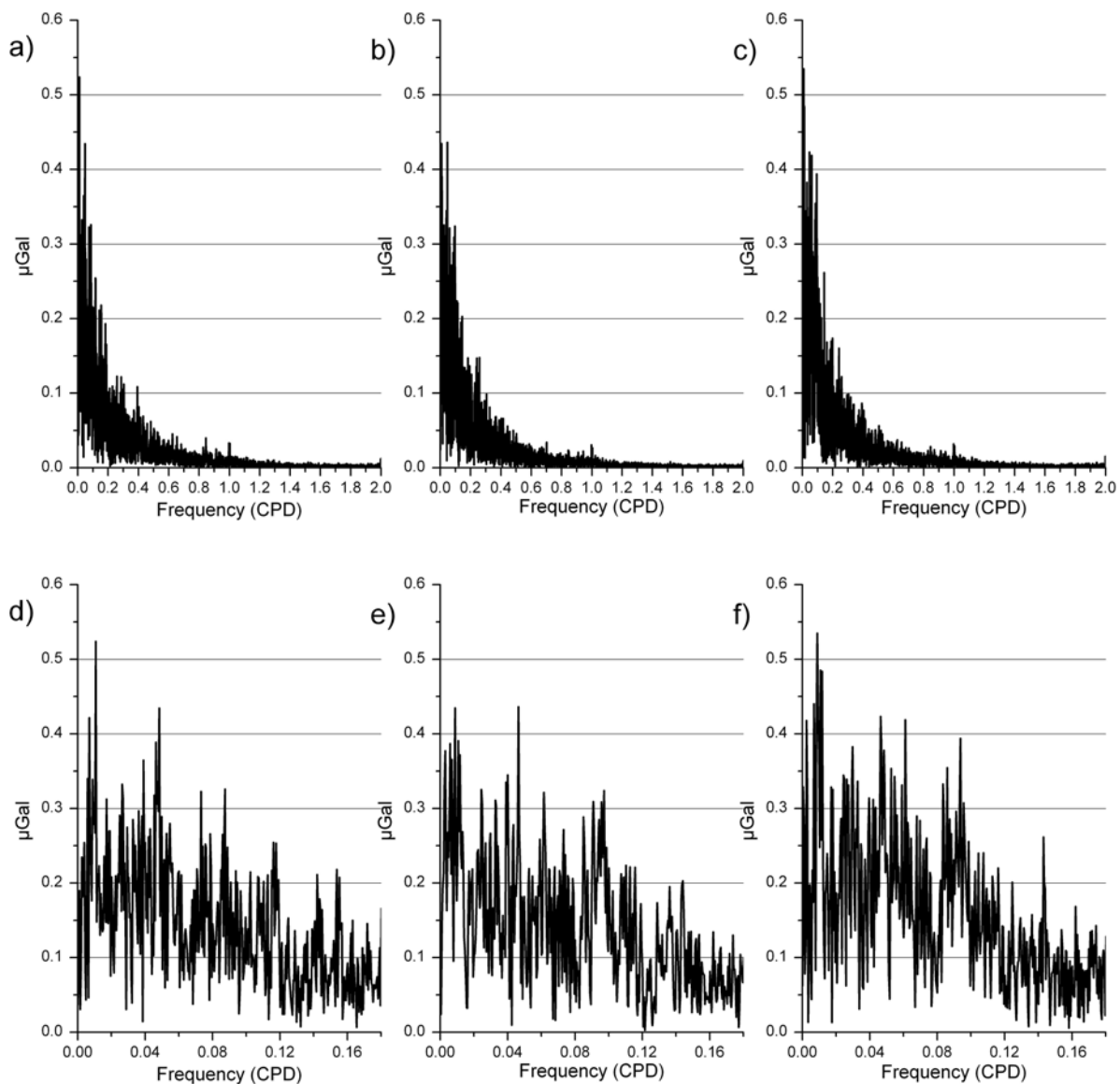
Figure 9

Amplitude spectra of different atmospheric effects from 2004/01/01 to 2007/12/31
a) reduction 3D+2D , b) reduction 2D data , c) admittance factor
enlarged
d) reduction 3D+2D , e) reduction 2D data , f) admittance factor

Fig.9a, b, c show the amplitude spectra of the reductions using (3D+2D) data, 2D data, and an admittance factor respectively. The amplitudes of the reduction based on 2D data have a 6% smaller value than the reduction based on (3D+2D) data and are 12% smaller than the reduction using an admittance factor on average in the spectral range between 0 and 2.0 CPD. To investigate in particular the range of long-period tides, the range between 0.0 and 0.18 CPD is enlarged (Fig.9d, e, f). The amplitude of the reduction using 2D data is 1.3% smaller than the reduction using (3D+2D) and 12% smaller than the reduction using an admittance factor in this range on average. The amplitude difference

between the reduction based on (3D+2D) data and 2D data in the range of long-period tides (1.3%) is smaller than that in the range between 0 and 2.0 CPD (6%). These differences in the amplitudes are seen in the gravity residuals after carrying out the tidal analysis, due to the fact that either a too large or too small atmospheric reduction is applied to the gravity data.

3-3 Result of tidal analysis

It is also investigated how the different atmospheric reductions affect the tidal analysis. The tidal analyses are carried out using "BAYTAP-G and -L" (Tamura et al., 1991). The data cover 3 years. For the analysis, the atmospheric reductions derived from the ECMWF data are interpolated to 1h sample. In order to analyze the long-period Earth tides using BAYTAP-L, the data are re-sampled to 1 day interval.
 Fig.10a shows the SG data from Moxa station after removing steps and spikes from 1st of January, 2004 to 31st of December, 2006. The SG data have a peak-to-peak amplitude of 250μGal. Fig.10 b, c, d) show the gravity residuals after applying the three atmospheric reductions discussed before. Additionally the Earth tides, which are computed using different tidal factors determined after application of different pressure corrections as well as polar motion correction, are removed from the gravity observations. We calculate polar motion with IERS (International Earth Rotation Service) data using the well-known formula (IAGBN, 1992)

$$\delta g = -\delta \times 10^8 \times \omega^2 \times a \times 2 \times \sin\varphi\cos\varphi \cdot (x\cos\lambda - y\sin\lambda)\,\mu\text{Gal.} \quad (9)$$

where δg is gravity variation caused by polar motion , δ is 1.164 for the spherical elastic Earth, x and y (rad) are the coordinates from IERS , ω is Earth's rotational velocity (7292115×10^{-11} (rad/s)), a is equatorial radius (semi-major axis) of reference ellipsoid (6378136.3(m)), and ϕ and λ are respectively latitude and longitude of the observation site. In order to subtract the SA and SSA tide, the theoretical model of DDW (Dehant et al., 1999) is used.
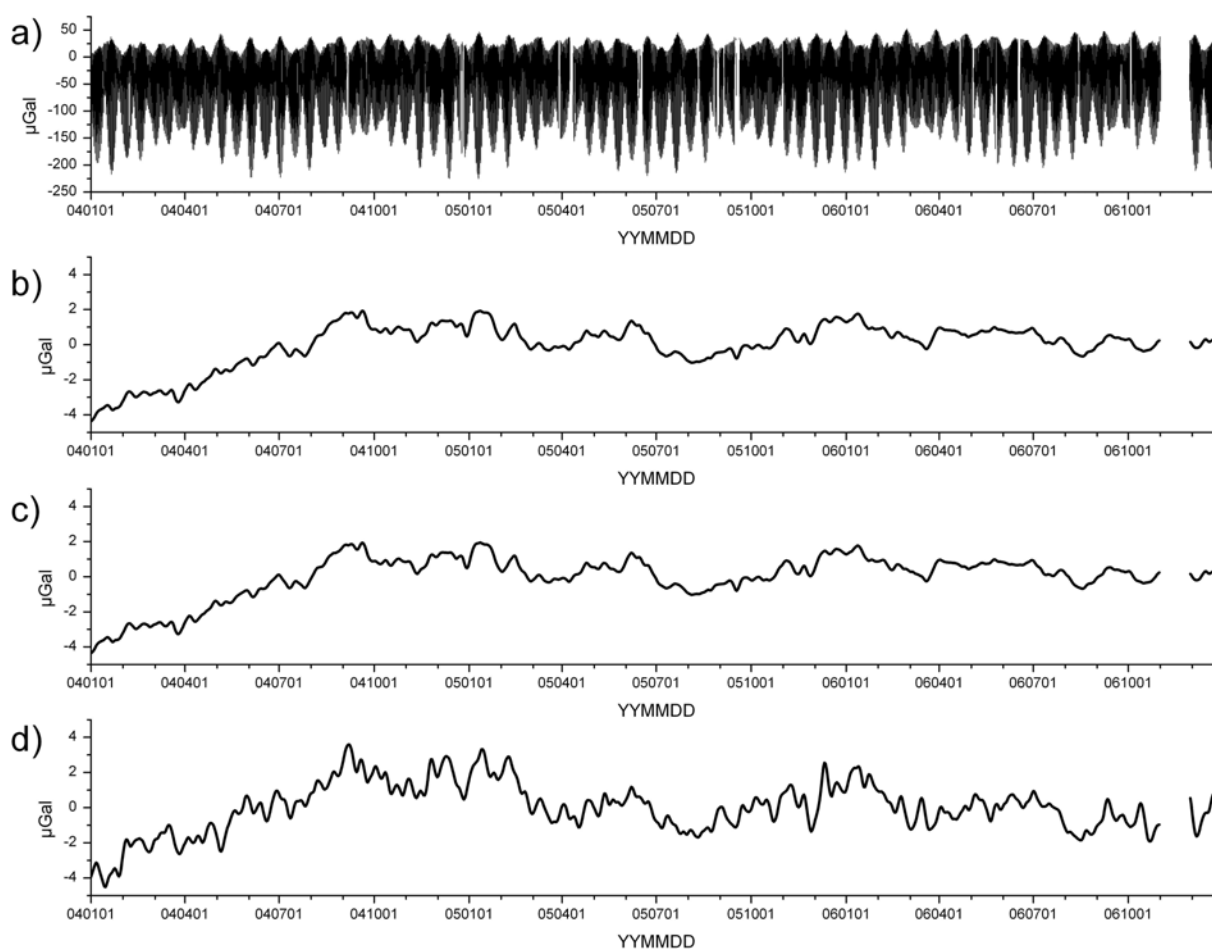
Figure 10
SG observation and gravity residuals from Moxa station after removing tides and atmospheric effect using different reductions from 2004/01/01 to 2006/12/31
a) SG data (after removing steps & disturbances)
b) reduction 3D+2D , c) reduction 2D data , d) admittance factor

The two reductions (Fig.10b, c) based on a physical approach yield similar gravity residual variations with a peak-to-peak amplitude of 7 µGal. The gravity residuals obtained by using an admittance factor (Fig.10d) contain stronger variations with a peak-to-peak amplitude of 1-3 µGal with periods of 5 days to 30 days which do not occur for the other two reductions.

In order to investigate in which period bands differences occur, Table 1 shows the mean amplitude of the gravity residuals after applying different atmospheric reductions for five period bands; periods longer than 1000 days, between 1000 and 250 days, between 250 and 50 days, between 50 and 15 days and 15 and 2 days.

Period bands		μGal	difference (%)		μGal	difference (%)
1000 d < T	2D data (3D+2D) data admittance	0.3894 0.3071 0.3695	26.81	2D+temp data (3D+(2D+temp)) data admittance	0.2930 0.2937 0.3695	0.0025
250 d < T < 1000 d	2D data (3D+2D) data admittance	0.1924 0.2356 0.4028	-18.31	2D+temp data (3D+(2D+temp)) data admittance	0.2506 0.2495 0.4028	0.0045
50 d < T < 250 d	2D data (3D+2D) data admittance	0.0945 0.0914 0.1248	3.30	2D+temp data (3D+(2D+temp)) data admittance	0.0914 0.0911 0.1248	0.0026
15 d < T < 50 d	2D data (3D+2D) data admittance	0.0281 0.0278 0.0544	1.02	2D+temp data (3D+(2D+temp)) data admittance	0.0288 0.0288 0.0544	≈
2 d < T < 15 d	2D data (3D+2D) data admittance	0.0010 0.0010 0.0034	≈	2D+temp data (3D+(2D+temp)) data admittance	0.0013 0.0013 0.0034	≈

Table 1
Mean amplitude of gravity residuals for reductions based on (3D+2D) data, 2D data (with and without temperature-dependent part) and an admittance factor for different period bands and difference between the physical approaches (%)

For comparison, results derived from the 2D- reduction without temperature variations are also shown in the table 1. If the temperature effects are not included, the gravity residuals applying the reduction based on (3D+2D) data is 1 - 3% different from the gravity residuals based on 2D data in the period band between 15 and 250 days on average. In the period band between 250 days and 1000 days, 18% of deviations exist between the gravity residuals based on the physical approaches. This result indicates that the reduction based on 2D data removes not only the signal related to the atmosphere in this period band but also other signal. However, if we include the temperature-dependent component, the differences between reductions using 3D data and 2D data become nearly zero. The application of an admittance factor leads to 1.2 - 3.4 times larger amplitudes than the other two methods in the considered five period bands. An explanation for this is that the spatial and temporal scale of air mass movements is more or less proportional (Fortak, 1971), for instance if the scale of the atmospheric mass movement is 1 km, then the associated temporal variation is in the range from 50 sec to 8 min, but if the spatial scale of atmosphere is 500 km, then the temporal variation is about 3 h to 8 days. With increasing spatial extension of an atmospheric mass, the deformation component increases, thus more of the attraction part is compensated. This in turn results in a reduced admittance factor for lower frequencies. Applying an admittance factor which is determined from short-period tides therefore leads to a well known too big

reduction in the long-period tides range. This explains why the amplitude of the reduction using an admittance factor is larger than the other two and the amplitude spectra of the reduction using an admittance factor is 11% - 12% larger than the others in the spectral range of long-period Earth tides.

Concerning the result of the tidal analyses, the sampling rate of the ECMWF data is 6 h, therefore, only the long-period tidal parameters are discussed. The amplitude factors using physical approaches do not have large discrepancies. All tidal factors and phases derived from the physical approaches are in agreement within the error bars of (3D+2D).

Concerning the amplitude factors between the reduction using (3D+2D) and using an admittance factor, the amplitude factor of MM, MF, MSTM and MSQM are not in agreement within the error bars of (3D+2D). The error values of the reduction based on an admittance factor are 44 - 73% larger than that of the reduction using (3D+2D) data.

For the differences between the phase values using (3D+2D) data and using an admittance factor, MM, MF and MSQM are not in agreement within the error bars of (3D+2D). The error bars of the reduction using an admittance factor have 42% - 72% larger than the reduction using (3D+2D) data.

Finally, table 2 shows the amplitude factor of the polar motion signal. This factor is estimated between the theoretical gravity polar motion signal, which is determined by use of equation 9 with $\delta=1.0$, and the gravity residuals after applying the different atmospheric reductions, removing the tides and drifts. There is a 1.5% difference between the value of the factor after applying the reductions using 2D data including temperature and 3D data, however, these differences are within the associated standard deviation.

atmospheric reduction	amplitude factor	standard deviation
(3D+(2D+temp))	1.147	0.017
2D+temp	1.164	0.017
(3D+2D)	1.147	0.017
2D	1.165	0.017
admittance	1.159	0.023

Table 2
Amplitude factor of the polar motion signal derived after applying different atmospheric reductions

4, Conclusions

From computing the attraction effect of 6 zones up to 15° from Moxa station using 3D data from ECMWF and comparing it with the attraction effect derived

from 2D data (pressure and temperature) and a standard atmosphere, we find that the difference in the attraction effect from the zone up to 0.5° around the station, the ring-shaped zone of 0.5° - 1.5°, 1.5° - 3°, and 3° - 5° are respectively 4.5 µGal, 3 µGal, 0.8 µGal and 0.26 µGal. In contrast, the differences from the ring-shaped zone of 5° - 10° and 10° - 15° is below 0.2 µGal. We infer, therefore, that it makes sense to calculate atmospheric attraction effect up to 5° using 3D data

The difference between the physical reductions and the use of an admittance factor amounts to around 3 µGal with a RMS value of 0.4 µGal in a time span of 4 years and the differences between both physical approaches have a peak-to-peak amplitude of 0.5 µGal including seasonal variations with an amplitude of 0.15 µGal and a RMS value of 0.1 µGal.

From spectral analysis of these three reductions, it emerges that in the spectral range between 0.0 CPD and 0.18 CPD, the amplitude of the reduction using (3D+2D) data is 12% smaller than that of the reduction using an admittance factor on average and 1.3% larger than that of the reduction using 2D data (pressure and temperature). Moreover, in the spectral range between 0.0 to 2.0 CPD, the difference between the reduction using (3D+2D) data and 2D data becomes larger (6%). On the other hand, the difference between the reduction using (3D+2D) and an admittance factor is nearly the same value (12%).

Concerning the tidal analysis, the error bars of the reduction based on an admittance factor are 44% - 73% for the tidal factors and 42% - 72% for the phases larger than the reduction using (3D+2D) data by comparing the results. However, there are no visible improvements between the results based on the physical approaches.

Comparing the mean amplitude of the gravity residuals for five different period bands yields also no dramatic differences between the two physical reductions. If we do not consider the temperature-dependent component in the reduction using 2D data, there are 18% differences between both data sets. Moreover, we show that the amplitude of the residuals after a reduction using an admittance factor is 1.2 - 3.4 times larger than for the other two methods in the five period bands. This is explained by the fact that the impact of atmosphere cannot be represented using only one admittance factor for all frequencies due to the different spatial extensions of air masses and the associated velocities. This emphasises once more the findings by Warburton and Goodkind (1977), Crossley et al. (1995) and Neumeyer (1995). The reductions using (3D+2D) data or 2D data do not have this problem because they can be estimated directly using the atmospheric cells. The reductions derived from physical approaches capture the atmospheric effects better than the reduction derived from an admittance factor.

With regard to the development of an improved reduction on a physical basis, the consideration of 3D data and 2D data with a temperature-dependent component leads almost to the same result in the tidal analysis. A 1.5% difference exists between both physical approaches considering temperature variations in the determination of the amplitude factor of the polar motion signal.

The effect of actual vertical atmospheric distribution is not obvious; however, this accuracy is necessary for further studies of small long-period geodynamic signals such as the polar motion or long-period non-tidal mass shifts in the

oceans. The effect has a peak-to-peak amplitude of 2.2-2.7 µGal (Kroner et al. 2009). A reduction model should be at least one order of magnitude more accurate than the effect which is to be investigated. Therefore, it is recommended to use the more sophisticated atmospheric reduction model discussed in this paper.

References

Boy, J.P., Hinderer, J., Gegout, P.,1998. Global atmospheric loading and gravity. Phys. Earth Planet. Int., **109**,161-177.

Boy, J.P., Gegout, P., Hinderer, J., 2002. Reduction of surface gravity from global atmospheric pressure loading. Geophys. J. Int., **149**, 534-545.

Crossley, D., Jensen O.G., Hinderer J., 1995. Effective barometric admittance and gravity residuals. Phys. Earth Planet. Int., **90**, 221-241.

Crossley, D., Hinderer, J., Casula, G., Francis, O., Hsu, H.T., Imanishi, Y., Jentzsch, G., Kääriänen, J., Merriam, J., Meurers, B., Neumeyer J., Richter, B., Shibuya, K., Sato, T., 1999. Network of superconducting gravimeters benefits a number of disciplines, EOS, Trans. Am. Geophys. U., **80**, 121-126.

Dehant, V., Defraigne, P., Wahr, J.M., 1999. Tides for a convective Earth, J. Geophys. Res, **104**, 1035-1058.

ECMWF, Higher resolution model upgrade - 2 February 2006, Operational upgrades.

Farrell, W.E., 1972. Deformation of the Earth by surface loads.Rev. Geophys. Space Phys., **10**, 761–797.

Fortak, H., 1971. Meteorologie. Carl Hebel Verlagsbuchhandlung, Berlin and Darmstadt.

Guo, J. Y., Li, B. Y., Huang, Y., Deng, T. H., Xu., Q. S. and Ning, S. J., 2004. Green's function of the deformation of the Earth as a result of atmospheric loading. Geophys. J. Int., **159**, 53-69.

IAGBN,1992. Absolute Observations Data Processing Standards.

Kroner, C. & Jentzsch, G., 1999. Comparison of different barometric pressure reductions for gravity data and resulting consequences. Phys. Earth Planet. Int., **115**, 205-218.

Kroner, C., Jahr, Th., Jentzsch, G., 2004. Results from 44 months of observations with a superconducting gravimeter at Moxa/Germany. Journal of Geodynamics, **38**, 263-280.

Kroner, C., Thomas, M., Dobslaw, H., Abe, M., Weise, A., 2009. Effect of non-tidal mass shifts on observations with superconducting gravimeters. Journal of Geodynamics., accepted.

Merriam, J.B., 1992. Atmospheric pressure and gravity. Geophys. J. Int., **109,** 488-500.

NASA (National aeronautics and Space Administration) U.S. Standard Atmosphere, 1976, U.S. Government Printing Office, Washington, D.C., 1976.

Neumeyer, J., 1995. Frequency dependent atmospheric pressure correction on gravity variations by means of cross spectral analysis. Bulletin d'Information des Marées Terrestres, **122**, 9212-9220.

Neumeyer, J., Hagedoorn, J., Leitloff, J., Schmidt, T., 2004. Gravity reduction with three-dimensional atmospheric pressure data for precise ground gravity measurements. Journal of Geodynamics, **38**, 437-450.

Neumeyer, J., Schmidt, T., Stoeber, C., 2006. Improved determination of the atmospheric attraction with 3D air density data and its reduction on ground gravity measurements. Dynamic Planet - monitoring and understanding a dynamic planet with geodetic and oceanographic tools ; IAG Symposium, Cairns, Australia, 22-26 August, 2005 - International Association of Geodesy Symposia, **130**, 541-548.

Sun, H.-P., Ducarme, B., Dehant, V., 1995. Theoretical calculation of atmospheric gravity Green's functions. Proc. 2nd Workshop on non tidal gravity changes, intercomparison between absolute and superconducting gravimeters', Cahiers du Centre Européen de Géodynamique et de Séismologie, **11**, 223-237.

Tamura, Y., Sato, T., Ooe, M., Ishiguro, M., 1991. A procedure for tidal analysis with a Bayesian information criterion. Geophys. J. Int., **104**, 507-516.

Warburton R. J. & Goodkind J. M., 1977. The influence of barometric - pressure variations on gravity. Geophys. J. R. Astr. Soc., **48**, 281-292.

BLANK PAGE

A New Tidal Gravity Station at Hurghada, Red Sea, Egypt

R. M. Hassan[2], K. H. Zahran[1], G. Jentzsch[2] and A. Weise[2]

1National Research Institute of Astronomy and Geophysics, Helwan, Egypt
2 Friedrich- Schiller- University, Institute of Geosciences, Jena, Germany

Abstract

The Red Sea region is one of the seismically active regions in Egypt due to the tectonic movements in the Red Sea. The evaluation of the seismic activity and recent crustal movements in this region is an important point of scientific interest. The LaCoste and Romberg gravimeter D-218 was installed in the tidal gravity station on the ground floor of the main building of the Seismological Centre at Hurghada, Red Sea, Egypt. One year of continuous gravity observations (February 2008 to February 2009) are available to conduct the current study. The main objectives are to determine the response of the crust to the tidal forces and, in consequence, to supply reductions for the geodetic observations, which were initiated due to the continuous seismological activities in this region. The tidal parameters of Hurgada station have been determined by least squares adjustment and the standard deviation of the analysis is ± 5.6 nm/s^2. The residuals reach about 20 nm/s². The amplitude spectrum shows a noise level in the diurnal band of 5.5 nm/s² and 6 nm/s² in the semidiurnal band.

1. Introduction

Hurghada city is located in a seismically active area close to the triple junction of the African plate, Arabian plate and Sinai sub-plate. The boundaries of these three plates are seismically active and are represented by three seismic source zones: the northern part of Red Sea, the southern part of Gulf of Suez and the Gulf of Aqaba seismic zones (Fig. 1). The National Research Institute of Astronomy and Geophysics (NRIAG) has established a seismic network (ENSN) to study the seismic activity and a geodetic network to monitor the recent crustal movements. Thus, a tidal gravity station at Hurghada is of great importance in this region. In the gulf areas and shelf regions usually a lateral change of the tidal constituents is observable due to the complicated tidal wave propagation against the boundary of the shelf and the influence of the bottom and coastal friction in shallow water areas. The anomalous behavior of the tidal constituents in Gulf regions has made the accurate prediction of tides in these regions of considerable importance for various geophysical, geodetic and oceanographic applications. NRIAG has successfully established tidal gravity stations at both Cairo (Zahran et. Al, 2004) and Aswan (Hassan, 2007 ; Hassan et al., 2009 a & b). An additionl tidal gravity station has been established at the ground floor of the main building of Hurghada seismological center to achieve a higher accuracy for geodetic and geophysical observations, so high precaution in the observation and advanced analysis technique has to be applied.

2. Objectives of Hurghada Tidal Gravity Station

The objectives of Hurghada tidal gravity station are summarized as follows:
a- Carrying out continuous gravity observations to determine the local elastic parameters of the Earth's crust to the tidal forces;
b- Providing Earth tide reductions for gravity measurements and other precision measurements (satellite positioning and leveling);
c- Determining the observed ocean tide loading parameters
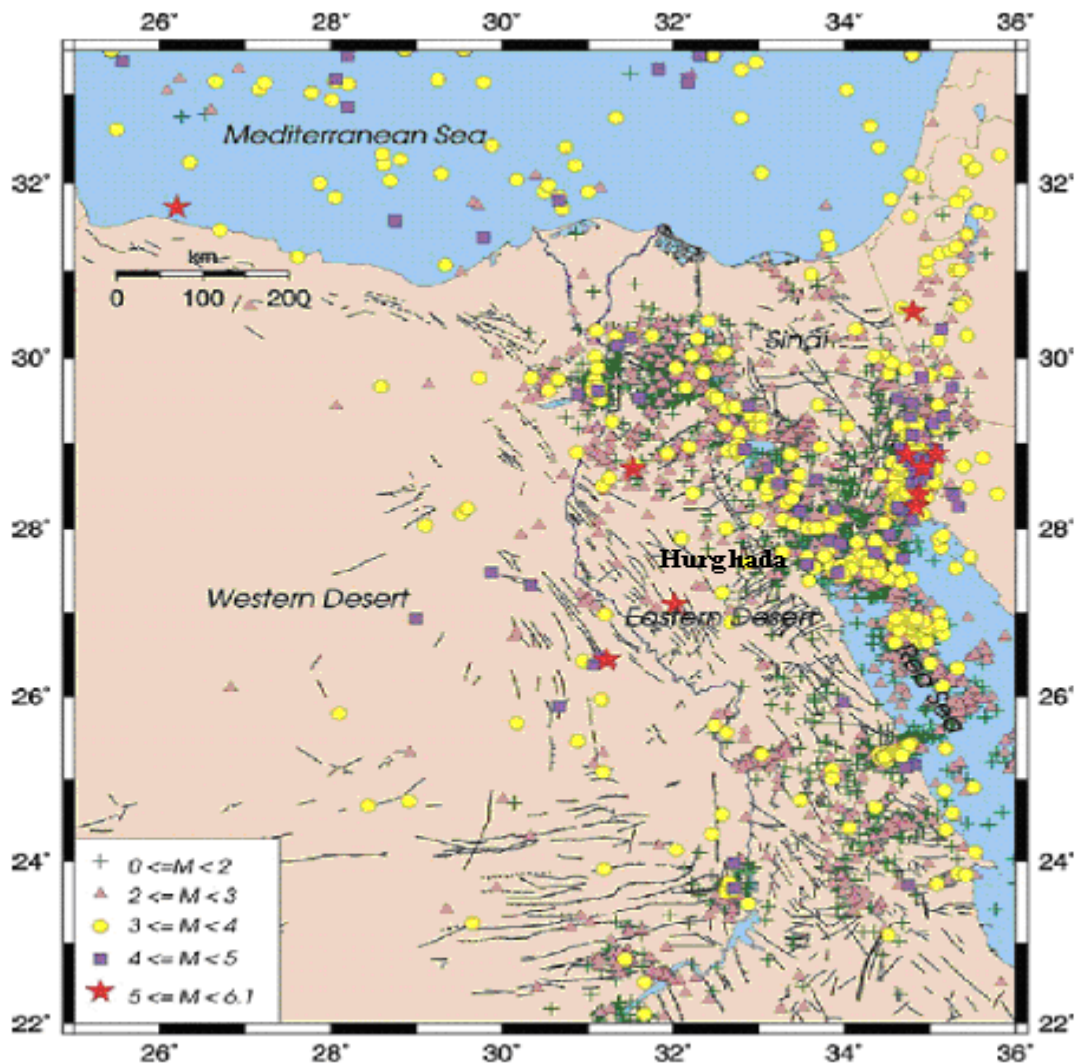d- Comparing the recent ocean tide models with the observed ocean tide loading

Figure 1. Local earthquakes recorded by ENSN from Aug. 1997 to Dec. 2004.

3. Hurghada Station

Hurghada tidal gravity station is located in Hurghada city (Fig. 2) at the ground floor of the main building of the Seismological Centre at Hurghada, which is close to the shore line of the Red Sea (about 250 meters). The station coordinates are 27.313° N and 33.832° E, and the elevation is 77.25m. A wooden box chamber that consists of double walls of wood and insulation material between the double walls was designed to keep the sensor (gravimeter) isolated from the surroundings. The sensor was installed on a pillar connected to the bedrock, inside the wooden box room, which is separated from the construction of the building. The gravimeter used is the LaCoste-Romberg meter D-218 with electrostatic feedback. The temperature stability in the sensor room is better than 1°C per day. The recording system consists of a multi-channel A/D-converter to provide the feedback output to the computer (Fig. 3). Besides, an UPS (uninterruptible power supply) guarantees for safe power supply and a Laptop is used to download the data.
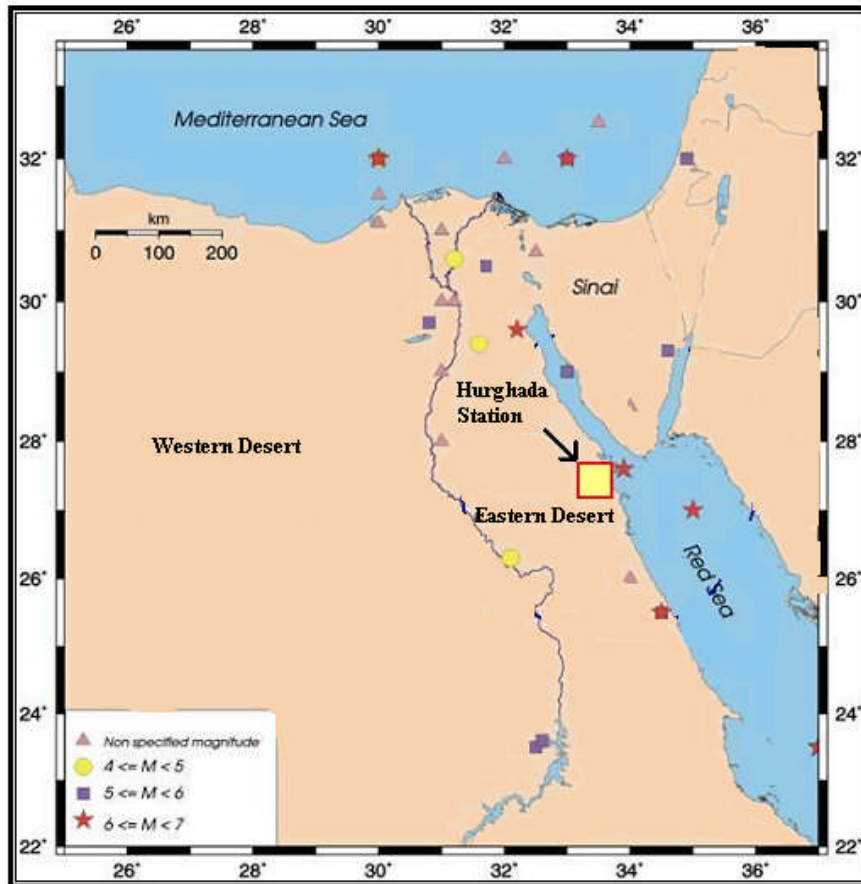
Figure 2. Location of Hurghada tidal gravity station.

Figure 3. Lacoste and Romberg Gravimeter D-218 in the measuring room of Hurghada
station (left) and recording system (right).

4. Recording of Data

The recorded data were stored in a computer using software which was designed under Q-basic. Because of the response time of the feedback system there was no additional anti-aliasing filter. The data comprise three channels: two channels for the long and cross levels of the gravimeter and the third one for the feedback output. Data were logged in a high resolution sampling interval of 5 seconds. The data were stored in files, each of one hour capacity. The ETERNA format used was described by Wenzel (1994). It was adopted for the exchange of high precision and high rate Earth tide data by the working group on High Precision Tidal Data Processing at its meeting in Bonn 1994 (Jentzsch, 1995). The recording of tidal gravity data started in February, 2008, and is still going on. The changes in air pressure and temperature affect the quality of the recorded data. Besides, the data contain some gaps due to power failure. The raw data, with all noise and local perturbations, are shown in Fig. 4. The data contain, in general, a high drift. Because the station is located in a region of seismic activity, any seismic activity is clearly observed in the raw data. A period of one year (Feb. 2008 to Feb. 2009) was used for the tidal analysis.
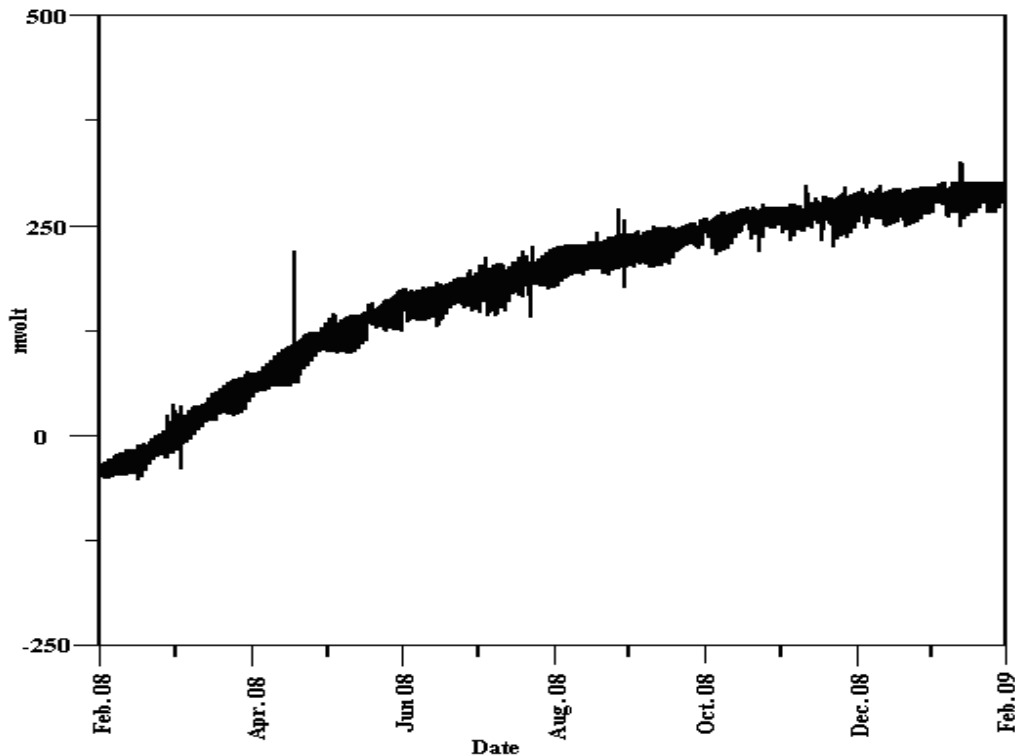

Figure 4. Raw data recorded from Feb. 2008 to Feb.2009 at Hurghada station (calibration factor 1mvolt = 12.88 nm/s^2) .

5. Analysis of Hurghada Tidal Gravity data

The tidal analysis was carried out using the program ANALYZE of the ETERNA 3.4 package (Wenzel, 1996, 1997), using the Hartmann and Wenzel (1995a, b) tidal potential catalogue. A numerical digital high-pass filtering was applied in order to eliminate the long periodic drift of the instrument. The analysis of data contained two main steps, first: data pre-processing

and second: data analysis. In the first step the 5 second data files for each day were combined to one single file per day, and then, all files were combined to one file. The data were numerically filtered and sampled at 1 min interval. Afterwards, the 1 min data were calibrated and corrected for drift. The corrected one minute samples were finally numerically filtered and decimated to one hour sampling interval, using the program DECIMATE. The hourly samples have been used for tidal analysis. Fig. 5 shows the pre-processed hourly samples of the recording period.
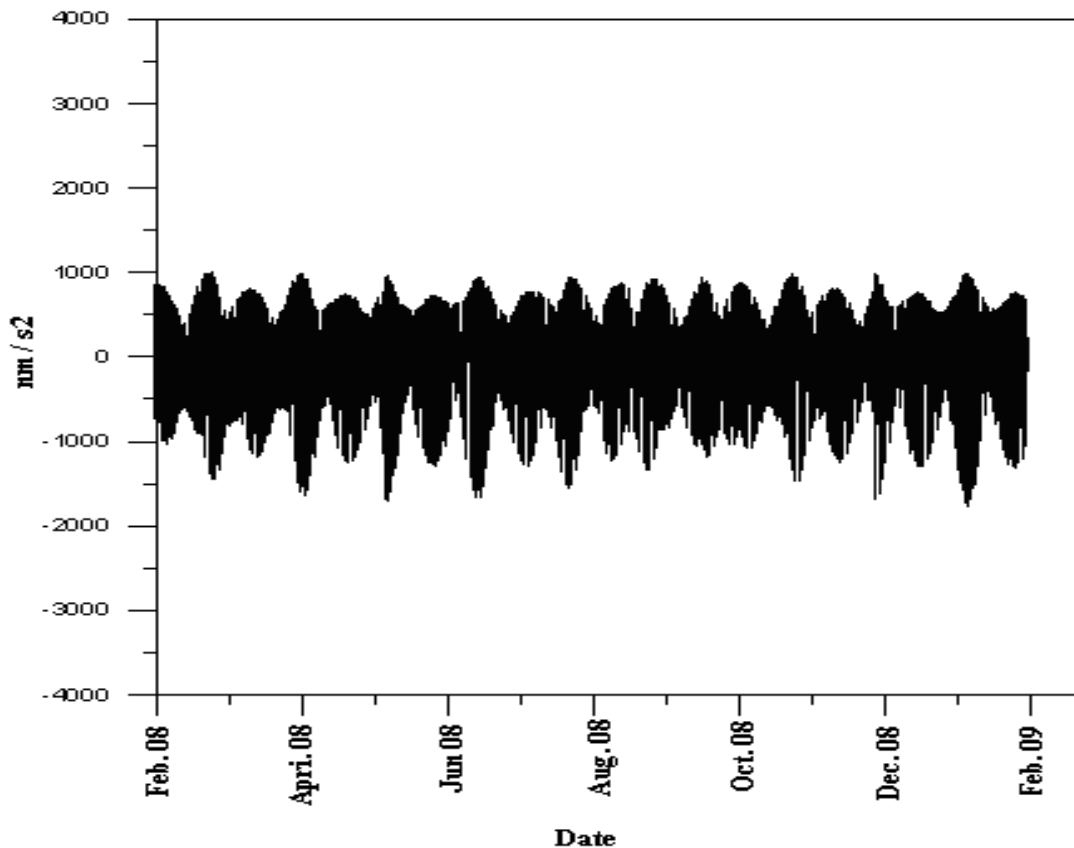

Figure 5. Hourly data at Hurghada station after pre-processing and high pass filtering.

6. Results of Tidal Analysis

The adjusted tidal parameters, using ETERNA 3.4, are given in Tab. 1. It can be noticed that some waves show an amplitude factor close to the global amplitude factor, i. e., 1.16. Most of the wave groups have a phase shift close to zero except S1, because S1 is strongly affected by thermal variations. Generally, low errors can be recognized in the semidiurnal band, especially for wave groups of large amplitudes as M2, both in amplitude factor and phase shift. The standard deviations are high for M1, S1 and L2 in phase shift. This could be due to the strong air pressure variation and the high thermal variation during the day which is very clear in S1. The standard deviations of all phases are affected by the error in the quartz clock. Also the standard deviations are very high for most of the tidal waves of higher frequencies (>2.4 cpd) because of the small amplitudes.

Table 1: Adjusted tidal parameters of Hurghada station.

Tidal Wave	From cpd	To cpd	Amplitude Th. nm / s²	Amplit. Factor	Stand. dev. %	Phase shift (degree)	Stand. dev. (degree)
Q1	0.501370	0.911390	48.4448	1.1354	0.351	-0.252	0.204
O1	0.911391	0.947991	253.0250	1.1289	0.076	0.058	0.044
M1	0.947992	0.981854	19.8995	1.1029	1.358	-0.931	0.787
P1	0.981855	0.998631	117.7320	1.1321	0.213	0.154	0.122
S1	0.998632	1.001369	2.7830	1.1706	12.551	20.35	6.964
K1	1.001370	1.880264	355.8535	1.1121	0.064	-0.047	0.036
N2	1.880265	1.914128	113.4428	1.1477	0.232	-0.010	0.136
M2	1.914129	1.950419	592.5144	1.1489	0.049	0.005	0.029
L2	1.950420	1.984282	16.7475	1.1624	1.702	0.142	0.961
S2	1.984283	2.002885	275.6689	1.1384	0.100	0.024	0.058
K2	2.002886	2.182843	74.9228	1.1222	0.004	0.164	0.058
2MK3	2.451944	2.869714	2.8350	0.7927	0.035	-7.793	2.503
M3	2.898264	2.903887	10.3383	1.1538	1.104	0.370	0.667
MK3	2.927107	2.940325	0.5859	1.5732	0.142	-1.371	5.172
S3	2.965989	3.001000	1.3475	1.0898	0.058	-0.294	3.065
MN4	3.791510	3.833113	0.0601	2.8219	1.911	157.346	38.786
M4	3.500000	4.499999	0.1671	2.1661	35.356	-151.520	22.490
SN4	3.875000	3.901458	0.0144	10.5698	6.946	-164.754	37.656
MK4	3.936000	6.00000	0.0292	69.1009	25.398	113.794	21.056

7. Ocean Tide Loading Computation

Hurgada tidal station is of relatively small distance to the shore line, so precise computation of the ocean tide loading is needed. In order to compare the observed tidal parameters with the theoretical tidal signals, the ocean tide loading contribution has to be subtracted from the observed tidal parameters. The computation of ocean tide loading requires a model of ocean tides (Zahran et al., 2006). Nowadays, there is a great progress on ocean tide models, based on the data from TOPEX/POSEIDON. Ocean tide loading has been predicted for the coordinates of Hurghada tidal station, using the FES2004 ocean tide model (Lyard et al., 2006) and the online computation with the program OLMPP, M. S. Bos and H. G. Scherneck. The resolution of the ocean tidal model (FES2004) is 0.125°x0.125°. The computations were carried out applying the SPOTL-program (Agnew, 1996) at the coordinates of Hurghada tidal station. Table 2 shows the results of the ocean tide loading vectors and the corrected tidal parameters for the main tidal waves.

8. Discussion of Tidal Analysis Results

The evaluation of the discrepancy between observed /corrected and the theoretical parameters was obtained by computing the residual vectors (Table 3) which are in the range from 0.39 nm/s² for Q1 to 15.3 nm/s² for M2. The theoretical tidal parameters were estimated using the Dehant (1987) Earth model (Eanes, 1994). A systematic bias is existing in the ratio between the theoretical amplitude factors (Table 3) and the corrected ones (Table 2). This bias reaches 1.5% when considering the main diurnal and semi-diurnal tidal constituents. It is difficult to

explain such an effect only by the insufficient resolution of the ocean tides model in the Red Sea, as the ocean loading values associated with that bias represent twice the amplitude of the computed ocean loading for the diurnal waves and 50% of it for M2. One can suspect perhaps a change of the calibration factor of the instrument.

Table 2: Ocean tide loading computation at Hrghada station.

Wave	Amplitude nm / s²	Phase shift (degree)	Amplitude Factor corrected	Phase Shift corrected
Q1	0.7	-179.1	1.1109	-0.244
O1	1.9	176.9	1.1364	0.037
P1	0.8	145.2	1.1377	-0.042
K1	2.8	147.9	1.1188	-0.261
N2	4.4	-96.6	1.1528	1.905
M2	15.2	-76.2	1.1431	1.254
S2	4.4	-47.9	1.1278	0.626

Table 3: Discrepancies between theoretical and observed tidal parameters at Hurghada station.

Wave	Amplitude Theoretical	Amp. Factor Theoretical	Residual Vector nm / s²	Phase of residual vector
Q1	48.4448	1.1561	4.78	142.48
O1	253.0250	1.1559	5.01	177.89
P1	117.7320	1.1504	1.51	176.71
K1	355.8535	1.1349	5.96	162.34
N2	113.4428	1.1596	4.44	101.74
M2	592.5144	1.1596	18.02	124.68
S2	275.6689	1.1596	9.53	159.04

9. Gravity Residuals and Conclusions

The tidal gravity residuals are given in Fig. 6. The residuals have a general range of about ± 10 nm/s². No significant anomalies can be recognized in the residuals. The amplitude spectrum of residual gravity is very important to prove if the tidal waves are completely approximated or not. It can be noticed that tidal signals are still contained in the gravity residuals. The ANALYZE program allows the computations of the Fourier amplitude spectrum of the residuals (Fig. 7). It shows a noise level in the diurnal band of up to 5.5 nm/s² and in the semidiurnal band of 6 nm/s². Also at higher frequencies a noise level of 4.7 nm/s² can be recognized. The peaks correspond to shallow water components probably caused by ocean tide loading in the Red Sea. The significant energy in the residual spectrum may be due to the timing problem of the quartz clock, and air pressure variation, which was not considered during registration and analysis.
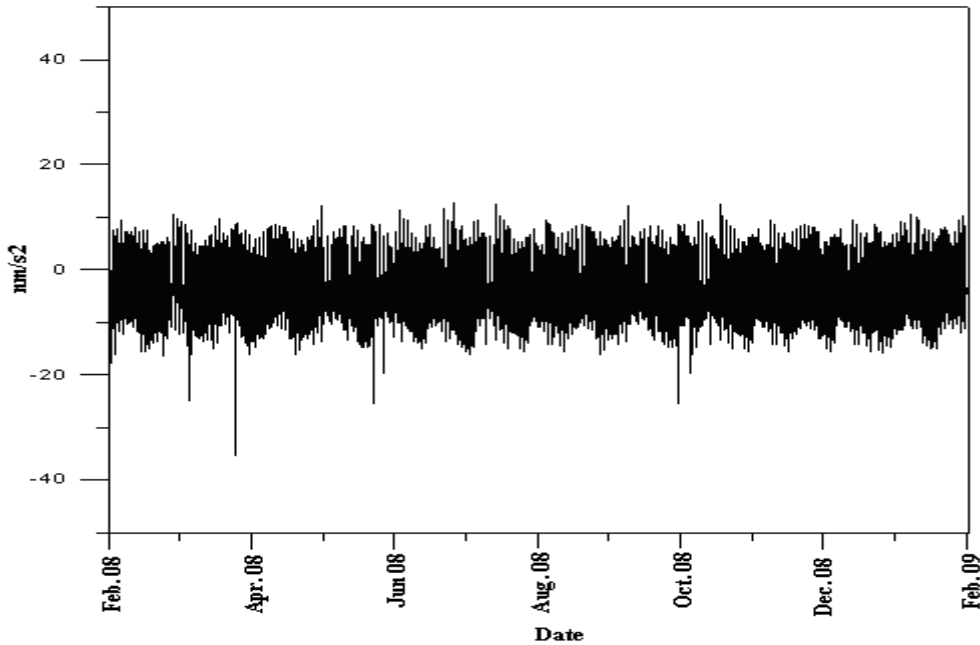
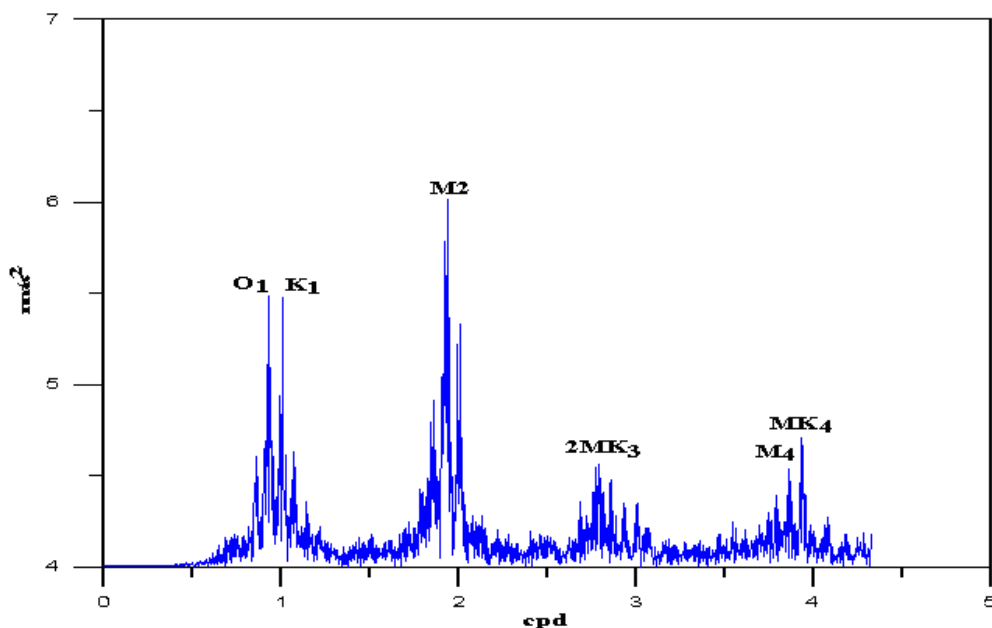Figure 6.Residual gravity at Hurghada station after tidal analysis.

Figure 7: Fourier amplitude spectrum of the residuals after tidal analysis at Hurghada station.

References

Agnew, D. C., 1996. SPOTL: Some programs for ocean - tide loading. Scripps Institution of Oceanography. SIO Reference Series 96-8.

Bos, M. S. and Scherneck, H. G., Online free ocean tide loading provider, http://www.oso. Chalmers .se/~loading.

Dehant, V., 1987. Tidal parameters for an inelastic Earth. PEPI, Vol. 49 pp. 97-116.

Eanes, J., 1994. Diurnal and semidiurnal tides from TOPEX/POSEIDON altimetry (Abstract). Eos Trans. AGU, vol. 75(No. 16), Spring   Meet. Suppl., 108p.

Hartmann, T., and Wenzel, H. G., 1995a. The HW95 tidal potential catalogue. Geophys. Res. Lett., vol. 22, pp. 3553-3556.

Hartmann, T., and Wenzel, H. G., 1995b. Catalogue HW95 of the tidal potential. Bull. d' Inf. Marées Terrestres, vol. 123, pp. 9278-9301.

Hassan, R. M., 2007. Tidal gravity observations at Nasser Lake area, Aswan, Egypt. Dissertation, Geophysics Department, Faculty of Science, Cairo University, 147 pp.

Hassan, R.M., Abdelrahman, E.M. , Tealeb, A. , Zahran, K.H. and Jentzsch, G., 2009a. Gravimetric Tide observation at Lake Nasser Region, Aswan, Egypt. Submitted to Bulletin d'Inf. Marées Terr., Proc.16 th Int. Earth Tide Symp., Jena, Sept. 1 – 5, 2008.

Hassan, R.M., Abdelrahman, E.M. , Tealeb, A. , Zahran, K.H. and Jentzsch, G., 2009b. Hydrological Signals due to the Seasonal Variation of Lake Nasser and its Effect to the Surrounding Crust as Deduced from the Tidal Gravity Observations. Submitted to Bulletin d'Inf. Marées Terr., Proc. 16 th Int Earth Tide Symp., Jena, Sept. 1 – 5, 2008.

Lyard, F. Lefevre, T. Letellier, and O. Francis, 2006. Modelling the global ocean tides: modern insights from FES2004. Ocean Dynamics, 56:394–415, 2006.

Jentzsch, G., 1995. Report of the Working Group on 'High Precision Tidal Data Processing'. Proc. 12th Int. Symp. Earth Tides, Beijing, August 1993, Science Press, Beijing.

Wenzel, H. G., 1994. PRETERNA a preprocessor for digitally recorded tidal data. Bull. d'Inf. Marées Terr., vol. 118, pp. 8722 – 8734.

Wenzel, H. G., 1996. The nanogals software: Earth tide data processing package ETERNA 3.30. Bulletin d'Inf. Marées Terr., vol. 124, pp. 9425 9439.

Wenzel, H. G., 1997. Analysis of the Earth tide observations. In: Wilhelm, H.,W. Zürn and H. -G. Wenzel (Eds). Tidal Phenomena. Lecture Notes in Earth Sciences, Springer Verlag, Berlin, Germany, 59-75.

Zahran K. H., T ealeb A., Groten E., Hassan R. M., Hamed T. A., and Rabah M. 2004. FINAL RESULTS OF GRAVITY TIME SERIES OBSERVATIONS AT HELWAN, CAIRO, EGYPT. NRIAG Journal of Geophysics PP. 75 84

Zahran, K. H., Jentzsch, G., and Seeber, G., 2006. Accuracy assessment of ocean tide loading computations for precise geodetic observations. J. Geod., vol. 42, 159-174.

BLANK PAGE